On the Use of High Performance Annular Fuel in PWRs

by

Bo Feng

Submitted to the Department of Nuclear Science and Engineering in Partial Fulfillment of the Requirements for the Degree of

Bachelor of Science in Nuclear Science and Engineering
and
Master of Science in Nuclear Science and Engineering

at the
Massachusetts Institute of Technology
June 2008

© Massachusetts Institute of Technology, 2008. All rights reserved.

Signature of Author: _____
Department of Nuclear Science and Engineering
May 9, 2008

Certified By: _____
Mujid S. Kazimi, Ph.D.
TEPCO Professor of Nuclear Engineering
Thesis Supervisor

Certified By: _____
Pavel Hejzlar, Sc.D.
Principal Research Scientist
Thesis Reader

Accepted By: _____
Jacquelyn C. Yanch, Ph.D.
Chair, Committee on Graduate Students

MASSACHUSETTS INSTITUTE OF TECHNOLOGY
JUL 24 2008
LIBRARIES
ARCHIVES

On the Use of High Performance Annular Fuel in PWRs

By
Bo Feng

Submitted to the Department of Nuclear Science and Engineering on May 9, 2008, in partial fulfillment of the requirements for the Degrees of Bachelor of Science and Master of Science in Nuclear Science and Engineering

Abstract

Recently, MIT's Center for Advanced Nuclear Energy Systems developed a new high burnup annular fuel that features both internal and external cooling. Implementation of this fuel design in current pressurized water reactors (PWRs) will allow power uprates up to 50% while maintaining or improving its existing thermal and safety margins. Each annular fuel assembly is arranged in a 13x13 array but has the same side dimensions as a 17x17 solid fuel assembly. Even at much higher power densities, the peak fuel temperatures are substantially lower and the MDNBR is comparable to that of solid fuel at 100% power. The main motivation for utilizing this fuel is the lower capital construction cost per kilowatt of electrical production compared to new reactors using solid fuel.

To elaborate on the previous work, three remaining issues were addressed: the shutdown margin deficiency at 50% uprated power, effect of inner channel flow restrictions due to crud buildup and obstructions, and the economic impact of a fleet of reactors using high burnup annular fuel. All of the work was done using computer codes specializing in core neutronics, thermal hydraulics, and fuel cycle analysis.

The reduced shutdown margin was found to be caused mainly by a reduction in control material volume coupled with a higher power density. This issue was resolved by changing the control material from traditional Ag-In-Cd to 25 wt% B-10 enriched B_4C. Increasing the control rod surface area was also investigated as a possible solution but it was revealed that any departure from the cylindrical shape would lead to a reduction in control volume which resulted in decreased rod worth.

Simultaneous oxide growth and crud buildup on the inner cladding of the annular fuel was simulated in a whole core thermal-hydraulics model to determine the maximum thickness that the annular fuel can tolerate while maintaining an MDNBR greater than 1.3 under transient overpower conditions. Under very conservative conditions, the maximum tolerable thickness was calculated to be a uniform 50 μm layer of combined oxide and corrosion on the inner and outer cladding surfaces of the hot rod. Under full power conditions, the fuel was found to be able to tolerate a 35-40% blockage of the hot rod's inner channel. However, the prospect of plugging can be regarded as very hypothetical since debris filters in PWRs have a mesh spacing smaller than the fuel's inner channel diameter.

The fuel cycle analysis code CAFCA SD was modified to include the capability to model the effect of LWRs using high burnup annular fuel on the US fuel cycle. At a given date, annular fuel can be introduced to the once-through fuel cycle via Generation II reactor uprates or construction of Generation III reactors. Results showed that constructing new 1.5 GWe reactors using annular fuel resulted in the greatest reduction in the cost of electricity due to its low capital construction cost. Total spent fuel was also reduced due to the reduced amount of reactors required to fulfill power demand. However, compared to traditional 4.5 wt% enriched solid fuel, using the higher enriched annular fuel for an entire fleet of LWRs would require a greater uranium mining rate.

Overall, all three of these studies alleviate some concerns about annular fuel and serve to boost its attractiveness and feasibility for use on an industrial scale.

Thesis Supervisor: Mujid S. Kazimi
Title: TEPCO Professor of Nuclear Science and Engineering
Professor of Mechanical Engineering

Acknowledgements

I would like to thank Prof. Kazimi for providing me with the opportunity to work with him as well as suggesting and helping me with the topics for my thesis, Dr. Pavel Hejzlar for his help and for being an invaluable advisor for my undergraduate and graduate research, Dr. Ed Pilat for all his help and conversations, Prof. Shatilla for his help and instruction in reactor physics, Tyler Ellis for all his great advice and assistance with my codes, Rodney Busquim e Silva and Laurent Guérin for their help/teamwork on CAFCA, and Paul Romano for his help with Squadron and MCODE.

I want to also thank Dr. Zhiwen Xu for suggesting the method to increase Boron-10 in CASMO as well as for leaving behind very well-documented and organized work on which my research was based. He made my life so much easier.

I would also like to thank my girlfriend of almost 4 years, Daphne, for always making sure that I'm working when I'm not spending time with her because according to her, my research is the only thing that can be considered more important.

Lastly, I must thank my parents for four years of financial support. Thank you for working hard everyday to pay for my education as well as raising me for 18 years. I know tuition wasn't cheap but I'll make sure that you'll get a great ROR on your investment.

Table of Contents

List of Figures

List of Tables

Nomenclature

ABR 1.5	Actinide Burner Reactor
AIC 2.1	Silver Indium Cadmium (Ag-In-Cd)
BOC 1.3	Beginning of Cycle
CAFCA 1.5	Code for Advanced Fuel Cycles Assessment
CONFU 1.5	Combined Non-Fertile and UO_2 fuel
CMS 1.2.2	Core Management System
DNBR 1.1	Departure from Nucleate Boiling
EOC 1.3	End of Cycle
EPRI 1.2.1	Electric Power Research Institute
FBR 1.5	Fast Breeder Reactor
FFF 1.5.1	Fertile-Free Fuel
HFP 1.3	Hot Full Power
HLSD 1.5	High Level Structure Diagram
HZP 1.3	Hot Zero Power
IA 1.3	Insertion Allowance
IXAF 1.1	Internally and eXternally cooled Annular Fuel
LWR 1.1	Light Water Reactor
MCNP 1.6	Monte Carlo N-Particle transport code
MCODE 4.1.3	MCNP-ORIGEN Depletion Program
MDNBR 1.1	Minimum Departure from Nucleate Boiling Ratio
MOC 1.3	Middle of Cycle
MTC 1.3	Moderator Temperature Coefficient
NERI 1.1	Nuclear Energy Research Initiative
PWR 1.1	Pressurized Water Reactor
REA 1.3.5	Rod Ejection Accident
ROR 1.2.3	Rate of Return
SDM 1.1	Shut Down Margin
SPD 1.5	Structure-Policy Diagram
SWU 4.1.4	Separative Work Unit
TRU 1.5	Transuranics
ULWR 4.1	Uprated Light Water Reactor
VIPRE 1.2.1	Versatile Internals and Component Program for Reactors
WS 1.1.1	Westinghouse Solid fuel full power case
XF 1.1.1	IXAF fuel Full power case
XU 1.1.1	IXAF fuel Uprated power case

1. Introduction and Background

1.1. Motivation

The very competitive price of electricity from nuclear power in the U.S. has led to nuclear power plants operating at over 90% capacity factor in recent years to satisfy the growing energy demand. As a result of this constant market demand for cheaper electricity, nuclear power utilities have pursued power uprates for their plants since the 1970s in order to increase electrical output and subsequently operating profits. To increase the power output of a reactor, typically more highly enriched uranium fuel and/or more fresh fuel is used. Using high-burnup fuel allows the reactor to produce more thermal energy while maintaining its fuel cycle length and minimizing capital investment.

However, any dramatic increase in power density must be accommodated by more advanced core designs in order to satisfy all the normal safety requirements, including equivalent or better thermal margins. Increasing the surface-to-volume ratio reduces the increased maximum fuel temperatures operating at uprated powers but in the past, this was only achieved by decreasing the size and increasing the number of cylindrical fuel pellets. However, there are limits to how small solid pins can be before they lack the rigidity to resist vibrations and avoid the penalty of corrosion of thinner cladding [Kazimi et al., 2006].

Therefore, annular fuel geometry had been proposed at MIT which would allow a substantial increase in power (up to 150%) in existing and future Pressurized Water Reactors (PWRs) while maintaining or improving its safety margins. This new fuel design, called IXAF (Internally- and eXternally- cooled Annular Fuel), utilizes an annular shape which allows coolant flow inside and outside of the fuel rods and is shown below:

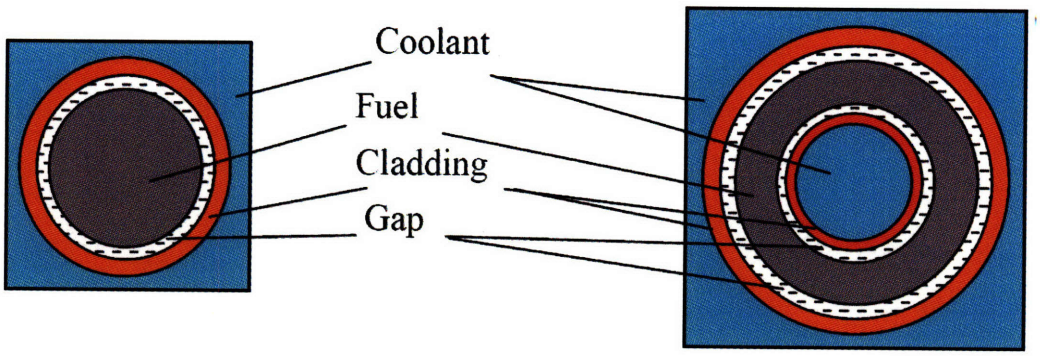

Figure 1-1 Solid and internally and externally cooled annular fuel (from Kazimi et al., 2006)

This design is very promising for implementation with high power density fuel due to two inherent features: (1) reduction of heat conduction path thickness, which improves the margin from peak fuel temperature to melting and (2) increased heat transfer surface area which improves the margin for Departure from Nucleate Boiling Ratio (DNBR). A comprehensive study on developing the IXAF for PWRs, led by MIT and funded by the U.S. DOE Nuclear Energy Research Initiative (NERI), was concluded in 2006 with detailed analyses in thermal hydraulics, neutronics, fuel performance including first scoping irradiation tests at the MIT reactor, fuel manufacturing, and economics. The overall results reveal a very promising innovative fuel design that would allow PWR uprates up to 150% power.

However, there are a few questions which deserve further investigation: (1) the need to increase the shutdown margin (SDM) for the annular fuel core at 150% power due to the higher fissile loading and shift of the neutron spectrum, (2) the effect on the minimum departure from nucleate boiling ratio (MDNBR) of potential partial blockage of the inner channel, such as simultaneous crud and corrosion buildup, and (3) the impact of using high burnup fuel in the once-through fuel cycle. This thesis addresses all three topics in detail, but for a better understanding of its results, the necessary background on IXAF and the individual topics themselves is provided in the following sections.

1.2. Annular Fuel Project Background

This section is not meant to give a complete overview or detailed results from the annular fuel project but to highlight the important factors which lead to the finalized annular fuel core design. Specifically, emphasis is placed on the thermal hydraulic and neutronic design approaches and fuel manufacturing economics.

1.2.1. Thermal Hydraulics

The operating conditions of a Westinghouse 4-loop 18 month cycle 3411 MWt core at full power, as seen in Table 1-1, were used as the reference conditions which guided the design of the IXAF-fueled core geometry. The full power Westinghouse PWR core (WS) also served as the reference case for comparison studies with annular fuel cores at full power (XF) and 150% uprated power (XU). The annular fuel geometry was optimized using a whole core thermal hydraulic model written in VIPRE-01, a widely used code developed by Electric Power Research Institute (EPRI) and certified by the NRC for subchannel analyses of light water reactor (LWR) cores. There are fewer fuel rods in an assembly using annular fuel because in order to provide sufficient coolant flow rate through the inner channel, the fuel rod diameter must be significantly larger than that of the solid fuel rod of a WS assembly. Thus, annular fuel square array sizes (11x11 to 15x15) that fit in the fixed dimensions of the 17x17 WS assembly were first investigated for their thermal hydraulic performances. Due to the added inner cladding that takes up additional volume in the annular fuel assembly, the coolant and fuel volumes are slightly smaller than those of the solid fuel assembly. The fuel pin dimensions were selected to obtain at least 90% of the fuel volume in the WS design to minimize the cycle length penalty and a similar heavy metal-to-moderator ratio in an attempt to preserve key reactor physics parameters such as reactivity coefficients.

Table 1-1 Operating parameters and selected characteristics of the reference Westinghouse 4-loop PWR (from Xu et al., 2004)

Number of primary loops	4
Reactor thermal power (MWt)	3411
Plant electrical output (MWe)	1150
Power generated directly in coolant (%)	2.6
Power generated in the fuel (%)	97.4
Core	
Core barrel inside diameter/outside diameter (m)	3.76/3.87
Rated power density (kW/L)	104.5
Effective core flow area (m^2)	4.747
Active heat transfer surface area (m^2)	5546.3
Average heat flux (kW/m^2)	598.8
Primary Coolant	
System pressure (MPa)	15.51
Core inlet temperature (°C)	292.7
Average temperature rise in reactor (°C)	33.4
Total core flow rate (Mg/s)	18.63
Effective core flow rate for heat removal (Mg/s)	17.7
Average core inlet mass flux (kg/m^2-s)	3729
Fuel Rods	
Total number	50,952
Cladding material	Zircalloy-4
Fuel density (% theoretical density)	94
Active fuel height (m)	3.66
Fuel Assemblies	
Number of assemblies	193
Number of heated rods per assembly	264
Number of grids per assembly	7
Location of first spacer grid above start of heated length (m)	0.3048
Grid spacing (m)	0.508
Grid type	L-grid
Number of control rod thimbles per assembly	24
Number of instrument tubes	1
Rod Cluster Control Assemblies	
Neutron absorbing material	Ag(80)-In(15)-Cd(5)
Cladding material	Type 304 SS
Cladding thickness (mm)	0.46
Number of clusters Full/Part length	53/8
Number of absorber rods per cluster	24

The optimum assembly designs with respect to DNBR performance at 100% power were found to be the 12x12 and 13x13 arrays, as can be seen in Figure 1-2. However, due to the likelihood of increased heat flux to the outer channel after thermal expansion and swelling of the fuel pellets, a higher outer channel minimum departure from nucleate boiling ratio (MDNBR) was preferred. Therefore, the 13x13 array was selected as the optimum design from a thermal hydraulic perspective. Table 1-2 and Figure 1-3 compare the 13x13 annular fuel array geometry with that of the reference 17x17 solid fuel array.

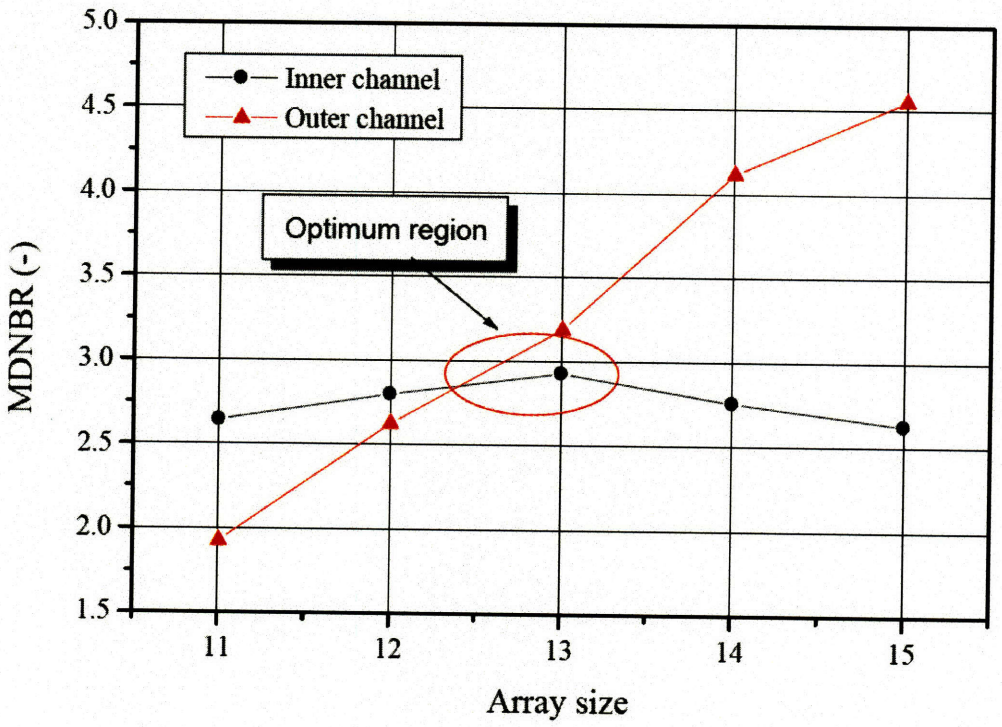

Figure 1-2 Inner and outer channel minimum DNBR at 100% power as a function of annular fuel array sizes (from Kazimi et al., 2006)

Table 1-2 Dimensions [cm] of annular fuel elements of optimum arrays and the reference solid fuel array (from Kazimi et al., 2006)

Array	D_{cii}	D_{cio}	D_{fi}	D_{fo}	D_{coi}	D_{coo}	Pitch
12x12	0.9533	1.0676	1.08	1.5400	1.5524	1.6667	1.789
13x13	0.8633	0.9776	0.99	1.4100	1.4224	1.5367	1.651
17x17-ref.	Solid pin	-	-	0.8255	0.8379	0.9522	1.263

*Subscripts, *ci, f,* and *co* designate inner cladding, fuel, and outer cladding, respectively; a second subscript designates outer (o) or inner (i) surface.

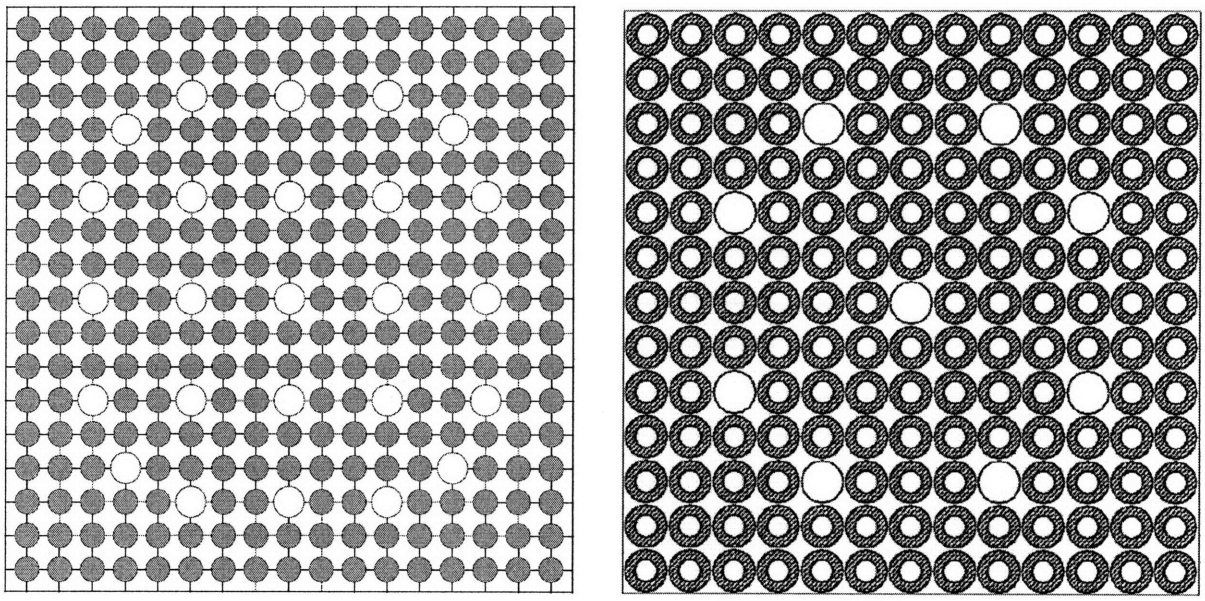

Figure 1-3 Comparison between the reference 17x17 solid fuel assembly (left) and the 13x13 annular fuel assembly (right) (from Kazimi et al., 2006)

It is important to note that the total number of guide tubes is decreased in the annular fuel assembly from 24 to 8 (the central water hole is reserved for instruments). Even though the individual control rods in annular fuel are larger, the reduced number of control rods in each assembly reduces the overall control rod volume in the annular fuel assemblies. This will be shown to be the main cause of the decreased SDM in the annular fuel cores.

In order to study the performance of IXAF-fueled cores at uprated power levels, the core power was taken from the nominal 3411 MWt to a 150% uprated 5117 MWt for the 13x13 array geometry. Thus, from a thermal hydraulic perspective, the XU and XF cores have the same basic core geometry, but the uprated core was modeled with 50% more coolant flow and power density. Even with the increased power density and the use of annular fuel, the MDNBR under transient conditions was calculated to be the same as that of the reference core with solid fuel at 100% power. The peak fuel temperature for the uprated core is still about 1300°C lower than the reference solid fuel, as shown in Figure 1-4:

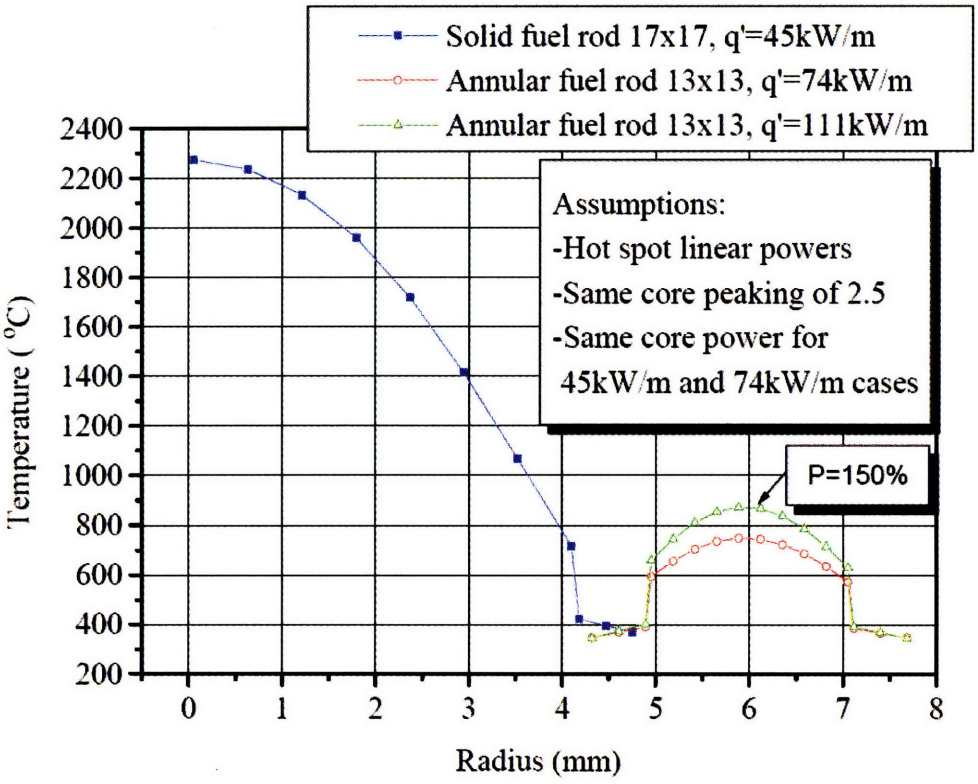

Figure 1-4 Comparison of fuel temperatures at the hotspot (from Kazimi et al., 2006)

1.2.2. Neutronic Performance

After the optimum dimensions of the IXAF had been determined primarily from thermal hydraulic analyses, the 150% power core and an 18-month fuel management scheme were designed using neutronic analysis. The design target was an 18 month cycle length at 90% capacity factor, under the constraints of: a maximum boron concentration of 1750 ppm, a maximum radial pin power peaking of 1.65, and a hot spot factor of 2.5. Since the heavy metal loading for the XF and XU cores are relatively the same, higher enrichments are required for the annular fuel at 150% power.

Using a consistent design methodology and Studsvik's Core Management System (CMS) code package which consists of CASMO-4, TABLES-3, and SIMULATE-3, three cores were designed for the WS, XF, and XU cases. The annular core design followed the existing industrial 3-batch core approach with 72 reload assemblies (48 with 9.0% enrichment and 24 with 8.1% enrichment). The higher enrichment fuel batch stays in the core for 3 cycles while the lower enrichment fuel batch stays in for 2 cycles. The loading pattern of an equilibrium annular fuel core at 150% power rating is shown with peaking and burnups in Figure 1-5. The H and L designate high and low enrichment, the first two numbers after a letter indicate the number of rods with burnable poison coating (gadolinium), and the last two numbers the w/o of Gd in these rods.

It is important to note that the higher enrichment hardens the neutron spectrum and reduces the reactivity worth of the existing control rods. Other contributions to the reduced shutdown margin when transitioning from a solid to annular fuel core are the reduced number of control rods per assembly (8) and the retaining of the same number of control rod assemblies in the core (57). Otherwise, the XF and XU cores satisfied the design target and constraints and

showed comparable steady-state performance, including power distributions and reactivity coefficients, to the reference solid fuel core.

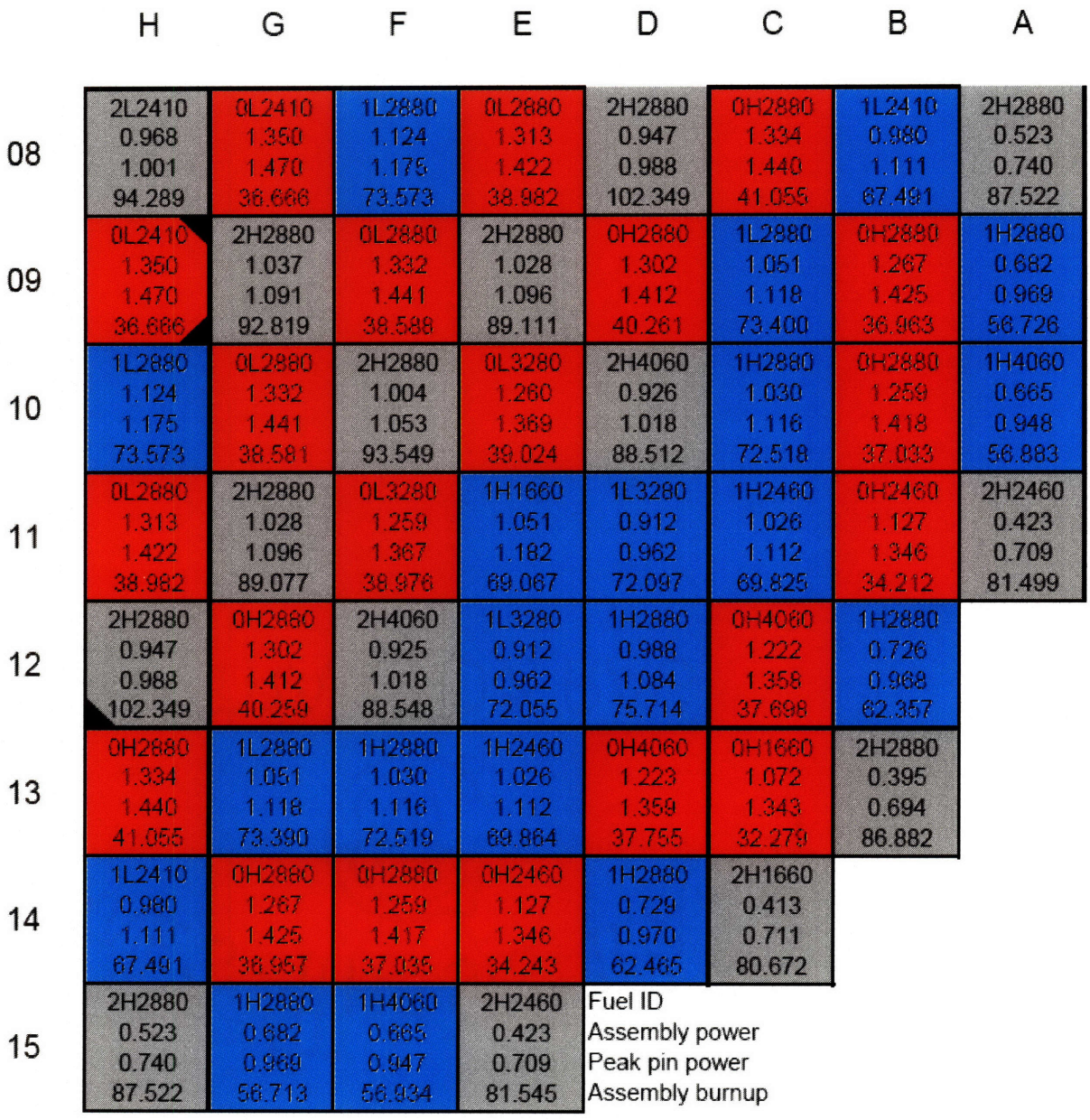

Figure 1-5 Assembly power distribution and burnup at end of 18-month cycle for the IXAF-fueled 150% power core (from Xu et al., 2004)

1.2.3. Economics

The economic analysis for IXAF was done by Westinghouse [Kazimi et al., 2006] to determine the additional fuel manufacturing cost as well as overall economic incentive for utilizing annular fuel. For the manufacturing cost effects, the baseline constraints and assumptions used in the evaluation were the permitting and operational constraints at the Westinghouse Nuclear Fuels plant in Columbia, South Carolina. This study did not take into account any enrichment costs so any additional cost resulting from this study would only result in additional fabrication costs. The manufacturing changes in fabricating annular fuel were found to be insignificant except for the additional cost of the zirconium inner cladding. This increased the fabrication cost from $0.005/kWhr(e) to $0.00502/kWhr(e).

To increase the power density of the annular fuel, Westinghouse decided to pursue increasing the mass of the fuel by extending the rod length from 12 to 14 feet and increasing the density from 95.5 to 97% theoretical density instead of increasing the U-235 enrichment. The reason the enrichment method was dropped was because it had an undesirable effect on all the wet process areas of the fabrication plant.

The three options of interest analyzed by [Kazimi et al., 2006] are: 1) new construction of a 1117 MWe solid fuel PWR, 2) uprate of a 1000 MWe solid fuel PWR to a 1800 MWe annular fuel PWR, and 3) new construction of a 1717 MWe annular fuel PWR. Option 2 was analyzed including costs for replacement power and un-utilized fuel value (Option 2a) and with only costs for new installed equipment (Option 2b). The summary and overall costs for the three of the options considered in this report are shown in Table 1-4 with the financial assumptions for the comparison in Table 1-3:

Table 1-3 Financial assumptions for comparison of annular and pellet PWR fuels (from Xu et al., 2004)

Price of Electricity	0.05 $/kWhr(e)]
Discount Rate	11 %/yr
Inflation Rate for Power Cost	1 %/yr
Inflation Rate for Fuel and O&M Costs	2 %/yr
Operating Rate	95 %/yr
Operating Time	20 years
Fuel Enrichment	5 %U235
Burnup	67 MWd/kg U
Plant Efficiency	35%

Table 1-4 Summary and overall costs of three considered options (from Kazimi et al., 2006)

Opt.	Description	Size (MW(e))	Fuel Cost ($/kWh(e))	O&M Cost ($/kWh(e))	Capital Cost ($/kW(e))	Total Capital Cost ($)	ROR (%)
1	New Solid Fuel PWR	1117	0.005	0.01	1313	1,466,853,397	6.9
2a	PWR Uprate all costs included	600 added to 1200, total 1800	0.00502	.005 on added 600 MW(e)	1817	1,090,200,000	6.3
2b	PWR Uprate component costs only	600 added to 1200, total 1800	0.00502	.005 on added 600 MW(e)	1381	828,600,000	11.6
3	New Annular Fuel PWR	1717	0.00502	0.0066	1103	1,893,299,218	11.5

A 3 year construction period is assumed for the new plant or components but for the uprate case (Options 2a and 2b), the plant was assumed to be offline for 12 months. Notice that if replacement power and unused fuel costs are included, the uprate option would have the lowest Rate of Return (ROR) as seen in option 2a. However, if these costs are ignored and only component costs are included (option 2b), then it would have the highest ROR. The Rate of

Return figures are the return on investments beyond what can be obtained in passive deposition of funds at banks. For a total return figure, one should add to this ROR the interest rate assumed, which for the Westinghouse study was 11%.

It was demonstrated by [Beccherle, 2007] that by using a fuel management scheme that gradually replaces the solid fuel with annular fuel one batch at a time before the uprate construction, the solid fuel will be fully utilized and will not contribute towards the capital cost of the uprate. The savings from fully utilizing the solid fuel before the uprate was calculated to be $71,000,000 [Lahoda et al., 2007] for the PWR. In addition, it was pointed out that by timing the uprate construction with a scheduled steam generator replacement the additional cost of the steam generators, estimated to be $150,000,000 [Lahoda et al., 2007], can be subtracted from the capital cost as well.

In [Lahoda et al., 2007], the total overnight cost of option 2a was actually $1,230,589,281 (2051 $/kWe) for a 1200 MWe reactor, with a replacement power cost of $224,694,000. However this overnight cost was then normalized from a 1200 MWe reactor to the AP1117 (option 1) to obtain 1817 $/kWe.

If the replacement power was assumed for a period of 1 year, then the cost of electricity assumed by Westinghouse can be calculated using Equation 1.1:

$$C_{rep} = \frac{C_R}{P_E \cdot CF \cdot T_{off}} \cdot \qquad (1.1)$$

where C_{rep} is the cost of replacement electricity, C_R is the total cost of replacement power ($224,694,000), P_E is the nominal electric power (1,200,000 kWe), CF is the capacity factor (0.95), and T_{off} is the offline period in hours (365 days x 24 hours/day= 8760 hours). Given these assumptions, the C_{rep} used by Westinghouse was $0.0225/kWhe.

1.3. Shutdown Margin

Shutdown margin is the instantaneous amount of reactivity by which a reactor is subcritical or would become subcritical from its operating condition, assuming all control rods are fully inserted except for the single rod with the highest integral worth, which is assumed to be fully withdrawn for conservatism [NEA, 2001]. In other words, the SDM is the surplus negative reactivity supplied by all but one of the available control rods after full insertion. It is important to note that the SDM will vary with burnup. Thus, it is necessary to maintain this margin to ensure complete shutdown at all times during the core lifetime. Typically, the minimum shutdown margin is 1.3 $\%\Delta\rho$ (1300 pcm) for a Westinghouse PWR operating at full power [Seabrook]. This safety criterion was also desired but not met by the initial design of the high burnup PWR cores using IXAF [Xu et al., 2004].

The annular fuel project used the CMS code package to model the entire core to calculate the SDM and other neutronic parameters. Specifically, the SDM was found by calculating the various reactivities in Equation 1.2:

$$(\rho_{allCRD} - \rho_{maxCRD})\ 0.9 - \rho_{HFPtoHZP} - \rho_{IA} = SDM \qquad (1.2)$$

Where ρ_{allCRD} = reactivity worth of all fully inserted control rods

ρ_{maxCRD} = reactivity worth of the control rod with the highest worth

$\rho_{HFPtoHZP}$ = difference between core reactivities at hot full power and at hot zero power (also known as the power defect)

ρ_{IA} = rod insertion allowance

SDM = shutdown margin

The values inside the parentheses make up the total available reactivity for shutdown which is multiplied by a factor of 0.9 for conservatism. Two reactivity values which must be deducted from this available reactivity are: (1) the reactivity insertion from taking the core from hot full power (HFP) to hot zero power (HZP) and (2) the rod insertion allowance (IA). The standard solid fuel WS case is used as an example of how the shutdown margin is calculated at three stages of an equilibrium 18-month cycle. All of the core wide reactivities from Equation 1.2 were calculated at beginning of cycle (BOC), middle of cycle (MOC), and end of cycle (EOC) when the average fuel burnups are 0.15, 9.5, and 18.784 MWd/kg, respectively, and are shown in Table 1-5. The calculation methods are explained in the proceeding sections. The lowest value of the shutdown margin for the WS core is 3861 pcm or 3.861 %$\Delta\rho$ which occurs at EOC.

Table 1-5 Values of the reactivity terms in Equation 1.2 for the WS core (from Xu et al., 2004)

Cycle Stage	BOC	MOC	EOC
ρ_{allCRD} [pcm]	7363	7853	8033
ρ_{maxCRD} [pcm]	101	106	113
Total Negative Reactivity [pcm]	6536	6972	7128
$\rho_{HFPtoHZP}$ [pcm]	1833	2187	2982
ρ_{IA} [pcm]	241	324	285
Total Positive Reactivity [pcm]	2074	2511	3267
SDM [pcm]	4462	4461	3861

1.3.1. Control Rod Worth

The reactivity worth of all the control rods, ρ_{allCRD}, was calculated by the difference between the k-effectives of the core with all control rods withdrawn, k_{ARO}, and all control rods inserted, k_{ARI} as shown in Equation 1.3:

$$\rho_{allCRD} = \rho_{ARO} - \rho_{ARI} = \frac{k_{ARO} - 1}{k_{ARO}} - \frac{k_{ARI} - 1}{k_{ARI}} = \left(\frac{1}{k_{ARI}} - \frac{1}{k_{ARO}} \right) \tag{1.3}$$

To get reactivity in terms of pcm (percent millirho), the result from Equation 1.3 is multiplied by 10^5. This value is then subtracted by the reactivity of the highest worth control rod, ρ_{maxCRD}, and multiplied by 0.9 to get the total negative reactivity.

1.3.2. Power Defect

When the reactor is shut down, the temperature of the fuel and moderator both decrease, and due to the reactor's negative Doppler and moderator temperature coefficients (MTC), this effect adds a significant amount of positive reactivity, otherwise known as the power defect. As seen in Table 1-6, this reactivity insertion is the most positive at EOC when the MTC is the most negative since the burnable poisons have been depleted and the soluble boron concentration in the coolant is virtually zero. The temperature drops across the fuel and moderator before and after shutdown are virtually the same at all stages of the cycle while the moderator temperature coefficient decreases from -27.1 to -73.3 pcm/°C from BOC to EOC.

Table 1-6 Reactivity feedback parameters of WS core at various burnups (from Xu et al., 2004)

	BOC	**MOC**	**EOC**
Burnup [MWd/kg]	0.15	9.5	18.784
Soluble Boron Concentration [ppm]	1428	756	0.03
Temperatures			
Avg. Moderator Temp at HFP [°C]	308.3	308.3	308.3
Avg. Moderator Temp at HZP [°C]	292.8	292.8	292.8
Avg. Fuel Temp at HFP [°C]	649.7	650.2	650.2
Avg. Fuel Temp at HZP [°C]	292.8	292.8	292.8
Feedback Coefficients			
Moderator Temp Coefficient [pcm/°C]	-27.11	-45.63	-73.31
Uniform Doppler Coefficient [pcm/°C]	-2.75	-2.75	-2.89
Power Coefficient [pcm/percent power]	-17.23	-20.36	-25.66
Power Defect [pcm]	1833	2187	2982

1.3.3. Control Rod Insertion Allowance

The IA is the allowed amount of negative reactivity inserted by a single bank (group) of control rods, as shown in Figure 1-6, during normal operation.

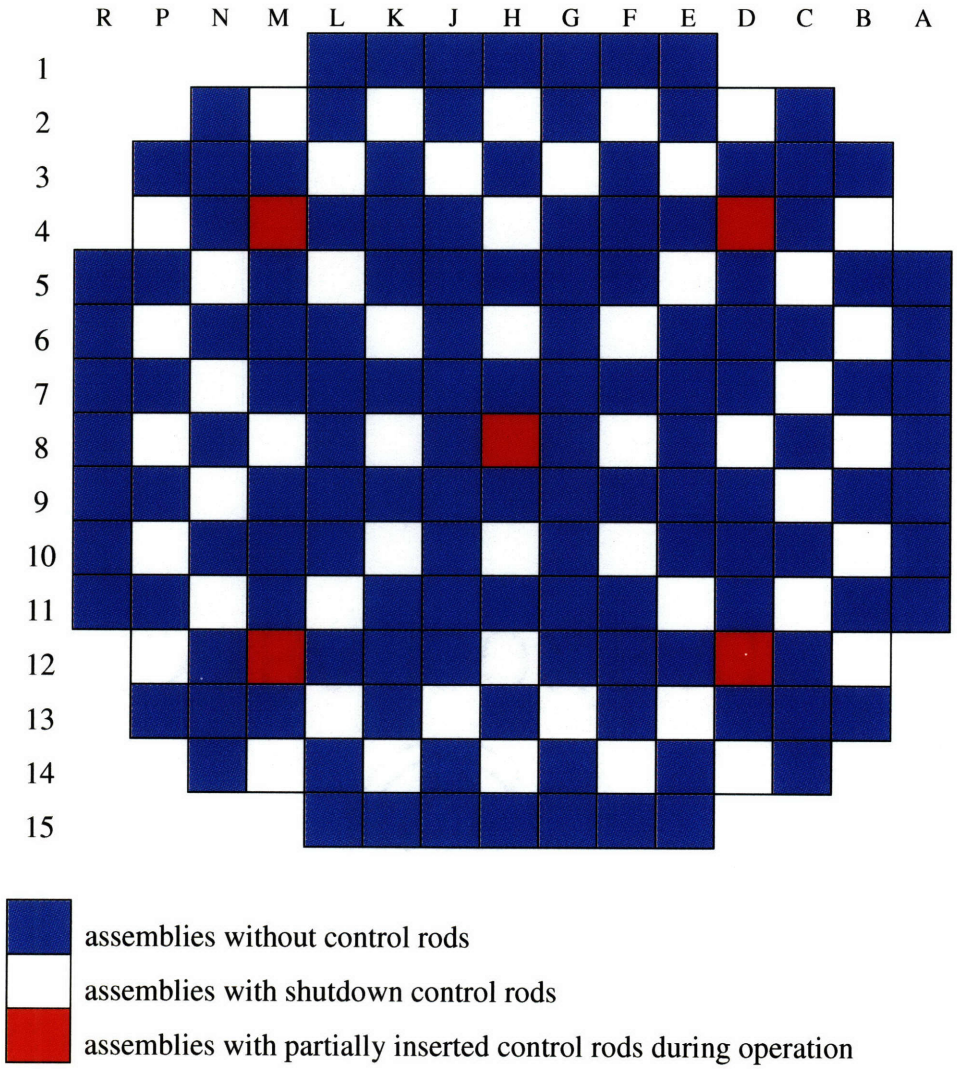

Figure 1-6 Control rods in PWR which are partially inserted during normal operation

These control rods are partially inserted in order to provide bite so the rods have a measurable differential worth when they are used to compensate for small changes in boron concentration, changes in temperature, and axial offset. The distance which the control rods are inserted for this purpose (126.8 cm) does not change with burnup but since the reactivity of the core does change with burnup, the amount of reactivity held by the IA changes as well. The negative reactivity from the IA is assumed to exist at all times so this value (ρ_{IA}) is subtracted from the total negative reactivity available in the SDM calculation.

1.3.4. Annular Fuel Shutdown Margin

The same methodology was used to calculate the shutdown margins for the XF and XU cores and the results are shown in Tables 1-7 and 1-8.

Table 1-7 Values of the reactivity terms in Equation 1.2 for the XF core (from Xu et al., 2004)

Cycle Stage	BOC	MOC	EOC
ρ_{allCRD} [pcm]	4250	4492	4525
ρ_{maxCRD} [pcm]	66	65	72
Total Negative Reactivity [pcm]	3766	3984	4008
$\rho_{HFPtoHZP}$ [pcm]	1298	1717	2429
ρ_{IA} [pcm]	239	314	211
Total Positive Reactivity [pcm]	1537	2031	2640
SDM [pcm]	2229	1953	1368

Table 1-8 Values of the reactivity terms in Equation 12 for the XU core (from Xu et al., 2004)

Cycle Stage	BOC	MOC	EOC
ρ_{allCRD} [pcm]	3767	3548	3583
ρ_{maxCRD} [pcm]	66	56	66
Total Negative Reactivity [pcm]	3331	3142	3165
$\rho_{HFPtoHZP}$ [pcm]	1614	1692	2795
ρ_{IA} [pcm]	236	351	152
Total Positive Reactivity [pcm]	1850	2043	2947
SDM [pcm]	1481	1099	218

By comparing Table 1-5 to Table 1-7, one can see that there is a substantial drop in SDM when using annular fuel for the same power level because the annular core utilizes only 8 control rods per rodded assembly as opposed to the WS's 24; the decrease in total control volume leads to lesser negative reactivity available for insertion. In addition, the XF fuel requires a higher enrichment for the same power density due to the slightly decreased fuel volume. This creates a harder spectrum for the annular fuel which leads to an additional decrease in total control rod worth. Specifically, the increased amount of U-235 absorbs slow neutrons and decreases the thermal flux in the core. A thermally black control rod will have less thermal neutrons to absorb and will have a reduced effect on neutronic control.

The XU assembly is identical to the XF assembly except that it has 1) even higher reload enrichments, 2) much more burnable poison pins, and 3) a higher soluble poison concentration during the early stages of the cycle in order to maintain the same cycle length at 50% higher power. All three of these factors contribute to an even harder spectrum which results in the shutdown margin for the XU core dipping below the 1300 pcm minimum sometime before the MOC as seen in Table 1-8.

Again, the shutdown margin decreases as a function of burnup for both the XF and XU cases due to the gradual decrease in the soluble boron concentration which leads to an increasingly negative MTC. Table 1-9 shows the reactivity feedback parameters used in the power defect calculation. Also, notice that the XF core has the lowest power defect. This is due to the lower fuel temperatures at HFP when using annular fuel at 100% power and the fact that the average fuel temperatures at HZP are virtually the same for all cores at each stage (293°C). In addition, the average moderator temperatures at HFP (308°C) and HZP (293°C) are the same for all cores at all stages so the moderator temperature decrease is constant when going from HFP to HZP.

Table 1-9 Reactivity feedback parameters for WS, XF, and XU cores at HFP (from Xu et al., 2004)

		BOC	MOC	EOC
Soluble Boron Concentration [ppm]	WS	1456	756	0.03
	XF	1503	660	0.02
	XU	1493	1086	0.05
Avg. Fuel Temp at HFP [°C]	WS	650	650	650
	XF	447	447	447
	XU	519	520	519
Moderator Temp Coefficient [pcm/°C]	WS	-27.11	-45.63	-73.31
	XF	-34.74	-53.60	-78.01
	XU	-37.26	-47.86	-81.11
Uniform Doppler Coefficient [pcm/°C]	WS	-2.75	-2.75	-2.90
	XF	-2.90	-3.02	-3.26
	XU	-2.77	-2.90	-3.17
Power Coefficient [pcm/percent power]	WS	-17.23	-20.36	-25.66
	XF	-12.43	-15.40	-20.57
	XU	-10.19	-11.04	-15.61
Power Defect [pcm]	WS	1833	2187	2982
	XF	1298	1717	2429
	XU	1614	1692	2795

1.3.5. Rod Ejection Accident Impact

One of the accidents analyzed in the previous study was the Rod Ejection Accident (REA) which is one of the specified transients addressed as part of the licensing process for PWRs. In this study, the control rod design for annular fuel was modified to increase its reactivity worth to provide greater shutdown margin so it is necessary to revisit REA analysis from the previous study [Kazimi et al, 2006]. The licensing analysis of this event generally seeks to initiate the accident from the worst possible initial condition, with the maximum possible ejected rod worth, and calculate the energy deposition in the fuel. In licensing analyses, the energy deposition is required to be less than 280 calories/gram at any axial location in the fuel rod. This is the main acceptance criterion for this event. Other acceptance criteria include

avoiding centerline melt conditions, and limiting the number of rods experiencing post-DNB conditions to less than 10% [Kazimi et al, 2006].

As described in Section 1.3.5, a single bank of control rods is partially inserted during normal operation. A REA assumes a mechanical failure of the control rod drive such that the reactor coolant system pressure would eject the control rod and drive shaft to the fully withdrawn position. Industry practice is to assume that the rod is ejected from the core, but does not breach the reactor coolant system pressure boundary. The ejection of the control rod represents a sudden insertion of positive reactivity, causing a surge in core power. The reactivity worth of the ejected rod determines the rate of initial power increase so for conservatism, the highest worth rod is assumed to be ejected. The increase in power causes a high neutron flux reactor trip (or a flux rate increase trip). However, it takes a few seconds for the unaffected control rods to insert into the core. The initial power increase, which occurs over milliseconds, is mitigated (self-corrected) by the fuel Doppler coefficient. The final power decrease occurs a few seconds later, caused by the insertion of the unaffected control rods. During this time, significant energy can be deposited in the fuel rod [Kazimi et al, 2006].

Since REA causes sudden insertion of positive reactivity in a particular region of the reactor core, an appropriate method of analysis was to use a coupled, three-dimensional, neutronic-thermal hydraulic calculation to determine the localized power response. This was then combined with a fuel rod thermal analysis to determine the energy deposition and fuel centerline temperature during the rapid rod ejection transient. A simplified approach is typically used in the current licensing analysis, which was derived from the more rigorous three-dimensional analysis, and benchmarked for a typical Westinghouse 4-loop 3411 MWt PWR. The simplified method used point kinetics calculations, with key parameters (Doppler coefficient and peaking factors) adjusted to account for the difference from the three-dimensional method. This approach was

done using SIMULATE-3 for the neutronics and RELAP5 for the thermal-hydraulics [Kazimi et al, 2006].

Neutronics calculations were carried out first to determine the most reactive rod at two initial conditions, namely, HZP and HFP, for the solid fuel at 100% power level and the annular fuel, at both 100% and 150% power levels. For each case, a static calculation was conducted with SIMULATE, where the most reactive rod was ejected. This provided static post-ejection peaking factors. Table 1-10 shows the results, for solid and annular fuel rod geometries at HZP and HFP conditions, for 100% power operation and for 150% power operation. Also shown for each case are the ejected rod worth and the fuel Doppler coefficient before the REA [Kazimi et al, 2006].

Table 1-10 Post-ejection physics parameters (from Kazimi et al, 2006)

	WS	**XU**	**XF**
HFP, EOC			
Maximum Rod Worth	27.6	19.8	18.1
Radial Peaking	1.576	1.563	1.514
Total Peaking	2.243	2.065	2.120
Doppler Coefficient [pcm/C]	-2.90	-3.26	-3.17
HZP, EOC			
Maximum Rod Worth [pcm]	274.0	130.4	110.5
Radial Peaking	3.648	2.549	2.120
Total Peaking	6.763	5.792	5.831
Doppler Coefficient [pcm/C]	-3.40	-3.44	-3.49

A system thermal-hydraulic calculation has been carried out with RELAP5 for HFP, modeling an average fuel rod and a hot rod. The hot rod is initially assumed to have the post-ejected peaking factors shown in Table 1-10. After that, the transient is initiated by inserting the positive reactivity shown in Table 1-10 for each case, over 0.05 seconds. The core power increases, the reactor trip signal occurs on high neutron flux, the initial power spike is mitigated

by the fuel Doppler coefficient, the other control rods are inserted, and the power finally decreases as the reactor is shut down [Kazimi et al, 2006].

The results are shown in terms of the fuel temperatures. Figure 1-7 shows the maximum fuel temperatures for HFP conditions. The transient is initiated at 1 second. The maximum fuel temperature for the solid rod is at the fuel centerline. For the annular rods, the maximum fuel temperature was taken at an interior node, biased closer to the center. It can be seen that the maximum fuel temperatures for the annular geometry are significantly lower (1200°C) than that for the solid rod (2200°C). The initial power increase was similar (on a relative basis) for all the cases, because the ejected rod worth was assumed similar. Hence the difference in temperatures is mainly due to the increased heat transfer area available for the annular rods. The large margin available indicates that the annular rods should be able to successfully withstand the rod ejection event even at 150% power level [Kazimi et al, 2006].

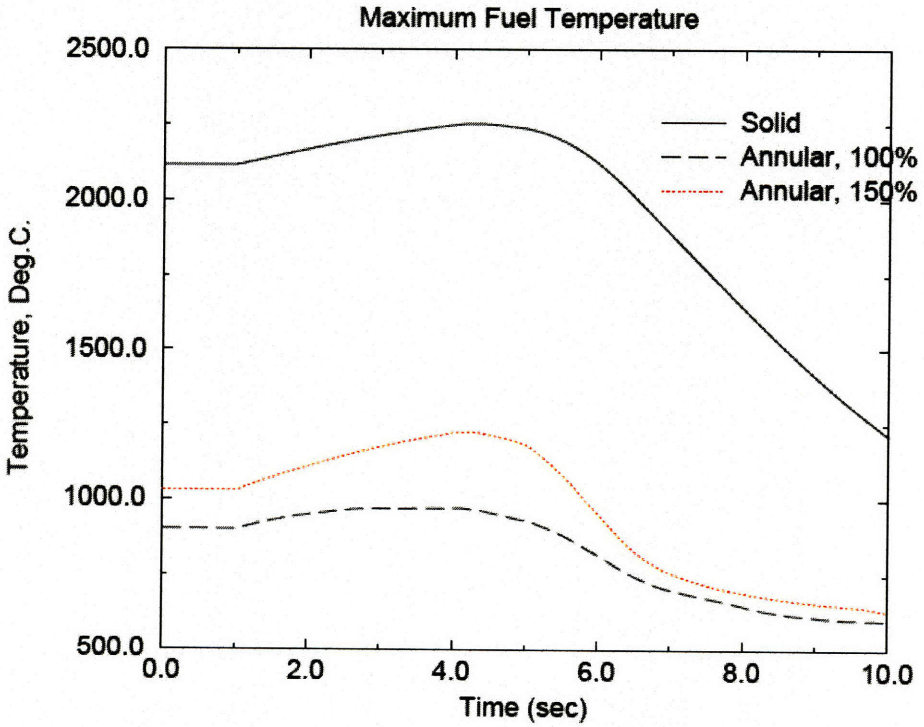

Figure 1-7 Maximum fuel temperatures for REA at HFP (from Kazimi et al, 2006)

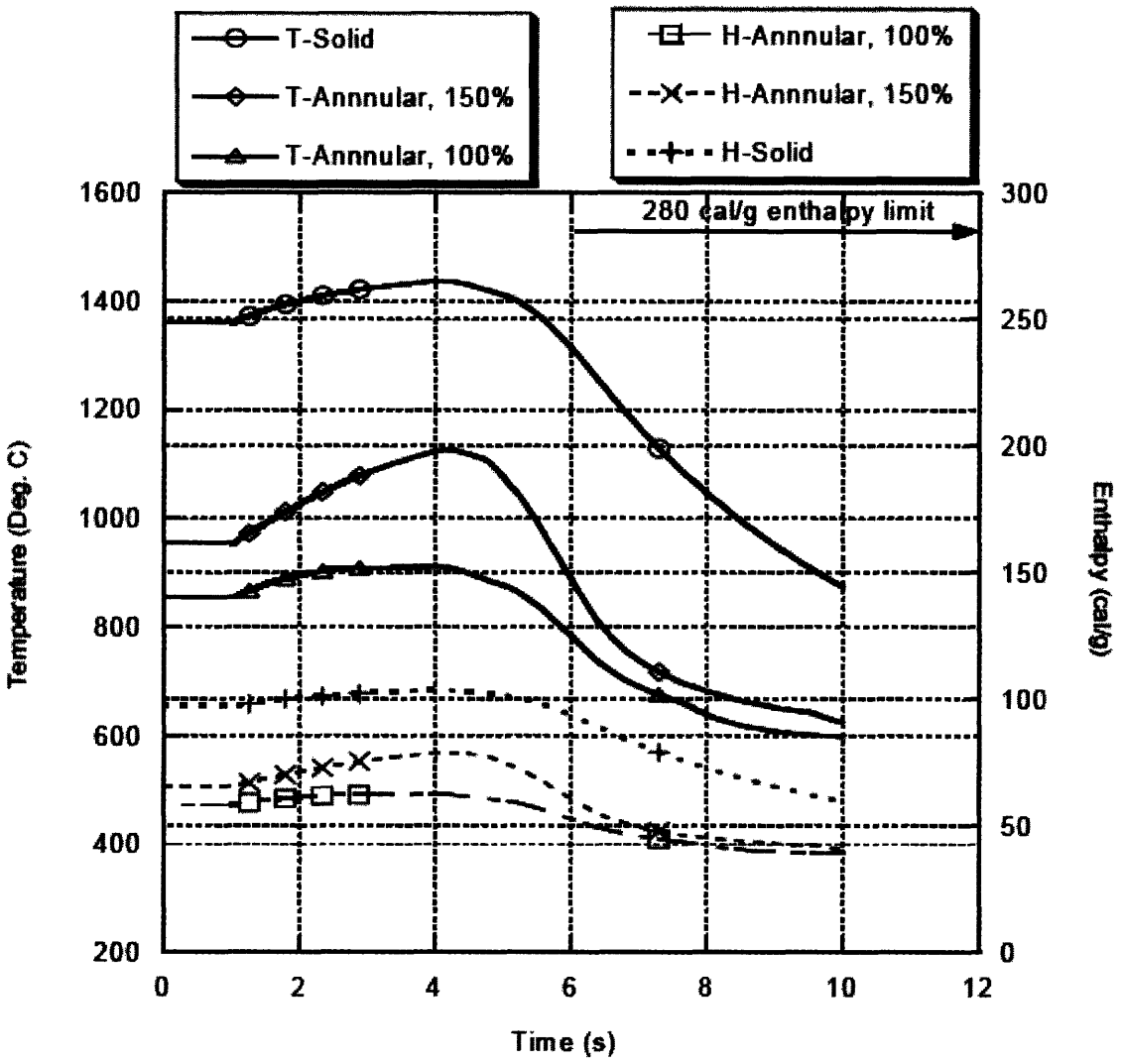

Figure 1-8 Average fuel temperatures and enthalpies for REA at HFP (from Kazimi et al, 2006)

Figure 1-8 shows the average temperature and enthalpy in the fuel. Notice that the 280 cal/g enthalpy limit is around 1550°C. The trend is the same as for the maximum temperature. The energy deposited in the fuel rod (calories/gram) can be calculated from the average fuel temperature. Because the average fuel temperatures for the annular rods are significantly less than that for solid rods, and the margin to enthalpy limit of 280 calories/gram is much larger for the annular fuel, it can be concluded that the annular fuel will perform better during REA than the solid fuel. Moreover, the large margin to energy deposition limits for annular fuel shows

better potential to meet the reduced energy deposition limit for high burnup fuels, once this limit is established [Kazimi et al, 2006].

As shown in Table 1-10, the ejected rod worths for HZP are considerably higher than those for HFP. On the other hand, the initial fuel temperatures would be significantly lower. The high neutron flux setpoint is also lowered at HZP (25% compared to 109%). Generally, HZP initial conditions provide a more limiting calculation for the rod ejection event. However, considering the results shown in Figures 1-7 and 1-8 for the HFP case and the data in Table 1-10 (lower rod worths, higher Doppler coefficients for annular rods), the results for HZP should be very similar to those for HFP, i.e., the annular rod performance, even at 50% higher power, would be better than that of solid rods [Kazimi et al, 2006].

1.4. Corrosion and Crud Buildup

Corrosion, for nuclear purposes, can be defined as the surface deterioration of a metal in the presence of water. In PWRs, it is of most concern for the Zircalloy cladding that is surrounded by high temperature, flowing coolant while exposed to high heat flux. The oxidizing environment in the core causes the metals to lose electrons and combine with oxygen ions from the water to form surface deposits (ZrO_2). This oxide layer on the cladding surface increases in thickness as the exposure time increases. In the annular fuel study, oxide thickness at end of cycle for a PWR using Zircalloy-4 was assumed to be 50μm with a thermal conductivity of 2 W/mK [Kazimi et al., 2006].

In addition to the ZrO_2 formed from the cladding, rust particles from other sources of the reactor such as piping, pumps, and other components also collect on the cladding surface. Altogether, this conglomerate is known as "crud" and can compose of many different oxides and exist in various sub-layers. Cladding surface scrapes from PWRs studied by EPRI in the 1990s have at times revealed at least 3 layers of different compositions which include nickel ferrite, nickel oxide, zirconium dioxide, and bonaccordite and at other times just a simple layer of nickel ferrite [Deshon et al., 2007]. It is also known that nickel metal deposits on fuel rods but it cannot always be measured due to its extreme solubility. The thickness of the combined crud and corrosion layer at end of cycle is typically less than 30μm but can reach 100μm locally in high duty units. Due to the unpredictability of crud composition and the difficulty of making such measurements, it has been suggested that the thermal conductivity of crud be on the order of 1 W/mK [Deshon et al., 2007].

1.5. Fuel Cycle Modeling

CAFCA (Code for Advanced Fuel Cycles Assessment) is a nuclear fuel cycle system model that has been in development at MIT for the last few years. The latest version, CAFCA SD (System Dynamics), developed by [Busquim e Silva, 2008], implements the code in a system dynamics environment using the program Vensim, developed by Ventana Systems, Inc. This section serves only as a brief overview of CAFCA based on more detailed descriptions from [Busquim e Silva, 2008].

System dynamics is a methodology for modeling and understanding the behavior of complex "feedback systems" over time. The term "feedback systems" refers to a situation where X affects Y, and Y in turn affects X through a chain of causes and effects. The technique is based on nonlinear dynamics and control theories where the goal is to identify system variables which shape the patterns of behavior. A computer model (in this case, CAFCA SD) is built to simulate the behavior of the system and used to test policies designed to change the system's behavior as desired.

CAFCA SD models the nuclear fuel cycle as a high level structure diagram (HLSD) and as a structure-policy diagram (SPD). The HLSD provides an overview of the model and the interconnections among its blocks without showing all of the details for the computer simulation while the SPD shows the details of the decision rules applied to the system functions. Figures 1-9 and 1-10 show examples of an HLSD and SPD, respectively, used in CAFCA SD. For details on all of the HLSDs and SPDs modeled in CAFCA SD, please consult [Busquim e Silva, 2008].

The code is driven by the main input of nuclear growth rate and LWRs are constructed at every time step based on this demand. In addition, advanced transuranics (TRU) recycling technologies such as Fast Breeder Reactors (FBR) with conversion ratio 1.0, Actinide Burner Reactors (ABR) with conversion ratio 0.0, and COmbined Non-Fertile and UO_2 Fuel (CONFU)

are constructed based on the amount of TRUs available for recycling. All three recycling technologies can occur by themselves or simultaneously. The mass transfer and accumulation of uranium and TRUs are traced throughout the entire cycle. Ultimately, an economic model calculates the various costs of the fuel cycle to determine the total cost of electricity.

1.5.1. High Level Structure Diagram

The high level structure diagram in Figure 1-9 shows the mass flow through the nuclear fuel cycle with all three advanced recycling technologies present. The front-end processes are represented by white blocks; the physical plants (reactors, separation plants, reprocessing plants) are represented by gray blocks; fresh fuel types are represented by green blocks; and spent fuels/TRUs in storage are represented by cylinders.

As seen in Figure 1-9, the front-end processes are mining, milling, conversion, enrichment, and fuel fabrication. Through these stages, the amount of uranium ore (U) mined is calculated based on thermal and fast reactor demand, the amount of "yellowcake" (U_3O_8) processed from ore is calculated after the milling stage, the U_3O_8 goes through the conversion stage to produce uranium hexafluoride (UF_6), the UF_6 from mined uranium and recycled uranium (from separation plants) is then enriched, and finally the enriched uranium is fabricated into traditional or CONFU fuel and the natural or depleted uranium is sent to self-sustaining FBRs. In addition, mass losses at each front-end stage are calculated and sent to a radioactive waste disposal site.

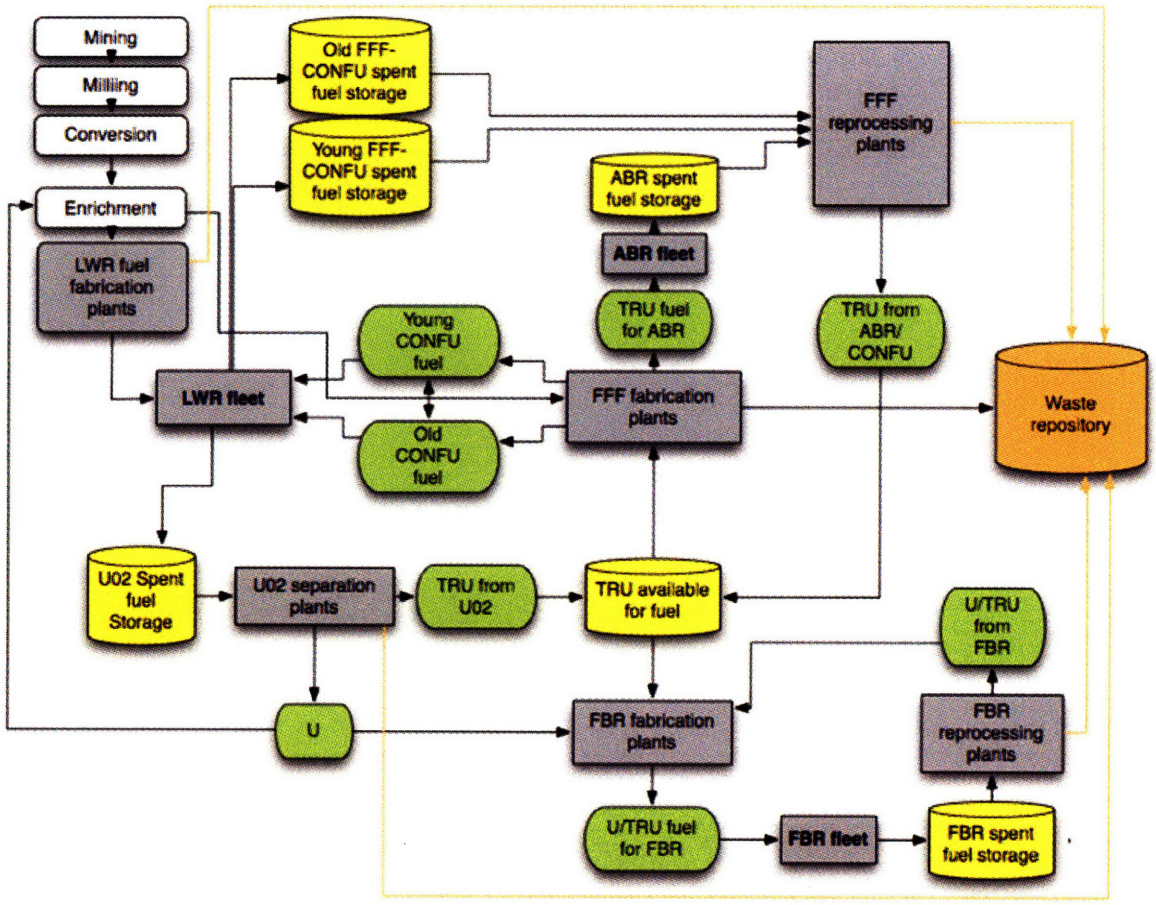

Figure 1-9 High level structure diagram of the nuclear fuel cycle (from Guérin, 2008)

Three options can be used either by themselves or simultaneously for recycling and burning of actinides: 1.) the CONFU assembly for LWRs 2.) the ABR fast burner reactor and 3.) the self-sustaining fast reactor, FBR. For the LWR-CONFU scenario, the LWR fleet is fed with UO_2 batches from traditional fabrication fuel plants or with young and old CONFU batches from Fertile-Free Fuel (FFF) fabrication plants. The spent UO_2 fuel from the LWRs is sent to cooling storage for 6 years and then to the UO_2 interim storage facility. The spent young and old CONFU batches are sent, after 6 and 18 years in cooling storage, respectively, to the CONFU interim storage facility. Then the spent fuel from the UO_2 interim storage is sent to separation plants where TRUs are separated from the uranium and losses are sent to the waste repository. The

TRUs available for fuel fabrication are then used by the FFF or FBR fabrication plants. FFF is used to produce young and old CONFU batches as well as ABR fuel. Spent ABR fuel is sent, after 6 years in cooling storage, to the ABR interim storage repository. After a short cooling time, spent ABR and CONFU fuels are then sent to the FFF reprocessing plants with reprocessing losses going to the waste repository. The reprocessed TRU is sent to the same place where the TRU from UO_2 fuel was sent to await fabrication. To produce fuel for the FBR, recycled uranium from UO_2 separation plants is mixed with TRUs to fabricate the U/TRU FBR fuel. After burning in FBRs and cooled in storage for 6 years, the FBR spent fuel is sent to the FBR interim storage facility. At the FBR reprocessing plants, U/TRU is separated from fission products and sent back to FBR fuel fabrication plants. During all processes, the mass losses are all sent to the radioactive waste disposal site [Busquim e Silva, 2008].

1.5.2. Structure-Policy Diagrams

The high level structure diagram in 1-9 is also a set of connected system blocks. The system-output of one block is the system-input for another connected block. There are many user-outputs which can be accessed at any time (i.e. SWU requirements, number of advanced fuel facilities, uranium needs, TRU inventory at interim storage, mass loading factor, incinerated TRU, fuel cycle cost, cost of electricity et cetera). Therefore the model is a chain of coupled structure-policy diagrams with feedback interactions among the blocks as shown in Figure 1-10. Each structure-policy diagram is a single-input single-output system that consists of two subsystems: system-structure and policy-structure. The first subsystem describes the structure while the second defines the decision rules. The complete nuclear fuel cycle is simulated by implementing structure-policy diagrams that relate system-inputs and system-outputs throughout the system's variables. The fleet of reactors and facilities are modeled as system-structure

diagrams while the policy-structure sets decision rules based on the state of the system. As soon as rules are applied, the state of the system changes, information about the new state is fed back to the system-structure. Then new decision rules are applied, closing the loop inside the block. This behavior occurs at every time step of the simulation.

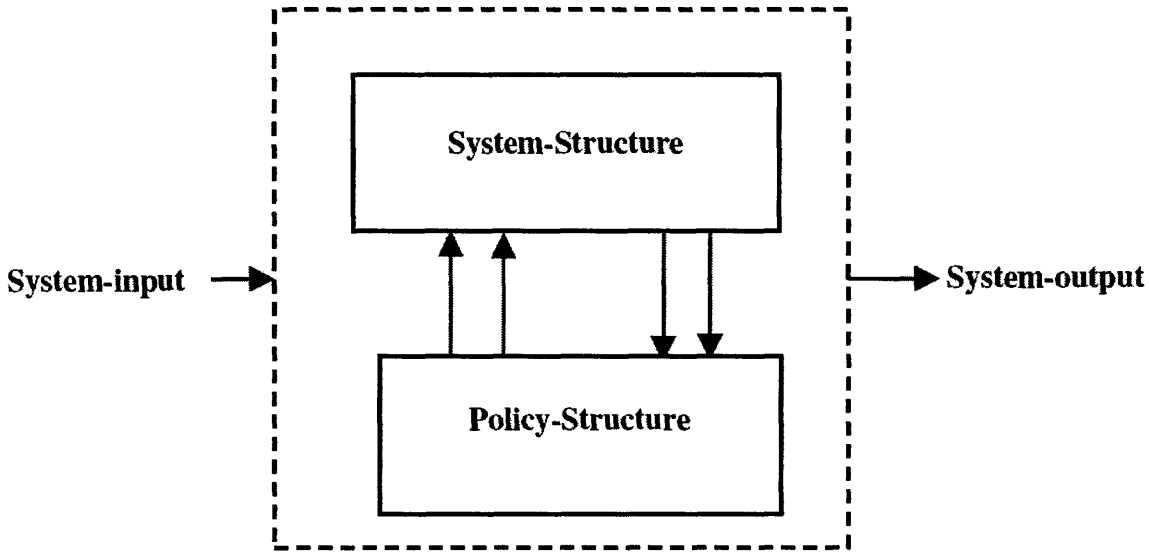

Figure 1-10 Structure-policy diagram of the system (from Busquim e Silva, 2008)

For example, the LWR SPD shown in Figure 1-11 is a power-demand driven system. The system-input is the expected nuclear demand growth rate. The forecasted LWR fleet required to fulfill the electricity demand is calculated based on the system-input. The number of reactors under commercial operation is represented by one stock, or state variable, and is increased by the construction rate and decreased by the decommissioning rate. The decommissioning rate changes only due to the end of a reactor's lifetime. LWRs are constructed in integer numbers based on preset constraints in the decision rules such as the difference between the forecasted LWR fleet and actual LWR fleet.

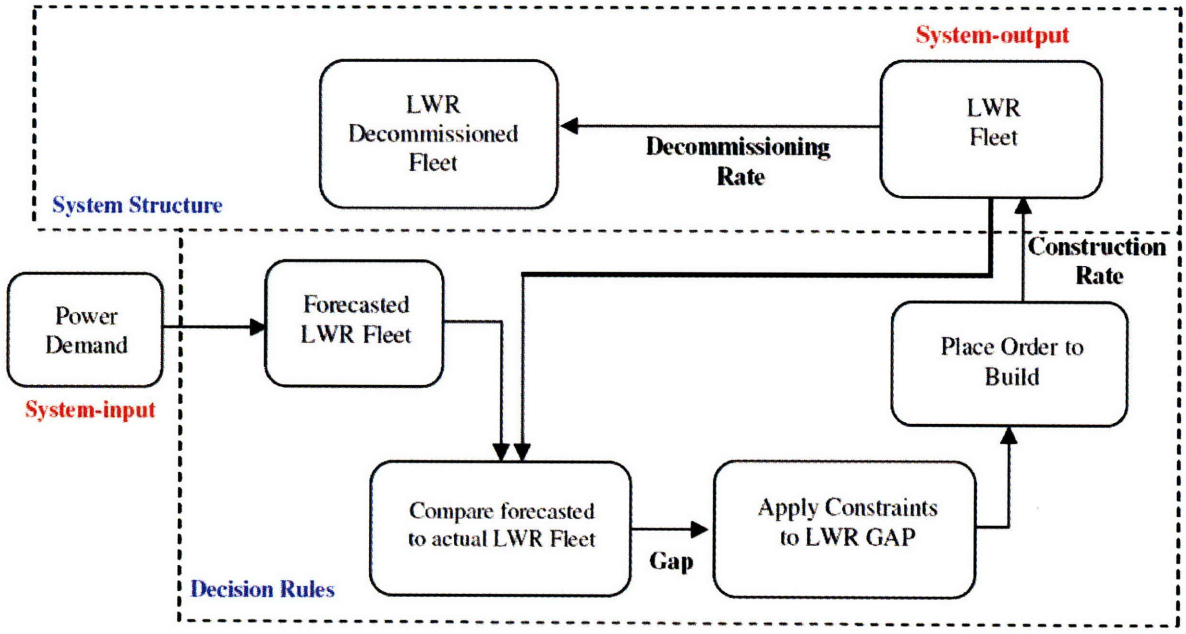

Figure 1-11 Structure-policy diagram for light water reactor construction/decommissioning (from Busquim e Silva, 2008)

The LWR SPD takes into account the age distribution of LWRs under commercial operation by modeling the reactors as 60 separate coflows. Coflows are system structures that track attributes of various items as they travel through the stock and flow structures. It is assumed that all items in each coflow are perfectly mixed, i.e. if there are 3 reactors in the 25 year old LWR coflow structure, it does not matter which one is selected for an uprate as long as the uprate demand is met. The detailed equations used in the structure-policy diagrams of the CAFCA SD model are described in [Busquim e Silva, 2008].

1.6. Objectives and Scope

Shutdown Margin

Although next generation nuclear reactors using IXAF may solve the SDM issue with different fundamental core designs, the possibility of implementing this fuel in current PWRs for power uprates up to 150% is an attractive and lucrative option for utilities. Thus, one of the objectives of this study was to find ways to modify the design of the already thermally-optimized XU and XF cores in order to maintain the 1.3%$\Delta\rho$ SDM during the entire cycle.

Different core modification approaches will be analyzed using the same SDM calculation methods done in the initial design. This consists of using the core analysis code package, CMS, for the SDM calculation and Los Alamos's Monte Carlo N-Particle (MCNP) version 4-C transport code for modeling as well as benchmarking the core modifications.

Inner Channel Thermal Hydraulic Issues

Due to the introduction of the inner channel for annular fuel, crud and corrosion buildup become an even greater concern for thermal performance and safety. The effect on the inner channel MDNBR of the hot rod due to crud buildup and zirconium corrosion will be analyzed using an annular core modeled in VIPRE-01. It will be assessed whether typical crud and corrosion thicknesses at end of cycle will result in inadequate thermal performance from the annular fuel. In addition, a partial blockage of the hot rod's inner channel entrance will be modeled to determine the maximum entrance blockage the fuel can withstand.

High Burnup Fuel Cycle

The impact of LWRs using IXAF on the once through and closed fuel cycles will be analyzed by implementing annular fuel into CAFCA SD. Specifically, the change in uranium consumption, TRU accumulation, and overall change in cost of electricity will be calculated through various scenarios of annular fuel introduction.

The descriptions of the core analysis codes used (CMS, MCNP, VIPRE-01, MCODE) are found in the Appendix.

2. Increasing Shutdown Margin

Without compromising the fuel's high burnup and high power density (two main draws of using IXAF), the desired approach for increasing the SDM was to increase the total reactivity worth of the control rods. Potential options include: (1) a higher worth control material; (2) more efficient control rod shapes; (3) higher number of control rods; and (4) reduced reload enrichment by increasing the number of reload fuel assembles. It should be noted that the Westinghouse PWR control rod design has been established with few major changes in the past 30 years and that any changes to the design will require additional cost to existing utilities. The annular fuel assembly design requires a different control rod assembly design but the overall number of control rod assemblies remains at 57 for the entire core which avoids redesigning of the reactor vessel head.

Options 1 and 2 require modifying only the control rod assemblies which will be redesigned anyway to accommodate the fewer control rods in the annular fuel assemblies. Although option 3 can be done by modifying the control rod assemblies with extended rodlets (similar to Combustion Engineering PWRs), it is a much more expensive modification than simply changing the control rod composition or shape. Option 4 would require an overhaul of the entire core design in order to maintain the high power density and 18-month cycle. In consideration of the minimum economic impact, only options 1 and 2 were pursued in this study.

2.1. Control Rod Material Modification

The first approach towards increasing the overall control rod worth for assemblies using annular fuel was changing the control rod material composition to one that had higher overall thermal neutron capture cross sections. This meant changing the standard Westinghouse Ag-In-Cd (AIC) control rods to one that is more thermally "black" to compensate for the reduction of control rods per assembly and increased power when using IXAF. To compare the reactivity worths of various control rod materials, a single annular fuel assembly was modeled in CASMO-4 with AIC, boron carbide (B_4C), and hafnium control rods. Figure 2-1 shows the reactivity worth of each control rod material in an XU assembly (8.7 w/o enrichment, poison-free) as a function of burnup. B_4C is seen to be able to provide approximately 40-50% higher rod worth for a single assembly compared to the other control materials. This provides a promising control rod material that can offset the increased reactivity, and this was selected for further analysis.

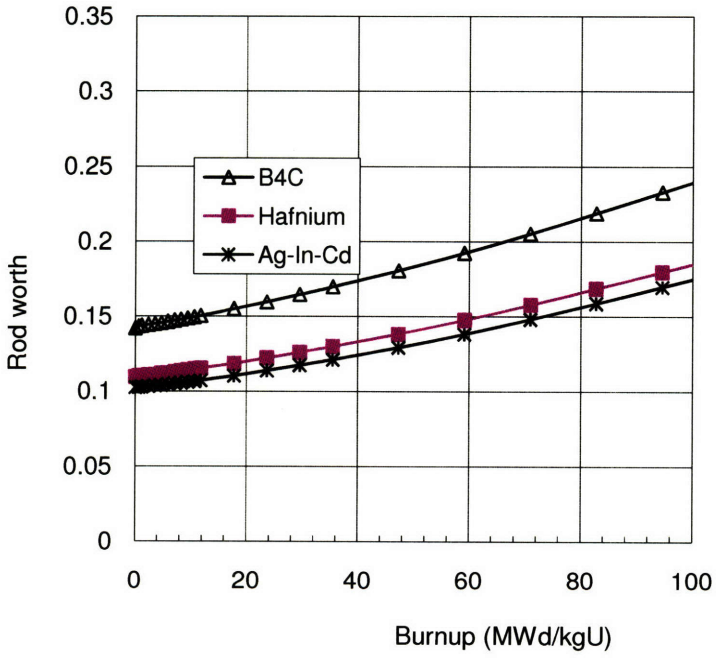

Figure 2-1 Control rod worth of various materials vs. burnup in XU assembly (8.7 w/o, no Gd)

2.1.1. Modeling Methodology

The SDM was calculated using all three codes of the CMS code package (CASMO-4, TABLES-3, and SIMULATE-3). It is a license-level code package widely used by industry for steady-state core analysis. The three codes are run in series: individual assemblies are modeled in CASMO-4 and cross sections and neutronic data is provided for various conditions and burnups, TABLES-3 converts the cross sections and other data into a binary library, and SIMULATE-3 uses the data from the library to calculate neutronic parameters of the entire core. The advantages of using the CMS code package are the credibility of the results for LWRs and the shorter computational time for burnup calculations compared to probabilistic codes like MCNP-4C. A more detailed explanation of the code suite can be found in Appendix B.

2.1.1.1. Uprated Core Model Description

The IXAF-fueled, 150% power core designed by *Xu et al.*, consists of the same amount of reload fuel assemblies (72) as the WS case and keeps a 3-batch fuel management scheme. As shown in Table 2-1, the fresh fuel has 24 assemblies at 8.1 w/o enrichment and 48 at 9.1 w/o with various gadolinia (Gd_2O_3) burnable poison loadings. The burnable poison loading is extended from 120 inches, as in the WS case, to the entire center fuel segment, i.e. 132 inches out of the 144 inch active fuel region. The assembly pin layout for various burnable poison loadings and the core loading pattern for the XU core are shown in Figures 2-2 and 2-3, respectively. It should be noted that the discharged fuel has an average burnup that is almost 70% higher than the current WS case. This is partly due to the 50% higher core power density, and partly due to the ~10% reduced fuel volume in the core. More details on the WS and XF equilibrium cores can be found in [Xu et al., 2004].

Table 2-1 Assembly description of the IXAF-fueled, 150%-power PWR core (from Xu et al., 2004)

Fuel ID	Type	Enrich (w/o)*	Number of Gd rods	Gd loading in Gd rods** (wt%)	Number of assm.	Total U loading (kg)	Exposure at EOC (MWd/kg)
0L2410	Fresh	8.1	24	10.0	4	1677.62	36.666
0L2880	Fresh	8.1	28	8.0	12	5038.15	38.717
0L3280	Fresh	8.1	32	8.0	8	3350.58	39.000
0H1660	Fresh	9.0	16	6.0	4	1695.88	32.281
0H2460	Fresh	9.0	24	6.0	8	3379.43	34.228
0H2880	Fresh	9.0	28	8.0	28	11756.55	38.509
0H4060	Fresh	9.0	40	6.0	8	3354.13	37.726
1L2410	Once	8.1	24	10.0	4	1677.62	67.492
1L2880	Once	8.1	28	8.0	12	5038.15	73.454
1L3280	Once	8.1	32	8.0	8	3350.58	72.077
1H1660	Once	9.0	16	6.0	4	1695.88	69.065
1H2460	Once	9.0	24	6.0	8	3379.43	69.844
1H2880	Once	9.0	28	8.0	28	11756.55	65.573
1H4060	Once	9.0	40	6.0	8	3354.13	56.909
2L2410	Twice	8.1	24	10.0	1	419.4	94.287
2H1660	Twice	9.0	16	6.0	4	1695.88	80.671
2H2460	Twice	9.0	24	6.0	8	3379.43	81.522
2H2880	Twice	9.0	28	8.0	28	11756.55	91.616
2H4060	Twice	9.0	40	6.0	8	3354.13	88.531
TOTAL					193	81110.03	

* The enrichment refers to center enrichment (not including axial blankets)

** The Gd loading refers to the weight percentage of Gd2O3 in UO2/Gd2O3. Also note that the burnable absorber active length is 132 inches centered in the active core.

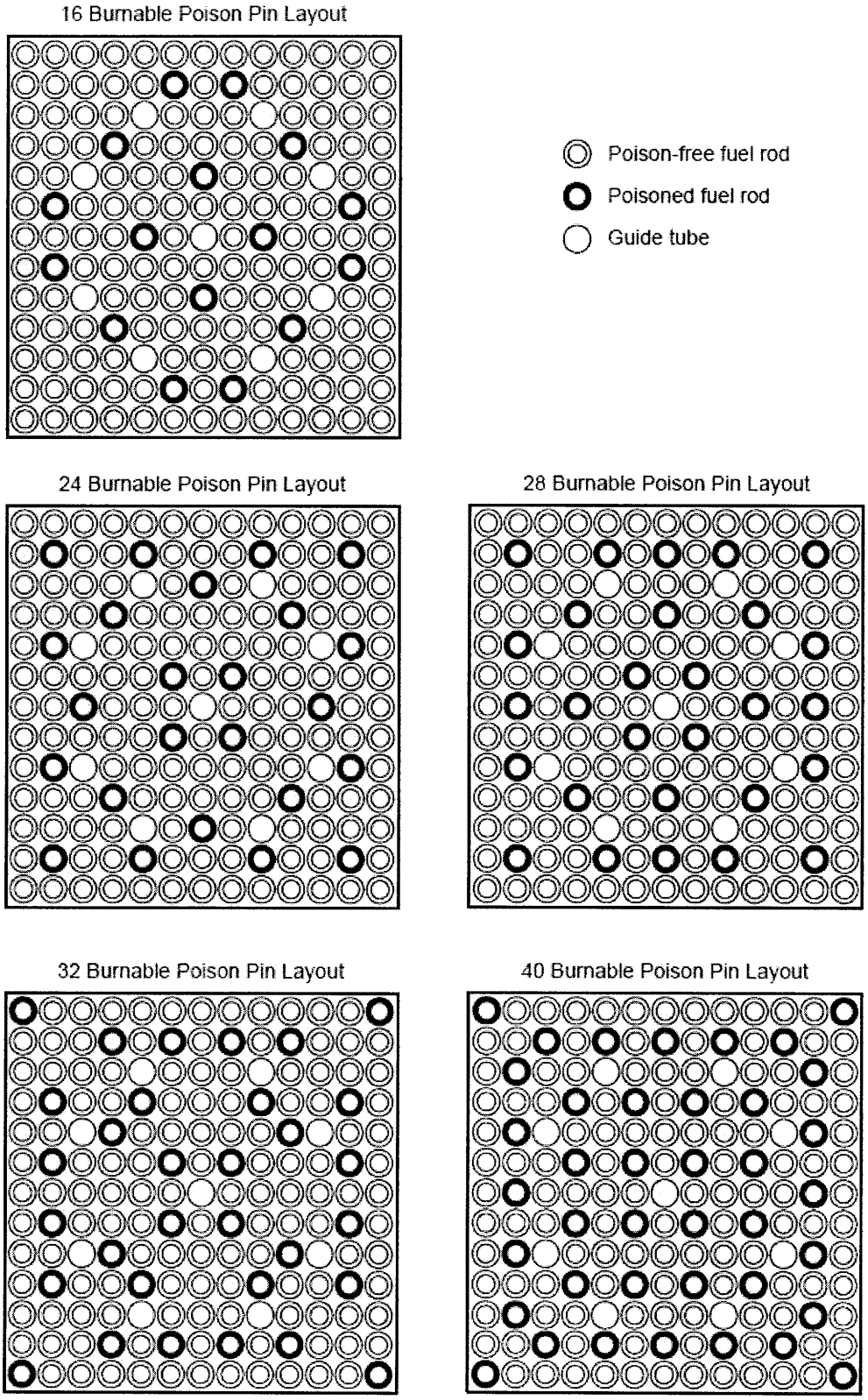

Figure 2-2 Assembly fuel pin layouts for the IXAF-fueled, 150%-power PWR core (from Xu et al., 2004)

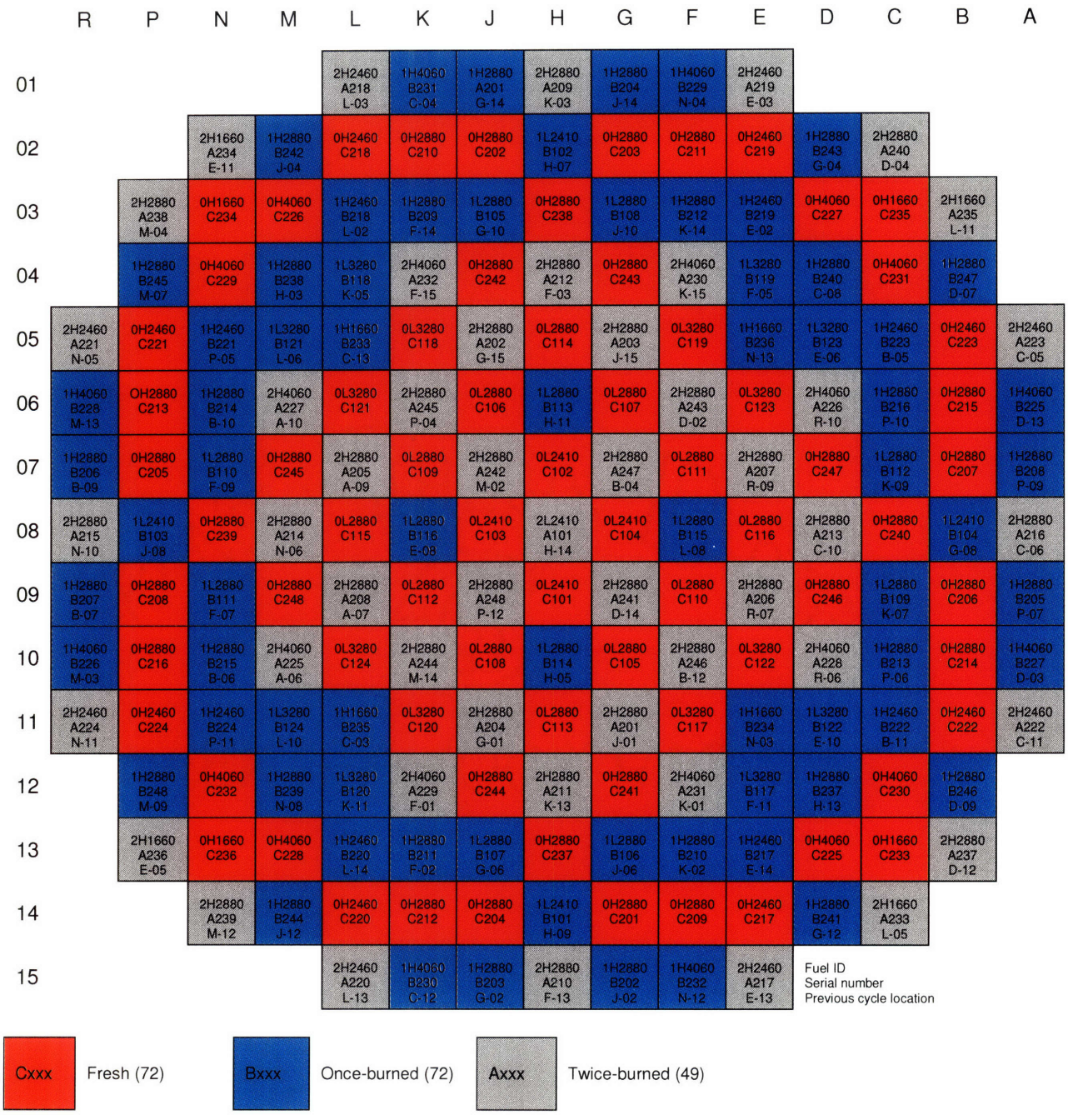

Figure 2-3 Core loading pattern for the IXAF-fueled, 150%-power PWR core

2.1.1.2. CASMO-4 Annular Fuel Adjustment

Since the CMS code package was developed and extensively benchmarked for existing LWR design and operation, novel features such as annular-shaped fuel can run into modeling issues. Benchmark cases between CASMO-4 and MCODE-1.0 made by *Xu et al.* to ensure the accuracy of the CMS code suite's results [Xu et al., 2004]. MCODE-1.0 is a code developed at MIT that couples the steady-state probabilistic code MCNP-4C with the depletion code ORIGEN-2.2 which was used for calculating k-infinite at various burnups [Xu et al., 2006]. As can be seen in Figure 2-4, the eigenvalue difference between CASMO and MCODE for the 17x17 solid fuel assembly is virtually constant and independent of burnup. This can be attributed to the difference in cross section libraries used by each code. However, for poison-free annular fuel, CASMO-4 initially over predicts the eigenvalue of the transport equation for low burnups and then under predicts it for higher burnups.

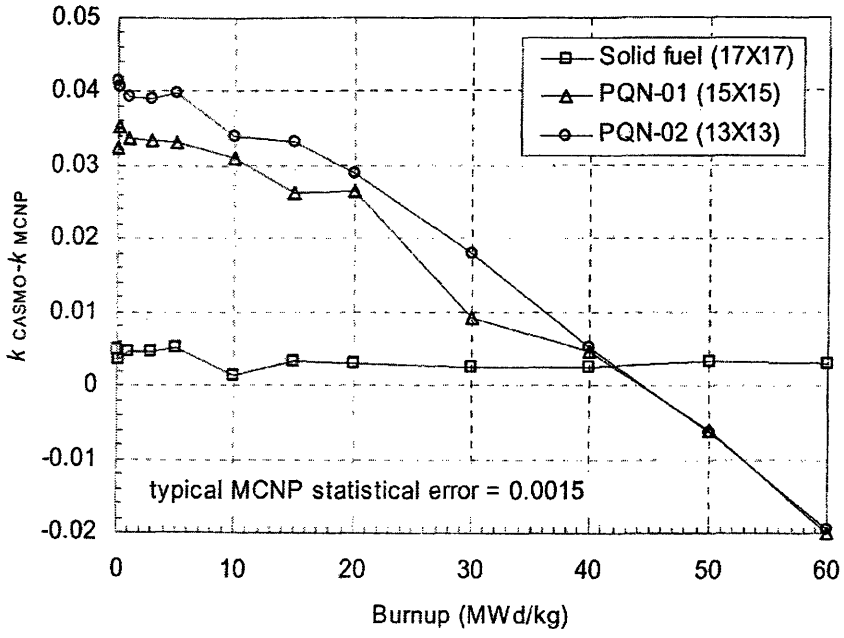

Figure 2-4 Eigenvalue differences between CASMO-4 and MCODE-1.0 for poison-free solid and annular fuel assemblies (from Xu et al., 2004])

After much detailed analysis and consulting with Studsvik personnel, it was determined that CASMO-4 did not take into account the epithermal U-238 captures that occur on the inner surface of the annular fuel, which should be present due to the introduction of water in the inner channel. This underestimation of U-238 capture initially results in a higher thermal flux, which causes an over prediction of the multiplication factor, but as burnup increases, lower than expected fissile Pu-239 levels resulting from U-238 capture reduce the multiplication factor, leading to the decreasing eigenvalue difference [Xu et al., 2004].

Since MIT did not have access to CASMO-4's source code, a MCNP-based correction factor developed by *Xu et al.* was implemented to account for the annular fuel modeling deficiency. Specifically, the U-238 levels were artificially increased in the CASMO assembly models to match the absorption levels calculated in an MCNP model. It was found that for annular fuel assemblies without burnable poison, the CASMO results closely resembled those from MCNP when the U-238 atom density was virtually increased by 20% and for annular fuel assemblies with poison, 30%. This method was adopted for all the CASMO runs to provide more accurate cross sectional and neutronic data for SIMULATE [Xu et al., 2004].

2.1.1.3. Cross Section Preparations

CASMO-4 models the individual assemblies with various properties (enrichment, burnable poison content) that make up the core. For the case of 50% uprated annular fuel, the 7 fresh assembly types used in the CASMO-4 calculations are indicated in Table 2-1. For each of these CASMO-4 assembly models, the following depletion and coefficient calculation cases were made for various simulated core conditions [Xu et al., 2004]:

- Base burnup case under nominal core average conditions with instantaneous branches;
- Low fuel temperature depletion with branches to nominal;
- Low moderator temperature depletion with branches to nominal;
- Low boron concentration depletion with branches to nominal;
- High fuel temperature depletion with branches to nominal;
- High moderator temperature depletion with branches to nominal;
- High boron concentration depletion with branches to nominal.

This realistic few-group preparation procedure produced 3-dimensional data tables containing cross sections and other neutronic data for each fuel segment as a function of burnup. This enables SIMULATE-3 to accurately model the entire core since three-dimensional core conditions vary considerably from location to location. TABLES-3 converts the data from the CASMO-4 assembly models into a master binary library that is readable by SIMULATE-3.

2.1.1.4. Whole Core Analysis

SIMULATE-3 calculates 3-D whole core steady-state parameters by reading the cross sectional and neutronic data from TABLES-3. An equilibrium core model was used to calculate the reactivities at BOC, MOC, and EOC in Equation 1.2 to solve the SDM. To achieve an equilibrium model, the first 9 cycles after the initial fresh core loading must be simulated by following the 3-batch refueling scheme indicated in Figure 2-3. SIMULATE-3 runs the first cycle and produces a restart file as input for the second cycle which in turn produces a restart file for the third cycle and so on until the 10^{th} or equilibrium cycle is reached. Using the equilibrium cycle restart file, commands are given in SIMULATE-3 to calculate the total control rod worth, reactivity of the highest worth control rod, the reactivity insertion allowance, and the reactivity

insertion from HFP to HZP. The SDM is then calculated by inserting these values in Equation 1.2. Figure 2-5 summarizes how the CMS code package was used for the neutronic calculations:

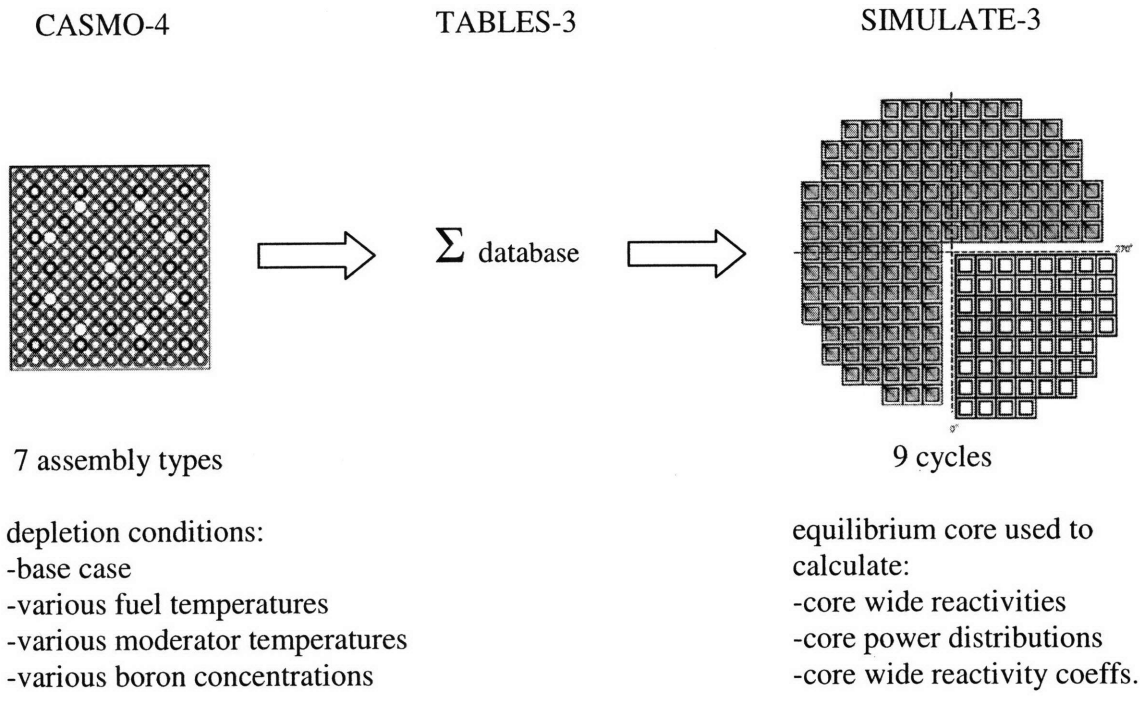

Figure 2-5 Schematic diagram of how the CMS code package is used to calculate the SDM

To investigate the effects of using B_4C control rods, the control rod material in the 7 CASMO fresh assembly files was changed from AIC to B_4C (with natural boron composition) and the entire aforementioned process represented by Figure 2-5 was rerun. Table 2-2 shows the differences between the two control rod types.

Table 2-2 Ag-In-Cd and B_4C control rod properties

Material	**Ag-In-Cd**	**B_4C**
Shape	cylindrical	
CR diameter	0.5751 cm	
CR structure inner diameter	0.5789 cm	
CR structure thickness	0.047 cm	
Guide tube inner diameter	0.711 cm	
Guide tube thickness	0.0575 cm	
Density	10.16 g/cm^3	1.76 g/cm^3
Composition	80 wt% Ag	21.74 wt% C
	15 wt% In	14.32 wt% B10
	5 wt% Cd	63.94 wt% B11

2.1.2. Results

Using the default B_4C composition for the control rods in CASMO-4, the reactivities in Equation 1.2 and SDM were calculated and shown in Table 2-3:

Table 2-3 SDM results for IXAF-fueled, 18-month cycle core at 150% power using natural boron B_4C control rods

Cycle Stage	BOC	MOC	EOC
ρ_{allCRD} [pcm]	4978	4714	4632
ρ_{maxCRD} [pcm]	78	69	80
Total Negative Reactivity [pcm]	4410	4181	4097
$\rho_{HFPtoHZP}$ [pcm]	1614	1692	2795
ρ_{IA} [pcm]	250	376	160
Total Positive Reactivity [pcm]	1863	2068	2954
SDM [pcm]	2546	2113	1142

Compared to Table 1-5, the SDM improved significantly due to the increased worth of the B_4C control rods but still did not meet the 1.3% $\Delta\rho$ (1300 pcm) at EOC. Upon closer analysis, the boron in the B_4C material in CASMO-4 is natural boron (ID 5000) which consists of 18.3 w/o B-10 and 81.7 w/o B-11 [Edenius et al., 1995]. It should be noted that the thermal cross section of B-10 is approximately 4 orders of magnitude larger than that of B-11 (3840 barns and 5 barns, respectively) [KAERI, 2000]. Thus the enrichment in B-10 in the B_4C control

rods could be tried. This is a very feasible adjustment since companies such as EaglePicher Boron, LLC, now owned by Ceradyne, Inc., offer boron carbide with up to 99% B-10 enrichment [Eaglepicher, 2008].

Modeling enriched boron in CASMO-4 cannot simply be done by replacing the natural boron in the control rod material (ID 5000) with increased levels of B-10 (ID 5010) and corresponding levels of B-11 (ID 5011) since the code only recognizes these as depletable burnable poison materials. Thus, it was suggested by Dr. Zhiwen Xu, one of the authors of the previous work on annular fuel and currently an employee of Studsvik, to simply increase the overall natural boron weight percent (ID 5000) since the small cross section of B-11 will have negligible effect on the results. Note that B_4C is 78.26 w/o natural boron and 21.74 w/o carbon.

A value of 25 w/o B-10 was set by changing the natural boron weight percent to the new natural boron weight percent found using Equation 2.1:

$$N_{B(new)} = N_{B(default)} * \left(\frac{E_{new}}{E_{default}} \right) \tag{2.1}$$

Where $N_{B(new)}$ = new natural boron weight percent (of B_4C)

$N_{B(default)}$ = default natural boron weight percent (of B_4C)

E_{new} = desired B-10 weight percent (of boron)

$E_{default}$ = default B-10 weight percent or 18.3 w/o (of boron)

The 25 w/o enriched B_4C resulted in the values in Table 2-4:

Table 2-4 SDM results for IXAF-fueled, 18-month cycle core at 150% power using 25% B-10 enriched B_4C control rods

Cycle Stage	BOC	MOC	EOC
ρ_{allCRD} [pcm]	5533	5052	4936
ρ_{maxCRD} [pcm]	81	73	84
Total Negative Reactivity [pcm]	4907	4481	4367
$\rho_{HFPtoHZP}$ [pcm]	1614	1692	2795
ρ_{IA} [pcm]	253	382	162
Total Positive Reactivity [pcm]	1866	2074	2956
SDM [pcm]	3040	2407	1411

Thus, the control rod worth increased by a sufficient amount to bring the SDM at EOC over the 1.3% $\Delta\rho$ minimum.

2.1.3. Rod Ejection Accident Analysis

For completeness, the REA analysis described in Section 1.3.5 must be revisited since the new control rod design for the XU core has higher worth. The same simplified approach was used in SIMULATE-3 to model the HFP case to determine the values in Table 2-5 below. The values from the XU case using Ag-In-Cd control rods calculated from the previous study are also included for comparison. Using the enriched B_4C control rods, the maximum rod worth and peaking factors increased slightly for the HFP case. The Doppler coefficients before the REA remained the same since the only difference between the two cores is the small amount of control rod worth difference between the partially inserted control rods. By realizing the large temperature margins shown in Figures 1-7 and 1-8, it can be assumed that the slight increases in rod worth and peaking are not expected to increase the peak or average fuel temperatures by a considerable amount. This was expected due to the inherently larger thermal margins of internally and externally cooled annular fuel. Thus, using the new control material will not pose a significant negative impact on the annular fuel's response to a REA.

Table 2-5 Post-ejection physics parameters for Ag-In-Cd and enriched B_4C control rods

	XF	XF
Control Rod Material	Ag-In-Cd	B4C
HZP, EOC		
Maximum Rod Worth [pcm]	110.5	163.6
Radial Peaking	2.12	2.291
Total Peaking	5.831	6.179
Doppler Coefficient [pcm/C]	-3.492	-3.492
HFP, EOC		
Maximum Rod Worth	18.1	21.9
Radial Peaking	1.514	1.534
Total Peaking	2.12	2.236
Doppler Coefficient [pcm/C]	-3.168	-3.168

2.2. Control Rod Shape Manipulation

Another control rod modification which could potentially increase the overall worth is changing the rod shape to increase the rod surface area. For this approach, cross-shaped and annular AIC control rods were considered. Since the CMS package was unable to model non-cylindrical control rods, the geometric manipulation was done in MCNP-4C. An annular fuel assembly model was created in MCNP and compared with its CASMO-4 counterpart. After the model was verified, the MCNP assembly was fully rodded with AIC and enriched B_4C cylindrical control rods to determine the necessary increase in rod worth from the shape modifications.

2.2.1. MCNP Model

Extensive benchmark work between CASMO-4 and MCNP-4C had already been done to develop the U-238 correction factor for CASMO. Using the same methodology as [Xu et al., 2004], a poison-free annular fuel assembly model was created and compared with the CASMO-4 model with the artificial U-238 atom density increase of 20%. This was done to create a MCNP model in which the control rod geometry can be changed. The MCNP model produced a slightly different k-infinite from the CASMO-4 model due to modeling inconsistencies with the original MCNP model used to develop the CASMO-4 U-238 adjustment factor by [Xu et al., 2004]. Unfortunately, the original MCNP model used for the benchmark studies in [Xu et al., 2004] were unavailable so there may be modeling discrepancies such as different cross section libraries, atom density calculations, number of neutron cycles and histories, et cetera which account for the difference in k-infinites. Regardless, the results are still in relative agreement with the CASMO model. Table 2-6 shows the model geometries, conditions, and eigenvalues for the unrodded assembly comparison:

Table 2-6 Comparison of CASMO and MCNP assembly models of poison-free annular fuel assembly at 4.95 wt% enrichment

Runs		
Code	CASMO-4	MCNP-4C
Model	Assembly	Assembly
Conditions		
Enrichment	4.95 wt%	4.95 wt%
Fuel Density	10.4 g/cc	10.4 g/cc
Fuel Temp	600K	600K
Clad Temp	N/A	593K
Mod Temp	583.1K	583.1K
Pressure	15.5MPa	15.5MPa
Burnable Poison	no	no
Geometry (cm)		
Inner Clad IR	0.4315	
Inner Clad OR	0.489	
Fuel pellet IR	0.495	
Fuel pellet OR	0.705	
Outer Clad IR	0.711	
Outer Clad OR	0.7685	
CRD ID	0.711	
CRD OD	0.7685	
Pitch	1.651	
Eigenvalues		
k-inf (BOL)	**1.38138**	**1.39093**
S.D.	N/A	0.00096

The worths of the AIC and enriched B_4C control rods were also compared to set the target k-infinite for the shape changes. Using the same geometries from Table 2-6, the eigenvalues were found to be in much better agreement as shown in Table 2-7.

Table 2-7 Comparison between CASMO and MCNP rodded assembly models

CRD material	AIC	B4C (enriched)
CRD shape	Cylindrical	Cylindrical
CRD radius [cm]	0.5751	0.5751
CRD circumference [cm]	3.61	3.61
K-inf (MCNP)	**1.1522**	**1.0845 (target)**
K-inf (CASMO)	**1.1569**	**1.08203**

Since the enriched B_4C has been proven to provide sufficient worth to solve the SDM issue, the k-infinite of the enriched B_4C control rod case run in MCNP was set as the target eigenvalue for the control rod shape modification cases.

2.2.2. Design Constraint

The main constraint of the control rod shape modification is to keep the control material within the control rod structure, indicated in light blue in Figure 2-6. This constraint was set to avoid redesign of the thermally-optimized assembly and allow smooth flow. Therefore, modifying the shape would require reducing the control material volume.

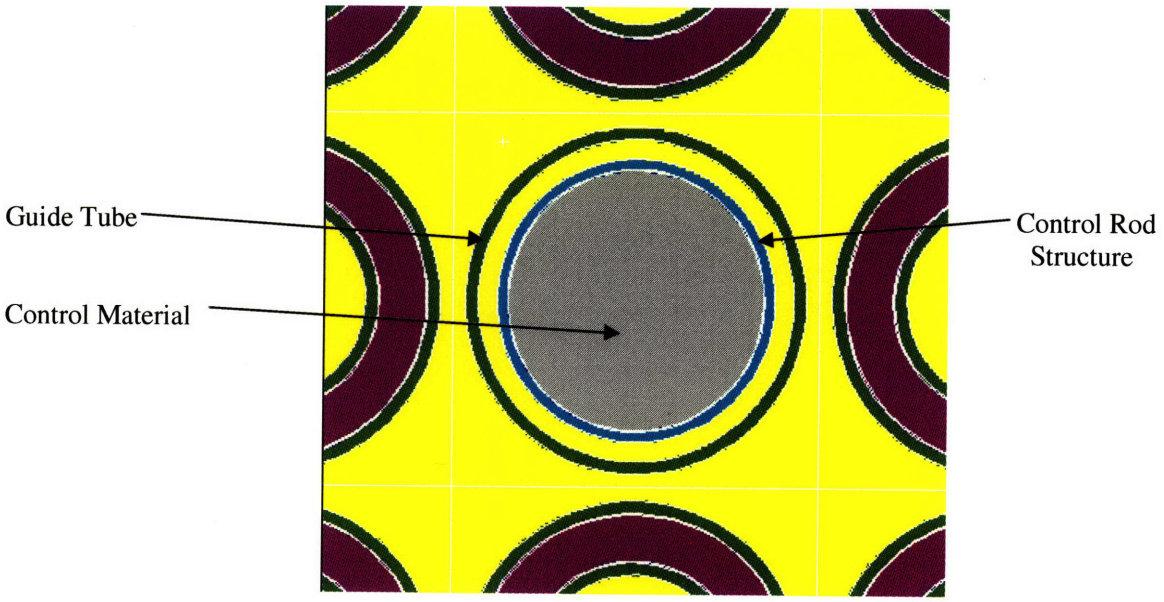

Figure 2-6 Standard control rod design for annular fuel assembly

2.2.3. Cross-Shaped Control Rod

The main idea behind the cross-shaped control rod was to increase the surface area where thermal neutron absorption takes place. To test if the theory worked, four 0.28 cm wedges were introduced to the cylinder (seen in Figure 2-7) to increase the surface area by about 12%.

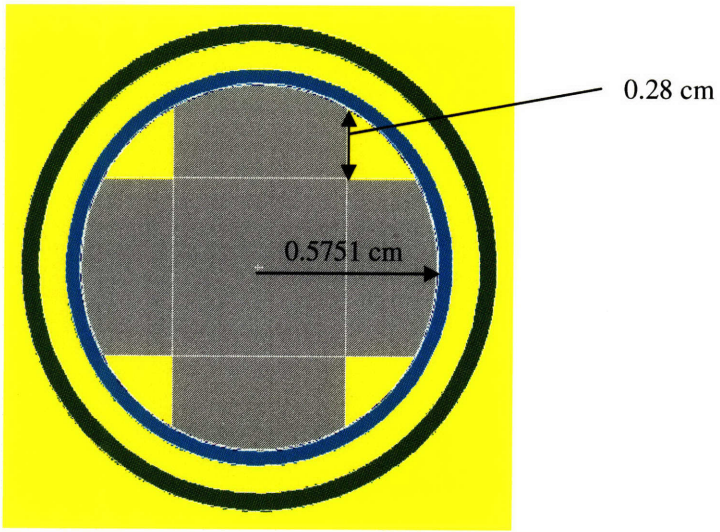

Figure 2-7 Dimensions of cross-shaped AIC control rod

The resulting MNCP calculation for this case resulted in a k-infinite of 1.1600, an increase from 1.1522 of the standard AIC case. It was determined that the decrease in control material volume was a much bigger factor than the increase in surface area and moderator volume in affecting the total control rod worth. Thus, the cross-shaped control rod design was discarded for the purpose of increasing control rod worth.

2.2.4. Annular Control Rods

The intention of the annular control rod design is to introduce an inner channel of coolant which could moderate the fast neutrons and induce their captures on the control rod's inner surface. An inner channel of 0.4 cm diameter was introduced in the standard AIC control rod as shown Figure 2-8. The resulting eigenvalue, 1.17033, was even greater than that of the cross-shaped control rod. This was due to the even greater reduction in control material volume.

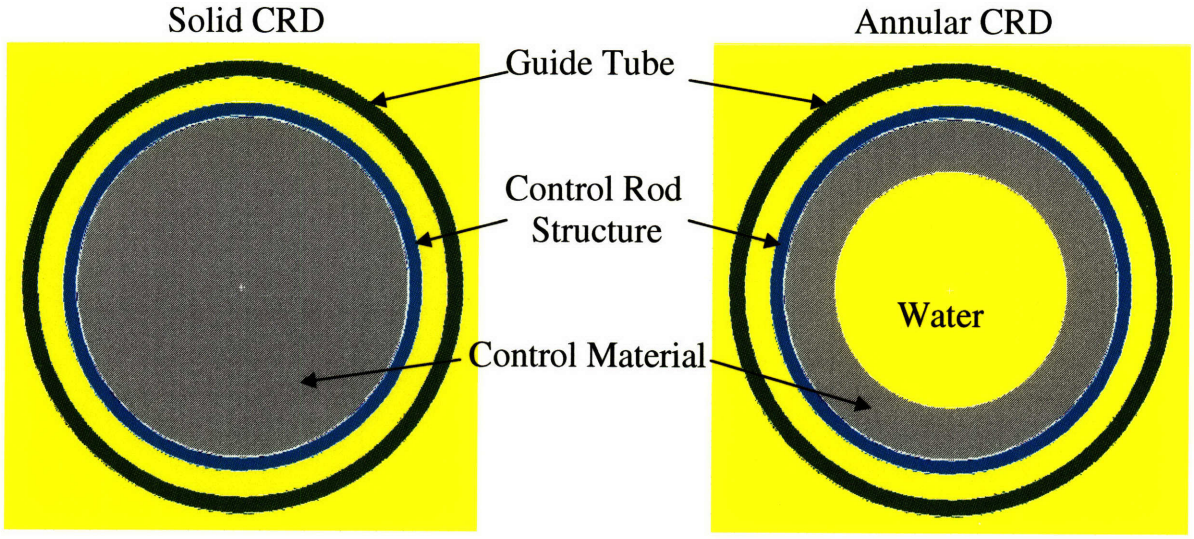

Figure 2-8 Annular and standard solid AIC control rods

To verify that this is the case, Figure 2-9 shows the difference in the total flux profile between the annular and solid control rods. It is apparent that fast neutrons are passing through the annular control rod into the inner channel and some are being captured on the inner surface. However, most of the neutrons simply pass through the entire control rod which results in the higher flux (thermal and fast) in the annular control rod inner channel. This is understandable since the inner channel is less than 1 cm in diameter and the mean free path of fast neutrons is of the same order of magnitude. This confirms that the control material volume remains the main geometric factor determining control rod worth.

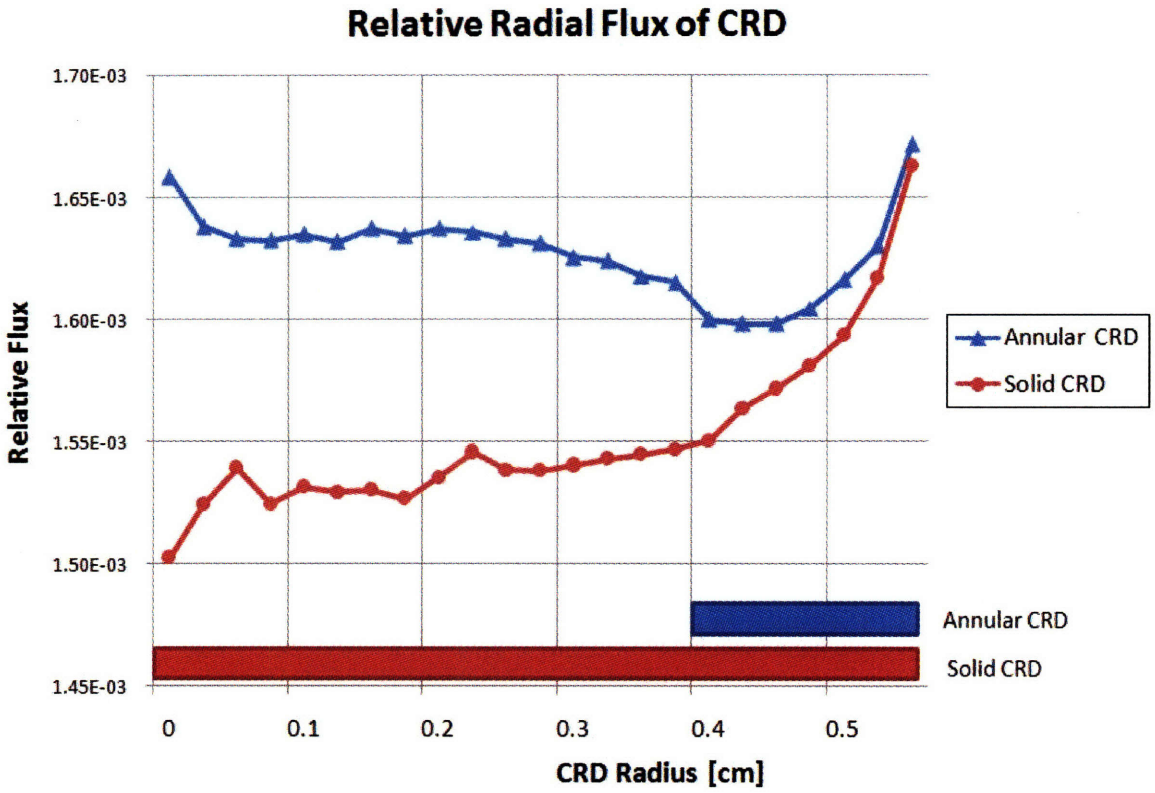

Figure 2-9 Relative radial total flux profile within the annular (blue) and solid (red) AIC control rods

2.3. Summary

The analysis of two approaches for increasing the shutdown margin for PWRs using annular fuel revealed that changing the material to 25% B-10 enriched B_4C while retaining the solid cylindrical geometry was the only successful approach. Changing the shape of the control rod did not pay off. It is possible that more advanced control rod designs using Ag-In-Cd may provide another solution, especially if the design is not constricted by the dimensions of the current annular fuel assembly, i.e. more control rod slots per assembly. It is also possible to increase the total number of control rods with extended rodlets from a single control rod cluster. However, the use of enriched boron control rods will most likely remain the cheapest and simplest approach.

3. Inner Channel Thermal Hydraulic Issues

To investigate the thermal effects of corrosion and crud buildup on annular fuel, a 1/8 core model was employed in VIPRE-01 to calculate the change in MDNBR as a result of increasing crud and oxide growth on the fuel rod with the highest local peaking factor and entrance blockage of its inner channel. First, a reference 150% power annular fuel fresh core was modeled in VIPRE-01. Second, the reference core was modified by adding various oxide and crud thicknesses to the surface at the inner channel of the hot rod to determine the maximum thickness allowed (maintaining a MDNBR > 1.3). Lastly, partial entrance blockage was introduced to the inner channel of the hot rod in the uncorroded reference core to determine the maximum allowable partial entrance blockage.

3.1. Reference Model Description

The geometry, core conditions, power distribution, and correlations used in the reference core model are described in this section and are taken from [Kazimi et al., 2006]. The models implementing corrosion/crud and blockage differ only in the hot rod geometry, so unless otherwise stated, all of the parameters described below pertain to the non-reference cases as well. A whole core model was used to properly account for mixing effects and core-wide flow distribution in order to obtain a more realistic and accurate MDNBR. In particular, the whole core model takes into account flow rate reduction in the hot channels due to increased pressure drop caused by increased subcooled, or possibly, saturated boiling.

3.1.1. Geometry

Although VIPRE-01 was originally developed for solid fuel LWRs, it has the flexibility to model annular fuel in the form of heated hollow cylinders composed of different materials. The hollow cylinder consists of 5 layers: outer cladding, outer gap, fuel annulus, inner gap, and inner cladding, which surround an internal channel of coolant. The external coolant is modeled with 4 adjacent external channels as indicated in Figure 3-1 below:

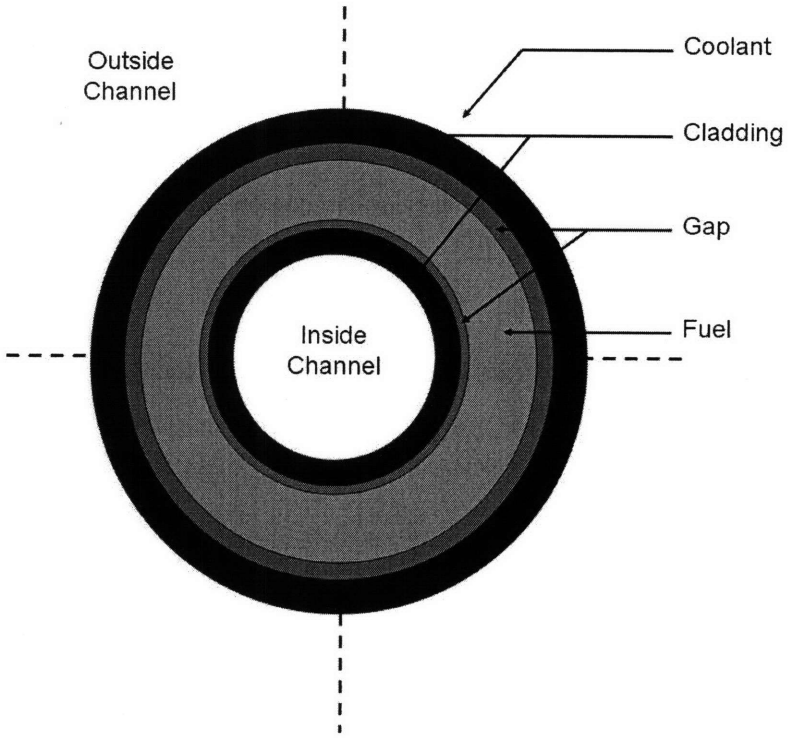

Figure 3-1 Schematic view of annular fuel pin modeled in VIPRE-01(from Beccherle, 2007.)

The VIPRE-01 model uses 1/8 symmetry on the assembly and core levels to minimize computation time. In addition, certain groups of fuel rods, channels, and assemblies are lumped together for further simplification. More detailed representation of the flow section is used for the hot region of the core. Figures 3-2 and 3-3 show the assembly and core layout with the

corresponding channel and rod numbering scheme used in the VIPRE-01 model. Note that the hot assembly was moved to the center of the core and surrounded by assemblies with the same power. This was done to minimize the effects of mixing among the outer channels of these assemblies and will yield conservative DNBR results [Feng et al., 2005].

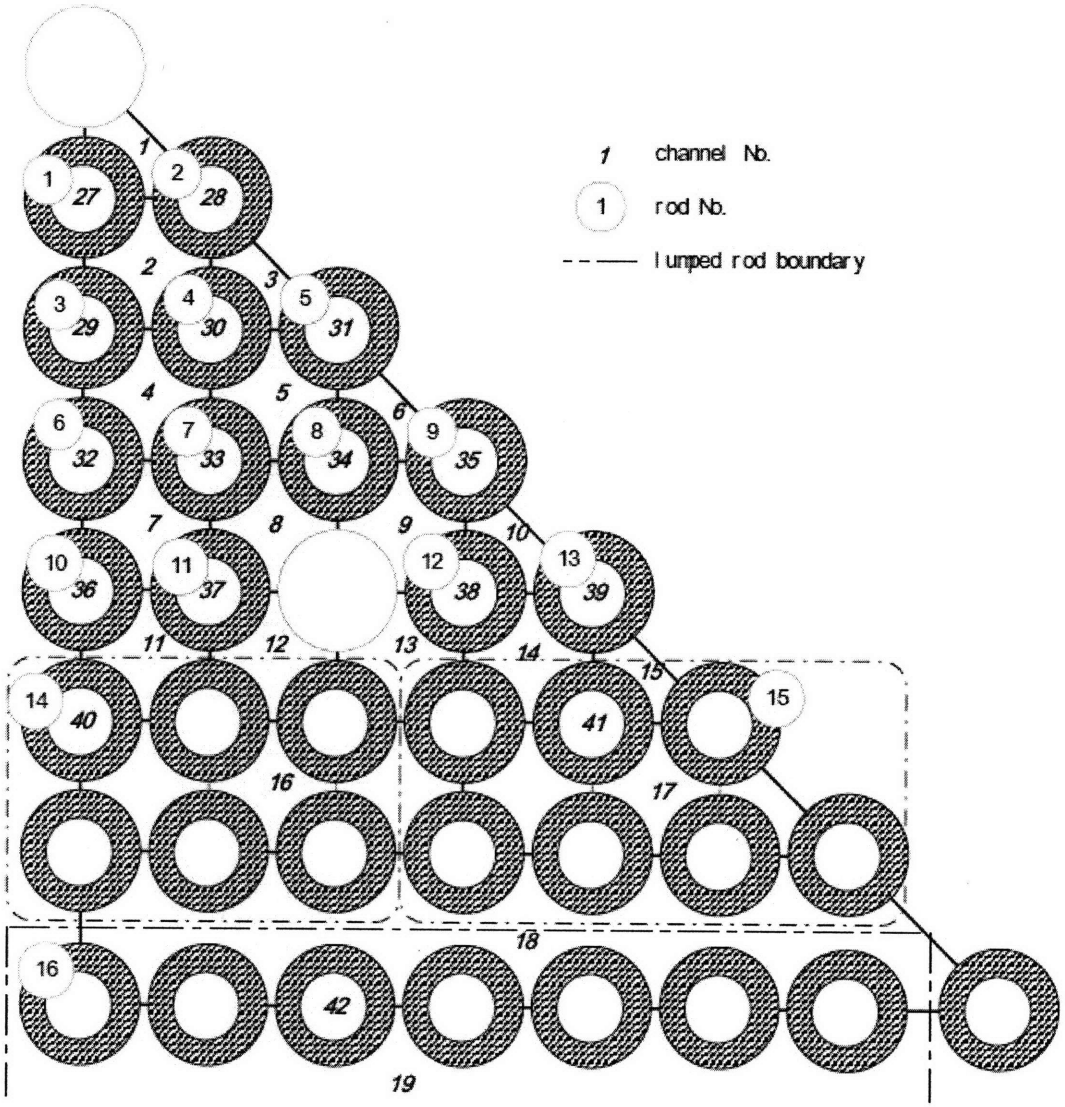

Figure 3-2 VIPRE-01 channel and rod numbering scheme for hot assembly (from Kazimi et al., 2006)

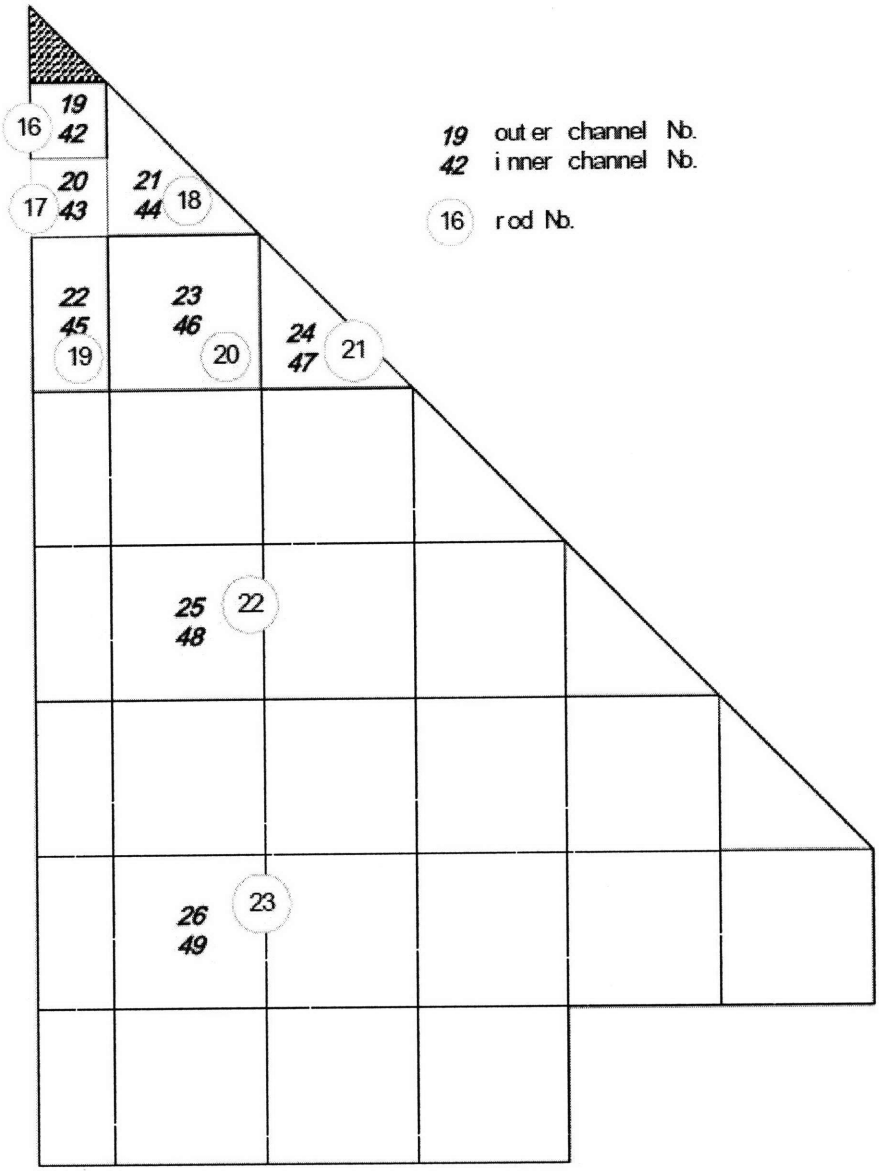

Figure 3-3 VIPRE-01 channel and rod numbering scheme for 1/8 core (from Kazimi et al., 2006)

The geometry of the reference model is described in Table 3-1. The assembly dimensions are based on the 13x13 lattice from Table 1-2 designed for a Westinghouse PWR core. Since VIPRE-01 does not calculate the channel flow areas automatically, they must also be supplied in the input. The channel flow areas and perimeters were calculated from the fuel geometry in Table 3-1, but special attention must be paid to the channels bordering the diagonal edge of the 1/8 assembly; channels 1, 3, 6, 10, and 15 have half of their areas sliced from the model so their flow areas and heated/wetted perimeters must be adjusted in the input. Also, flow through the guide tubes was modeled to be completely blocked in order to prevent coolant bypass. Therefore, the effective core flow rate for heat removal is the total core flow rate, reduced by 5% from 18.63 Mg/s to 17.7 Mg/s to account for the core bypass flow. The guide tubes contribute only to the wetted perimeter of their adjacent channels and have no effect on heat transfer in the system, so channels 1, 8, 9, 12, and 13 have reduced heated perimeters. It should be noted that since VIPRE-01 was developed in the 1980's primarily for U.S. utilities, the input is in British units.

Table 3-1 Geometry of VIPRE-01 reference model

Fuel Geometry	SI Units	British Units
Assembly Pitch	21.5 cm	8.465 in
Pin Pitch	1.651 cm	0.650 in
Rod Inner Diameter	0.864 cm	0.340 in
Inner Clad Outer Diameter	0.978 cm	0.385 in
Fuel Inner Diameter	0.991 cm	0.390 in
Fuel Outer Diameter	1.410 cm	0.555 in
Outer Clad Inner Diameter	1.422 cm	0.560 in
Rod Outer Diameter	1.537 cm	0.605 in
Guide Tube Diameter	1.537 cm	0.605 in
Core Active Length	366 cm	144 in
Channel Geometry*		
Outer Channel Area	0.871 cm^2	0.135 in^2
Inner Channel Area	0.587 cm^2	0.091 in^2
Outer Heated Perimeter	4.829 cm	1.901 in
Inner Heated Perimeter	2.713 cm	1.068 in

* For channels not bordering the diagonal edge or a guide tube (Channels 2, 4, 5, 7, 11, and 14)

3.1.2. Thermal Hydraulic Conditions

The thermal operating conditions described in Table 3-2 differ slightly from those described in Table 1-1 since this model is for the uprated annular fuel case. Specifically, the power density is increased by 50% along with a corresponding 50% increase in coolant mass flow. In addition, the inlet coolant temperature is increased by 2°C to account for possible non-uniformities of the core inlet temperature due to imperfect mixing.

Table 3-2 Thermal hydraulic core conditions employed in VIPRE-01 reference model

Core Conditions	SI Units	British Units
Operating Pressure	15.5 MPa	2248.12 psi
Inlet Temperature*	294.7°C	562.46°F
Total Flow Rate**	3.3187 Mg/s	7316.516 lb/s
Power per Rod**	195.5139 kW	
Overpower Margin (Transient)	18%	
Assembly Peaking Factor	1.587	

* The inlet temperature was increased by 2°C from the 100% WS case

** These conditions were given in the same format required in VIPRE-01 input

The Total Flow Rate and Power per Rod from Table 3-2 were calculated as follows:

$$\dot{M}_{VIPRE} = F_M * \dot{M}_{WS} * \frac{1}{8} \tag{3.1}$$

Where $\dot{M}_{VIPRE}$ = mass flow rate for uprated annular fuel 1/8 core

F_M = mass flow rate increase factor (1.5)

$\dot{M}_{WS}$ = effective core flow rate for heat removal from Table 1-1 (17.7 Mg/s)

$$P_{rod} = \frac{P_{core} * F_{OP}}{N_{assemblies} * N_{rods}} \tag{3.2}$$

Where P_{rod} = thermal power per rod [kW]

P_{core} = thermal power of uprated core (5,116,500 kW)

F_{OP} = overpower transient factor (1.18)

$N_{assemblies}$ = number of assemblies in the core (193)

N_{rods} = number of fuel rods per assembly (160)

The annular fuel assembly power distribution, shown in Figure 3-4, was calculated in MCNP while the core power distribution, shown in Figure 3-5, was the same distribution that the reference WS core used for licensing. Both are normalized to the assembly radial peaking factor of 1.587. The hot rod is indicated in red in Figure 3-4 below:

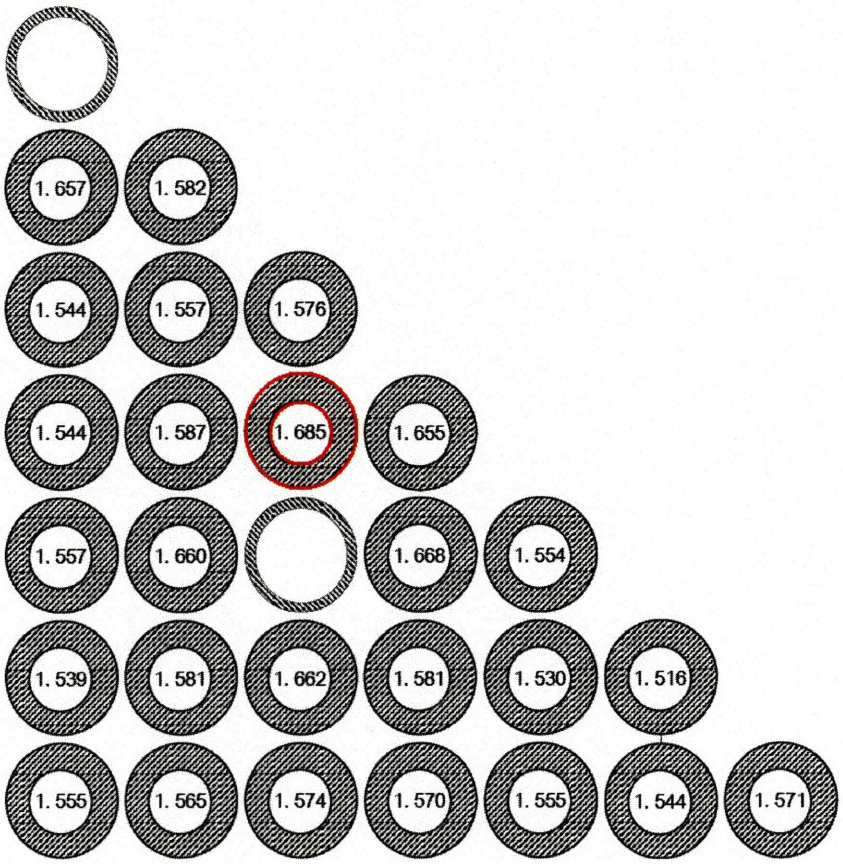

Figure 3-4 Hot assembly power distribution with hot rod indicated in red (from Kazimi et al., 2006)

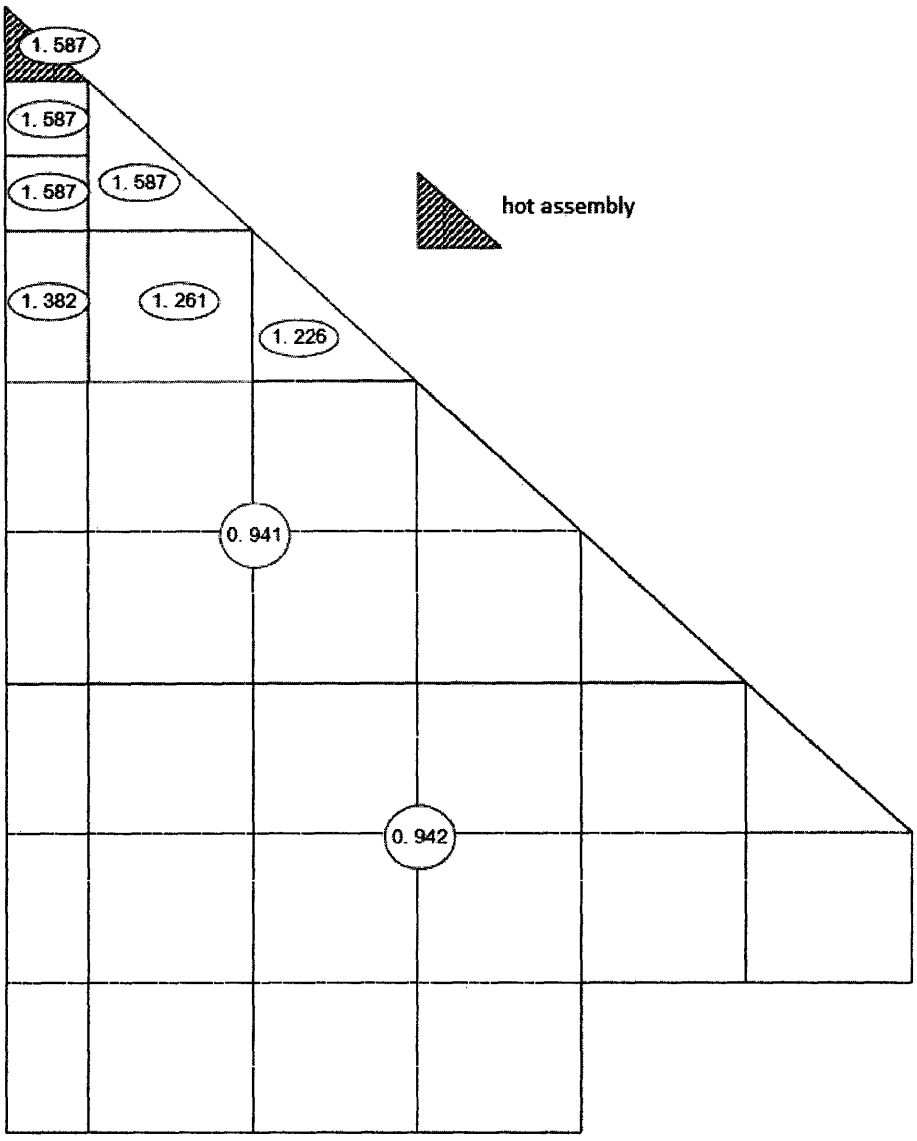

Figure 3-5 Core power distribution adopted for lumped assemblies (from Kazimi et al., 2006)

3.1.3. Correlations

Before the correlations are presented, two key parameters in VIPRE-01 that affect lateral heat and mass exchange among the outer channels should be discussed: the turbulent mixing coefficient β and the resistance to lateral flow.

The turbulent mixing model in the energy equation defines the cross flow w' (in *lb/sec-ft*) that results from an average axial flow $\overline{G}$ (in *lb/sec-ft*^{2}) in adjacent channels over a gap length s (in *ft*) in Equation 3.3:

$$w' = \beta \cdot s \cdot \overline{G} \tag{3.3}$$

A high β value will lead to a greater amount of mixing from cross flow. The mixing of the enthalpies among the channels leads to cold water taking place of steam bubbles in the hottest channel. This leads to an increase in the hot channel's flow rate which in turn increases the MDNBR. However, a turbulent mixing coefficient of 0.0 was used to yield conservative results. This is consistent with the NRC view, which states that unless a positive value of turbulent mixing can be shown experimentally, either no turbulent mixing or a conservatively small β should be used [Kazimi et al., 2006].

The resistance to lateral flow determines the pressure drop between adjacent channels that drives the crossflow. This pressure drop Δp_{cross} is defined in Equation 3.4 below:

$$\Delta p_{cross} = K_G \frac{|w|wv'}{2s^2} \tag{3.4}$$

where K_G is the lateral resistance coefficient, w is the cross flow in [kg/m-s], v' is the specific volume for momentum in [kg/m^3], and s is the gap width in [m]. A typical value for the lateral flow resistance coefficient between two rods is on the order of 0.5. This value is usually used in subchannel analysis since the crossflow resistance has insignificant effect on mass flux and

DNBR. However, for the VIPRE-01 whole core model a correlation was adopted from [Idelchik, 1986] for cross flow across a tube bundle in a square pitch. Equation 3.5 was derived using a pitch of 1.651 cm and rod diameter of 1.547 cm:

$$K_G = 7.333\mathrm{Re}^{-0.2} \tag{3.5}$$

where Re is based on the lateral velocity and rod diameter [Kazimi et al., 2006].

The correlations implemented in the VIPRE-01 model are summarized in Table 3-3 below. An additional conservative assumption made was that the turbulent momentum factor, which determines the extent at which cross flow mixes momentum, is zero. This implies that only enthalpy is mixed during cross flow [Kazimi et al., 2006].

Table 3-3 Correlations used in VIPRE-01core model for annular fuel (from Kazimi et al., 2006)

Turbulent mixing model	$\beta = 0.0$
Cross flow resistance coefficient	$K_G = 7.333\mathrm{Re}^{-0.2}$
Axial friction factor	$f_{ax} = \mathrm{Max}(0.32\mathrm{Re}^{-0.25}; 64\mathrm{Re}^{-1.0})$
Turbulent momentum factor	FTM = 0
Axial power profile	Chopped cosine, 1.55 peak-to-average ratio
Void Correlations	
Subcooled void correlation	EPRI void model
Bulk void/quality correlation	Zuber-Findlay drift flux model w/ coefficients developed for the EPRI void model
Two-phase friction multiplier	Columbia/EPRI correlation
Heat Transfer Correlations	
Single-phase flow	Dittus-Boelter correlation
Subcooled and saturated nuclear boiling	Thom + Single phase correlations
Critical Heat Flux Correlations	
Inner channel	W-3S correlation
	grid mixing factor = 0.0
Outer channel	W-3L correlation
	grid mixing factor = 0.043
	grid spacing factor = 0.066
	grid factor leading coefficient = 0.986
Form Loss Coefficients	
Inlet	0.4
Outlet	1.0
Mixing vane grids in outer channels	0.6

3.1.4. Results

The MDNBR occurs in channel 34 which is the internal channel of the hot rod. The outer channel MDNBR occurs in channel 6, which also faces the hot rod. The results in Table 3-4 are consistent with the original model from [Kazimi et al., 2006]. Figure 3-6 indicates that the MDNBR for both inner and outer channels occur at relatively the same distance along the channel, about 300 cm from the channel entrance.

Table 3-4 MDNBR results from reference VIPRE-01 model

		Mass Flux		Pressure Drop	
	MDNBR	[kg/s-m2]	[lb/hr-ft2]	[MPa]	[psi]
Inner Channel	1.366	5.83	4301.6	0.2426	35.19
Outer Channel	1.902	4.95	3652.8	0.2429	35.23

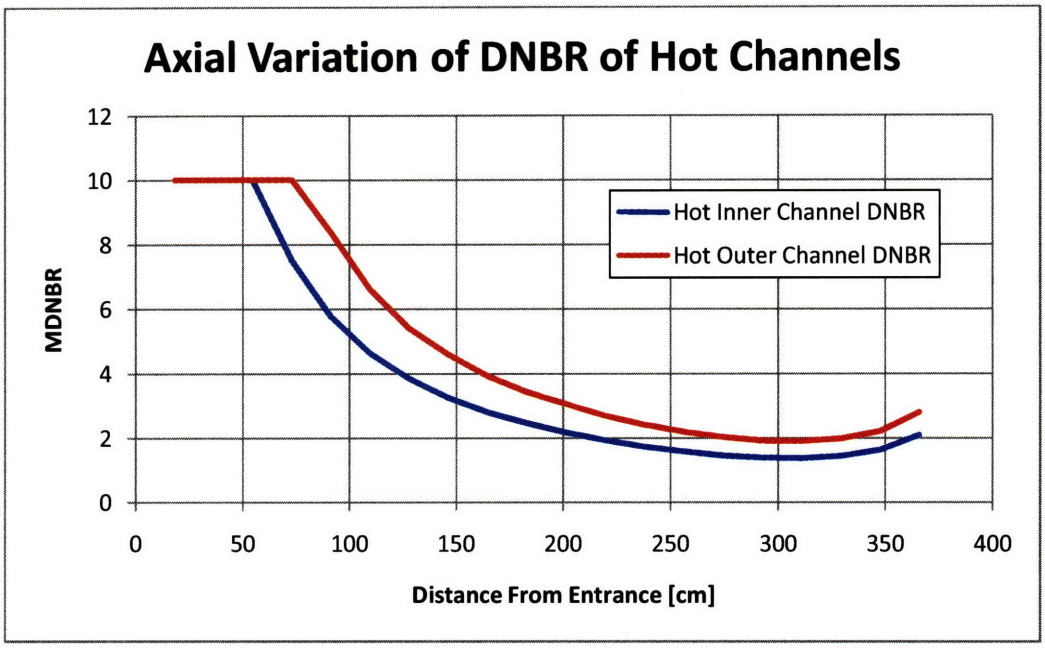

Figure 3-6 DNBR of hot inner and outer channels of reference VIPRE-01 model (annular fuel core at 150% power and flow)

3.2. Corrosion and Crud Modeling

3.2.1. Model Assumptions

The only change made to the reference model for corrosion and crud calculation was adding a uniform layer of crud and zirconium oxide on the inner and outer cladding surfaces of the hot rod. This assumption results in an even more conservative model because:

- The level of corrosion that is modeled does not develop until the EOC, and it was assumed that the corroded hot rod would still have a BOC power density
- The corrosion layer will decrease the flow areas inside and outside the hot rod resulting in a decrease in local coolant flow
- The corrosion occurs along the entire height of the hot rod which is unlikely due to the non-uniform axial power profile
- The corrosion occurs only on the hot rod; corrosion occurring on all fuel rods of the hot assembly would result in increased flow to the hot rod.

It was assumed that the oxide layer develops first and then a crud layer of equal thickness develops on top. This was done to simplify the VIPRE-01 input since the only required values were thickness and thermal conductivity of each layer. Although the ZrO_2 and crud may form a homogeneous layer simultaneously, the thermal conductivity of this mixed layer is assumed to be the weighted average of the two compositions and thus would not change the heat conduction through this layer.

3.2.2. Layer Thickness Calculation

Since ZrO_2 has larger molecular mass (123 g/mol) and lower density (5.9 g/cm^3) than zirconium metal (91 g/mol and 6.4 g/cm^3), the corroded part of the cladding will increase in

volume. The effect of ZrO_2 on the inner and outer diameters of the annular rod was calculated as follows:

For the outer cladding:

$$D_1 = D_0 - 2\delta_{Zr},\ V_{Zr} = \frac{\pi}{4}\left[D_0^2 - D_1^2\right],\ M_{Zr} = \rho_{Zr} V_{Zr}$$

$$M_{ZrO_2} = \frac{A_{ZrO_2}}{A_{Zr}} M_{Zr},\ V_{ZrO_2} = {M_{ZrO_2}}\Big/{\rho_{ZrO_2}}$$

$$D_2 = \sqrt{D_1^2 + \frac{4}{\pi} V_{ZrO_2}} \tag{3.6}$$

where δ_{Zr} is the corrosion thickness; D_0 is the original outer diameter; D_1 is the diameter inside the Zr oxide layer; V_{Zr}, M_{Zr}, A_{Zr}, and ρ_{Zr} are the volume, mass, molecular mass, and density of the oxidized Zr, respectively; V_{ZrO2}, M_{ZrO2}, A_{ZrO2}, and ρ_{ZrO2} are the volume, mass, molecular mass, and density of the ZrO_2 generated after oxidation, respectively; and D_2 is the cladding diameter after the zirconium oxidation.

Similarly, for the inner cladding:

$$D_1 = D_0 + 2\delta_{Zr},\ V_{Zr} = \frac{\pi}{4}\left[D_1^2 - D_0^2\right],\ M_{Zr} = \rho_{Zr} V_{Zr}$$

$$M_{ZrO_2} = \frac{A_{ZrO_2}}{A_{Zr}} M_{Zr},\ V_{ZrO_2} = {M_{ZrO_2}}\Big/{\rho_{ZrO_2}}$$

$$D_2 = \sqrt{D_1^2 - \frac{4}{\pi} V_{ZrO_2}} \tag{3.7}$$

where the meaning of each variable is similar to that in the expression for the outer cladding except now D_0 is the original inner diameter of the inner cladding [Kazimi et al., 2006]. Figure 3-7 illustrates the labeling scheme:

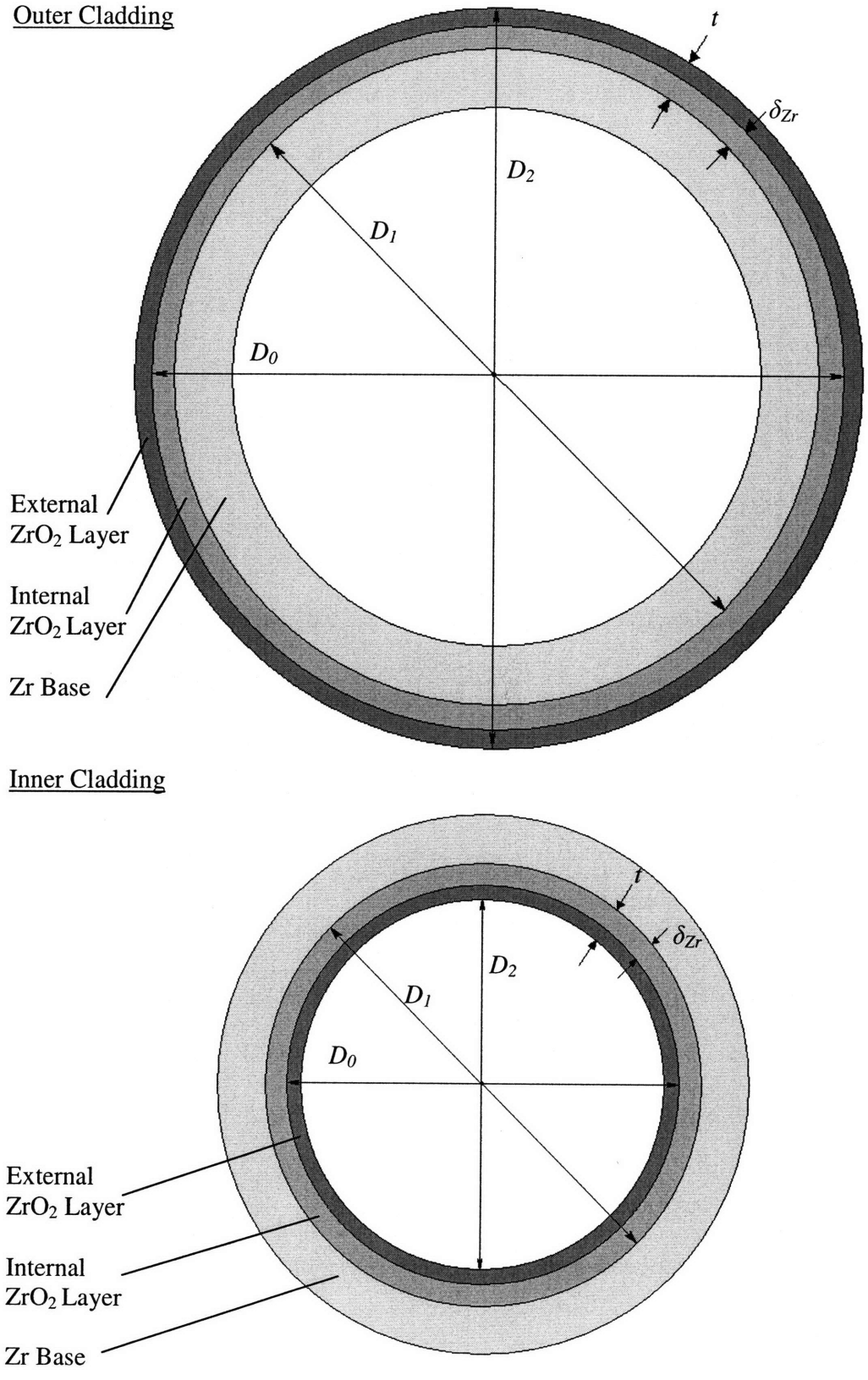

Figure 3-7 Outer and Inner cladding labeling scheme for zirconium oxide development (not drawn to scale)

Another important value is the total thickness of the zirconium oxide layer t:

$$t = \frac{|D_2 - D_1|}{2} \tag{3.8}$$

It should be noted that the inner t and outer t will be different but are extremely close for δ_{Zr} less than 100μm. For example, assuming a corrosion thickness of 20 μm, the values of the various diameters from Equations 3.6 through 3.8 are shown in Table 3-5:

Table 3-5 Diameter changes after zirconium oxidation

	δ_{Zr}	D_0	D_1	D_2	t
outer [cm]	0.002	1.5367	1.5327	1.5386	0.002931
inner [cm]	0.002	0.8633	0.8673	0.8614	0.002936

In the VIPRE-01 model, it was assumed that on top of this ZrO_2 layer was an additional crud layer of thickness δ_C which was equal to δ_{Zr}. Altogether, the profile of the crud/oxide layer is shown in Figure 3-8:

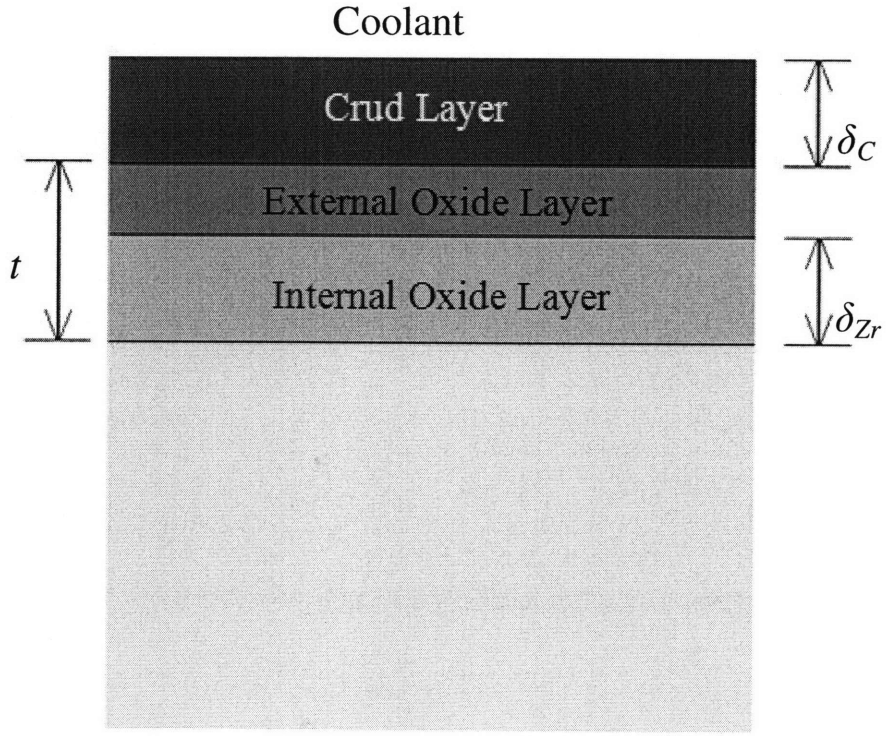

Figure 3-8 Profile of ZrO_2 and crud layers

For this study, δ_{Zr} and δ_C were varied simultaneously in the VIPRE-01 model from 10 μm to 50 μm, but ultimately the combined thickness L of the ZrO_2 and crud layers correspond to the thickness of the deposits found in PWR cladding surface scrapes where:

$$L = t + \delta_C \tag{3.9}$$

So for the case of δ being 20 μm, the combined corrosion thickness L is about 49 μm.

3.2.3. Thermal Conductivities

The thermal conductivity of ZrO_2 has widely been accepted to be about 2 W/mK. However, the thermal conductivity of crud (K_{crud}) from reactors has never been measured in its purest form. Due to its complex structure and the uncertainty of its composition varying from reactor to reactor, the thermal properties can only be estimated or partially measured. According to Kurt Edsinger of EPRI, Dr. Paul Cohen of NC State University reported values of 0.87 W/mK at 121°C by direct measurement and 0.80 W/mK by calculation based on magnetite (Fe_3O_4) at 65% porosity in water at 316°C. In Jennifer Uhle's MIT master's thesis, a value of 0.95 W/mK was used for magnetite at 60% porosity under forced convection to simulate steam generator deposits [Deshon et al., 2007]. For the purpose of this study, various thermal conductivities ranging from 0.75 to 2 W/mK were used to account for this uncertainty. The conductivity of crud is assumed to be lower than that of ZrO_2 since it has greater porosity. It will be shown later that overestimation of the thermal conductivity is a conservative assumption since a high conductivity favors the heat split towards the inner channel where MDNBR occurs.

3.2.4. Results

The maximum combined thickness L for a given crud conductivity was determined by varying both δ and K_{crud} simultaneously to determine the MDNBR which had to remain greater than 1.3 under the reference case conditions. The results are shown in Table 3-6 and Figure 3-9

which both indicate the conditions when MDNBR is less than 1.3. For a conservative assumption of K_{crud} = 1.0 W/K, the maximum combined corrosion thickness is about 50 μm, which is relatively large considering that typical thicknesses at end of life are less than 30 μm [Deshon et al., 2007]. This is also within the NRC limit on corrosion layer thickness of 100μm or 17% of the original cladding thickness.

Table 3-6 Inner and outer channel MDNBR as a function of combined corrosion thickness and crud thermal conductivity

Inner Channel

		Crud K [W/mK]			
δ [μm]	*L*[μm]	0.75	1	1.5	2
10	24.66	1.355	1.345	1.336	1.331
20	49.31	1.33	1.313	1.295	1.285
30	73.95	1.302	1.277	1.252	1.239
50	123.2	1.236	1.201	1.161	1.142

Outer Channel

		Crud K [W/mK]			
δ [μm]	*L*[μm]	0.75	1	1.5	2
10	24.66	1.819	1.823	1.828	1.827
20	49.31	1.741	1.744	1.752	1.753
30	73.95	1.661	1.669	1.677	1.681
50	123.2	1.493	1.508	1.522	1.529

As expected, the MDNBR for all cases occur in the inner channel of the hot rod and also at the same axial location as the reference case (shown in Figure 3-6). The outer channel MDNBR also occurs in the same outer channel that borders the hot rod. It is interesting to note that as the crud thermal conductivity decreases, the inner MDNBR increases while the outer MDNBR decreases. This is attributed to the unequal heat split due to the annular geometry. A decrease in K_{crud} results in a greater increase in the thermal resistance of the inner cladding than

that of the outer cladding. So as K_{crud} decreases, more heat from the fuel is conducted through the outer cladding. A detailed calculation explaining this concept is in the Appendix A.

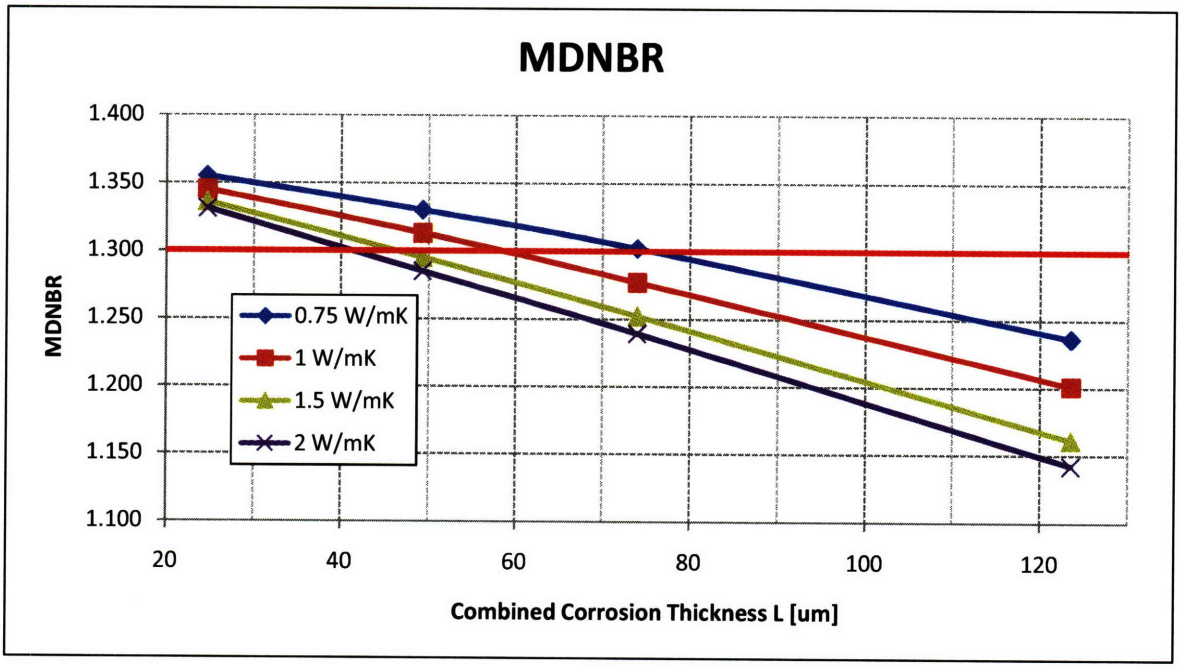

Figure 3-9 MDNBR as a function of combined corrosion thickness and crud thermal conductivity

Although increasing the thermal resistance of the cladding is helpful for MDNBR, increasing the combined corrosion thickness decreases the inner channel flow area which results in an increase in the local pressure drop. To maintain the same pressure drop, the flow through the hot channel is redistributed to other parts of the core, thus decreasing the mass flux as shown in Figure 3-10. Overall, increasing the thickness will decrease the MDNBR for any value of the thermal conductivity. However, the effect of increased cladding thermal resistance prevails over that of the reduced flow through the hot channel.

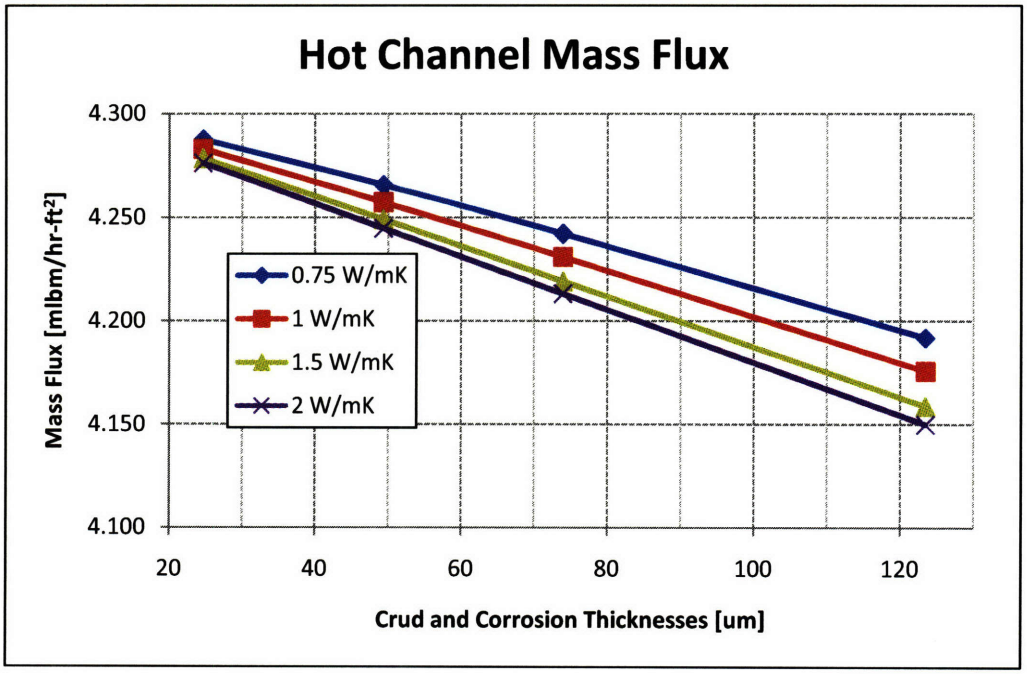

Figure 3-10 Hot channel mass flux as a function of combined corrosion thickness

3.3. Inner Channel Blockage

3.3.1. Model Assumptions

For the case of inner channel blockage, it was assumed that, in the unlikely event that inlet debris filters failed in a PWR, a hypothetical large particle would partially block the inner channel of the hot rod. The VIPRE-01 model was again used to simulate this event to determine the largest fractional channel blockage. All assumptions and parameters from the reference model were kept the same except for the overpower transient. This factor was reduced from 118% to 105% since a blockage accident and overpower transient are highly unlikely to occur simultaneously.

3.3.2. Blockage Calculation

The entrance blockage was modeled as an increase in the entrance form loss coefficient K_o using a correlation for flow through an orifice plate at a pipe entrance from [Idelchik, 1986]. The geometry is described in Figure 3-11 and the calculated values for K_o as a function of the orifice area to channel area ratio, f are shown in Table 3-7 and Figure 3-12. Equation 3.10 describes the relationship between K_o and the channel pressure drop:

$$\Delta P = \frac{\dot{m}}{2\rho A_c^2} \tag{3.10}$$

where ΔP is the pressure difference between the inlet and outlet of the channel, $\dot{m}$ is the mass flow rate through the channel, ρ is the coolant density, and A_c is the flow area of the channel.

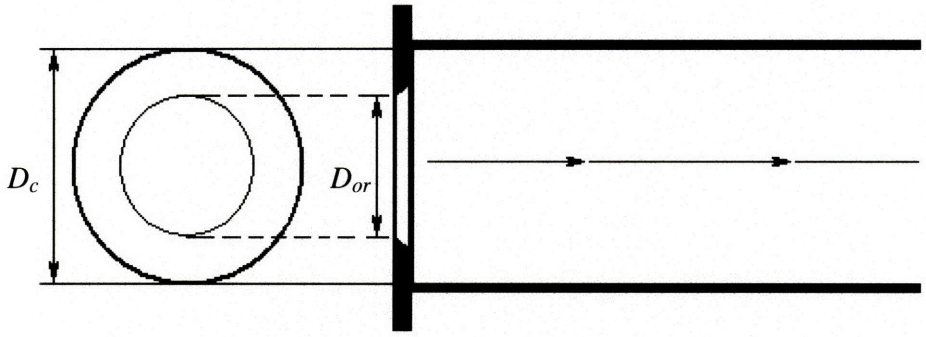

$$f = \frac{A_{or}}{A_c}, \quad A_{or} = \frac{\pi D_{or}^2}{4}, \quad A_c = \frac{\pi D_c^2}{4}$$

Figure 3-11 Geometry of correlation used for entrance channel blockage (from Idelchik, 1986)

Table 3-7 Entrance form loss coefficient as a function of ratio between orifice and channel areas (from Idelchik, 1986)

f	0.05	0.1	0.15	0.2	0.25	0.3	0.35	0.4	0.45
K_o	1100	258	98	57	38	24	15	11	7.8

f	0.5	0.55	0.6	0.65	0.7	0.75	0.8	0.9	1
K_o	5.8	4.4	3.5	2.6	2	1.7	1.3	0.8	0.5

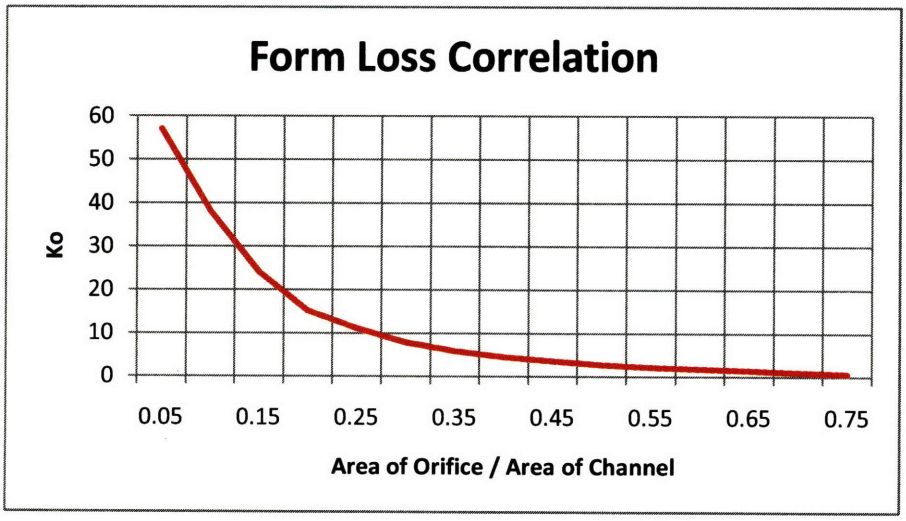

Figure 3-12 Regression function of Idelchik's entrance form loss correlation

This was the preferred approach as opposed to decreasing the entrance channel area in the VIPRE-01 model, because to simulate the effects of an entrance flow constriction, the area decrease must be modeled in the axial node after the entrance. This is because VIPRE-01 uses the hydraulic properties of the preceding node in order to calculate the velocity and mass flow for the current node. This would assume that the flow constriction occurs at the end of the first node (18 inches after the entrance) which would be inaccurate. Thus, the additional form loss resulting from the entrance blockage was calculated outside of the code to ensure that VIPRE-01 models the desired change correctly.

3.3.3. Results

The entrance form loss coefficient was gradually increased from 0.4 until the MDNBR dropped below 1.3, and then the corresponding f was approximated using Figure 3-12 and Table 3-7. The results are shown in Table 3-8 below:

Table 3-8 Effect of entrance blockage on MDNBR

K_o	f	MDNBR	Mass Flux [mlb/hr-ft^2]
0.4	1.0	2.51	4.7608
1	0.8-0.9	2.179	4.4254
3	0.6-0.65	1.384	3.6993
3.2	0.6-0.65	1.324	3.6478
3.3	0.6-0.65	1.292	3.623
3.5	0.6	1.237	3.5755

As the blockage increased, the mass flux decreased due to the whole core flow redistribution to accommodate equal pressure drops across each channel. The decreased mass flux was unable to remove as much heat from the inner channel, thus decreasing the MDNBR. The maximum blockage allowed under the assumed conditions was calculated to be 40 to 45%. If the power uprate were decreased from 50% to 10%, then the fuel can tolerate blockages up to

65% but as can be inferred from Figure 3-12, it becomes exponentially more difficult to accommodate blockage greater than 65% regardless of the power level.

3.4. Summary

A VIPRE-01 whole-core model was used to determine the effects of partial inlet blockages on the MDNBR in the hottest inner channel of uprated annular fuel cores. Under very conservative assumptions (118% overpower of a 50% uprated fresh core, central placement of hot assembly), a MDNBR of 1.3 was able to be maintained with a zirconium oxide and crud layer thickness of 50μm, a typical crud/oxide layer thickness for PWRs at EOC. Under the more realistic assumption of 105% overpower for normal operation of the uprated core, the fuel was found to be able to maintain the 1.3 MDNBR with a 35%-40% obstruction of the inner channel entrance.

4. Impact of Uprated Operation on the Fuel Cycle

4.1. CAFCA Modifications for Uprated Reactors

The existing version of CAFCA SD was unable to model two types of LWRs simultaneously, thus the source code was modified in order to simulate both LWRs and 50% uprated LWRs using annular fuel (UWLR) simultaneously: a new HLSD was created to represent the flow of ULWRs, the Mass Flow HLSD was modified to include the fresh and spent fuel compositions of the ULWR fuel, and the corresponding fuel and capital costs were updated in the Economics HLSD. Only the LWR and ULWR HLSD modifications are described in detail since their fundamental structures had to be changed while the Mass Flow and Economics HLSDs were simply updated to include new fuel and reactor types. Only basic details about the original code will be mentioned, so it is recommended to refer to Chapter 2 of [Busquim e Silva, 2008] for a fuller understanding.

4.1.1. ULWR from New Construction

There are two ways in which a ULWR is created: 1) through new construction and 2) by uprating an existing LWR. Although both pathways result in the same type of reactor, the uprated ULWR will enter the fleet with the LWR age maintained. The creation of ULWRs through the uprate method is more complex, so the construction of new ULWRs will be discussed first.

The ULWR Construction HLSD, which at this point does not include the uprate feature, is heavily based on the LWR Construction HLSD. The major difference is that construction of ULWR does not begin until the *introduction date for ULWR,* D_{ULWR} which is a variable designated by the user. It should be noted that CAFCA first calculates a fractional number of reactors needed to fulfill the electricity demand but the reactors are only constructed in integer

values. For example, although the *fractional ULWR construction order rate,* $R_{CO}^{ULWR}(t)$, at a given time may be 2.1 reactors per timestep, the *ULWR fulfilled order rate,* $R_{FO}^{ULWR}(t)$, is only 2 reactors per timestep. To implement the introduction date for ULWR construction, $R_{CO}^{ULWR}(t)$ was set to zero until the year D_{ULWR}. Afterwards , it is:

$$R_{CO}^{ULWR}(t) = Maximum\left[0, ADJ_{ULWR}(t) + R_{DR}^{ULWR}(t) + {R_{DR}^{LWR}(t)}/{UR}\right] \qquad (4.1)$$

where $R_{DR}^{ULWR}(t)$ and $R_{DR}^{LWR}(t)$ are the *ULWR decommissioning rate* and *LWR decommissioning rate*, respectively, *UR* is the *average uprate* (1.5 by default so 1 ULWR is ordered for every 1.5 LWRs decommissioned), and $ADJ_{ULWR}(t)$ is the *adjustment for fleet of ULWR* or difference between the number of reactors needed to fulfill the power demand and the current number of reactors evaluated as:

$$ADJ_{ULWR}(t) = \frac{F_{EST}^{ULWR}(t) - F_{ULWR}(t)}{\tau_{ULWR}} \qquad (4.2)$$

where $F_{ULWR}(t)$ is the *ULWR fleet under commercial operation,* τ_{ULWR} is the *ULWR fleet adjustment time*, the time constant in which the discrepancy would be corrected (default of 1 year), and $F_{EST}^{ULWR}(t)$ is the *forecasted ULWR fleet* evaluated as:

$$F_{EST}^{ULWR}(t) = \frac{P_N(t) - \sum_r F_r(t) \cdot P_r(t) \cdot CF_r}{CF_{ULWR} \cdot P_{ULWR}(t)} \qquad (4.3)$$

where $P_N(t)$ is the *nuclear power demand* and the terms in the summation $F_r(t)$, $P_r(t)$, and CF_r represent the number of reactors, net electrical output per reactor, and capacity factor, respectively, for the fleets of non-ULWR reactors (ABR, GFR, and LWR).

A major assumption made in the model is that once the annular fuel technology is implemented, all new light water reactors will be constructed as ULWRs since this is the most

economic option as shown by Table 1-4. Thus the *fractional LWR construction order rate* $R_{CO}^{LWR}(t)$ will be zero after the year D_{ULWR}.

4.1.2. ULWR from Uprate

If the uprate construction for LWRs is timed with that of a scheduled steam generator replacement, then the cost of the new steam generator would not be assigned to the capital cost of the uprate. In addition, the replacement power for the 3-month offline period for steam generator replacement is assumed to be covered by the operations and maintenance costs as well. If the steam generator is assumed to be replaced every 20 years, then the model assumes that the *available number of LWRs for uprate*, $A_{Ui}(t)$ at each time step is only non-zero for i = 20 or 40, where i is the coflow number (from 1 to 60) and the value $A_{Ui}(t)$ is equal to the number of LWRs under commercial operation that are i years old. However, not all of the LWRs available for uprates need to be uprated; the user can determine the *percent of available LWRs actually uprated* P_{AU}.

When an uprate occurs, a 20 or 40 year-old LWR is removed from the LWR fleet and added as a 21 or 41 year-old ULWR to the ULWR fleet during the same year. The off-line period of 1 year is not actually simulated; the power demand is assumed to be satisfied instantly. If this delay were to be modeled, additional ULWRs would be constructed during that period to try to make up for the demand. However, this off-line period is still accounted for in the Economics HLSD in terms of replacement power cost.

An *uprate rate* $R_{Ui}(t)$ is introduced as the outflow of the 20 and 40 year-old uprated LWRs from the ULWR fleet which is evaluated as a fixed delay with a delay of 1 year:

$$R_{Ui}(t) = Integer\left(R_{UAi}(t) \cdot P_{AU}\right) \tag{4.4}$$

where $R_{UAi}(t)$ is the *uprate availability rate*, which is equal to the rate at which 20 and 40 year-old LWRs become available. Notice that this is in units of [fractional reactors per time step] and different from $A_{Ui}(t)$ which is a measure of the discrete number of LWRs available. $R_{UAi}(t)$ is zero until D_{ULWR} and afterwards it is simply:

$$R_{UAi}(t) = R^{TRA}_{CR\ i}(t) \tag{4.5}$$

where $R^{TRA}_{CR\ i}(t)$ is the *transition LWR construction rate* modeled as:

$$R^{TRA}_{CR\ i}(t) = R^{LWR}_{FO}(t) \quad \text{if} \quad i = 1 \tag{4.6}$$

$$R^{TRA}_{CR\ i}(t) = R^{TRA}_{DR\ i-1}(t) \quad \text{if} \quad i = 2 \text{ to } 60 \tag{4.7}$$

where $R^{LWR}_{FO}(t)$ is the *LWR fulfilled order rate*. When $R_{Ui}(t)$ is greater than zero, the *transition LWR decommissioning rate* $R^{TRA}_{DR\ i}(t)$ must be adjusted so that the losses from the LWR fleet are not double counted:

$$R^{TRA}_{DR\ i}(t) = MAX\left(0, R^{TRA}_{IN\ i} + R^{TRA}_{LWR\,i} - R_{Ui}(t)\right) \tag{4.8}$$

where $R^{TRA}_{IN\ i}$ is the *transition rate for initial number of LWRs* and $R^{TRA}_{LWR\,i}$ is the *transition rate for LWR* which is just a fixed delay of 1 year for $R^{TRA}_{CR\ i}(t)$.

To avoid building or uprating an excessive amount of ULWRs, the *fractional ULWR construction order rate,* $R^{ULWR}_{CO}(t)$ from Equation 4.1 must be updated so that the fluctuations in the *adjustment for fleet of ULWR* $ADJ_{ULWR}(t)$ are minimized. This was done by ensuring that new ULWRs are only constructed based on the ULWR demand after all the uprates have occurred, thus giving the uprates precedence, even though it is the more costly option based on Table 1-4. To have new ULWR construction as the only option, the user can simply set P_{AU} equal to zero. So now Equation 4.1 becomes:

$$\text{if} \quad \frac{A_{Ui}(t) \cdot P_{AU}}{3} < ADJ_{ULWR}(t),$$

$$R_{CO}^{ULWR}(t) = Maximum\left[0, ADJ_{ULWR}(t) - \frac{A_{Ui}(t)\cdot P_{AU}}{3} + R_{DR}^{ULWR}(t) + \frac{R_{DR}^{LWR}(t)}{UR}\right] \quad (4.9)$$

if $\frac{A_{Ui}(t)\cdot P_{AU}}{3} > ADJ_{ULWR}(t)$

$$R_{CO}^{ULWR}(t) = R_{DR}^{ULWR}(t) + \frac{R_{DR}^{LWR}(t)}{UR} \quad (4.10)$$

Notice that the contribution of the uprates to fulfilling the ULWR adjustment is correctly modeled as $A_{Ui}(t)\cdot P_{AU}/3$ because for each uprate, 1.5 GWe is added by the ULWR and 1 GWe is removed due to removing an LWR from the fleet. This gives a net gain of 500 MWe for each uprate so 3 uprates are needed to satisfy the demand for a single ULWR from new construction.

If $R_{CO}^{ULWR}(t)$ was not modified to properly account for the ULWR fleet adjustment, then the $ADJ_{ULWR}(t)$ curve would fluctuate sinusoidally before finally converging to the exponential growth of the reactor demand. Although the adjustment does not affect the overall economics, the adjustment curves should match the power demand curve for results which are consistent with the model.

To account for uprates in the ULWR HLSD, the *transition ULWR construction rate* $RU_{CR\ i}^{TRA}(t)$ is set equal to the *uprate rate* of the LWRs that underwent the uprate:

$$RU_{CR\ i}^{TRA}(t) = R_{Ui-1}(t) \quad (4.11)$$

For example, the transition construction rate for ULWRs that are 21 years old is equal to the uprate rate of LWRs that are 20 years old. Thus, the age of the reactor is maintained through the fleet transfer.

Lastly, to account for the additional number of fresh cores needed per year due to uprated ULWRs, the *number of ULWR starting commercial operation per year* $F_N^{ULWR}(t)$ is now modeled as:

$$\frac{dF_N^{ULWR}(t)}{dt} = R_{FO}^{ULWR}(t) - O_{ULWR}(t) + \sum_i R_{Ui}(t) \quad (4.12)$$

where $R_{FO}^{ULWR}(t)$ is the *ULWR fulfilled order rate* and $O_{ULWR}(t)$ is a one year fixed delay applied to the fulfilled order rate.

4.1.3. Mass Flow Modification

Due to the annular fuel higher enrichment, lower mass loading, and different spent fuel composition due to higher burnup, the mass flow for ULWR fuel had to be tracked separately from that of LWR fuel. The modifications made to the Mass Flow HLSD to account for ULWR fuel are simply duplicates of all the stocks and flows in the original HLSD which accounted for LWR fuel. The only differences are the values in Table 4-1 and the fact that all ULWRs are only loaded with traditional UO_2 fuel as opposed to the option of both UO_2 and CONFU for LWRs. CONFU fuel has not yet been proven to be adaptable to the different conditions of ULWRs so it was not adopted in the modifications.

Table 4-1 Fuel properties for LWR and ULWR

	LWR	ULWR
Enrichment [wt%]	4.51	8.7
Feed Enrichment [wt%]	0.711	0.711
Tails Enrichment [wt%]	0.25	0.25
Mass Loading [MT/y]	17.15	15.54
Discharge Burnup [MWd/kg]	~50	83.4
Spent Fuel Composition		
U [wt%]	92.54	90.51
Pu [wt%]	1.32	1.96
FP [wt%]	5.83	7.29
MA [wt%]	0.31	0.24
U-235 [wt% U]	2.5	1.96
Np [wt% MA]	-	72.7
Am [wt% MA]	-	19.0
Cm [wt% MA]	-	8.3

The ULWR fuel enrichment was found by averaging over all the fresh assemblies in Table 2-1 and the ULWR mass loading per year was determined by multiplying the LWR mass loading, which is 17.15 MT/y for 1000 MWe LWRs [Busquim e Silva, 2008], by the ULWR/LWR total core mass ratio (0.905). The discharge burnups were calculated from the equilibrium WS and XU core descriptions from [Xu et al, 2004], so the 1 GWe LWR discharge burnup is approximated as that of a 1150 MWe PWR. The spent fuel composition for ULWR was calculated from an annular pin model (8.7 wt% enrichment, depleted up to 83 MWd/kg) using MCODE (an MCNP-ORIGEN Depletion Program) [Xu et al., 2006]. The fuel burnup is currently not an input for CAFCA but future modifications can use burnup as well as other inputs to correlations that calculate the spent fuel vectors. For example, Table 4-2 shows a correlation to calculate the weight fractions of the plutonium vector developed by [Xu, 2003].

Table 4-2 Approximate isotopic composition correlations for current PWR lattices with hydrogen-to-heavy metal ratios ~ 3.4 (from Xu, 2003)

For total plutonium:

$$\text{(kg Pu)/(kg initial heavy metal)} = 0.0193\left(\frac{B}{100}\right)^{0.565}$$

$$\text{(kg Pu)/(GWe*yr)} = \frac{70.45}{\eta\left(\frac{B}{100}\right)^{0.435}}$$

where B = burnup, MWd/kg;
η = thermodynamic efficiency.

For individual isotopes:

$$\frac{X48}{X49} = \left(\frac{0.0125}{X25(0)}\right)\left(\frac{B}{100}\right)^{2.47}$$

$$\frac{X48}{X42} = 9.73\left(\frac{X25(0)}{1-X25(0)}\right)\left(\frac{B}{100}\right)^{0.0339}$$

$$\frac{X40}{X49} = \frac{0.0354}{X25(0)}\left(\frac{B}{100}\right)^{1.01}$$

$$\frac{X41}{X49} = 1.47(1-X25(0))\left(\frac{B}{100}\right)^{0.152} - 1$$

where X4z = weight fraction of plutonium isotope of mass number ending in "z";
X25(0) = U-235 weight fraction in initial heavy metal.

The higher discharge burnup of the spent ULWR fuel results in a lower weight percent of uranium and subsequently a higher weight percent of fission products due to more fissions occurring during the fuel's in-core lifetime. The total Pu inventory also increases due to transmutation of U-238. Figure 4-1 shows the mass inventory of plutonium isotopes in UO_2 fuel as a function of burnup [Xu, 2003].

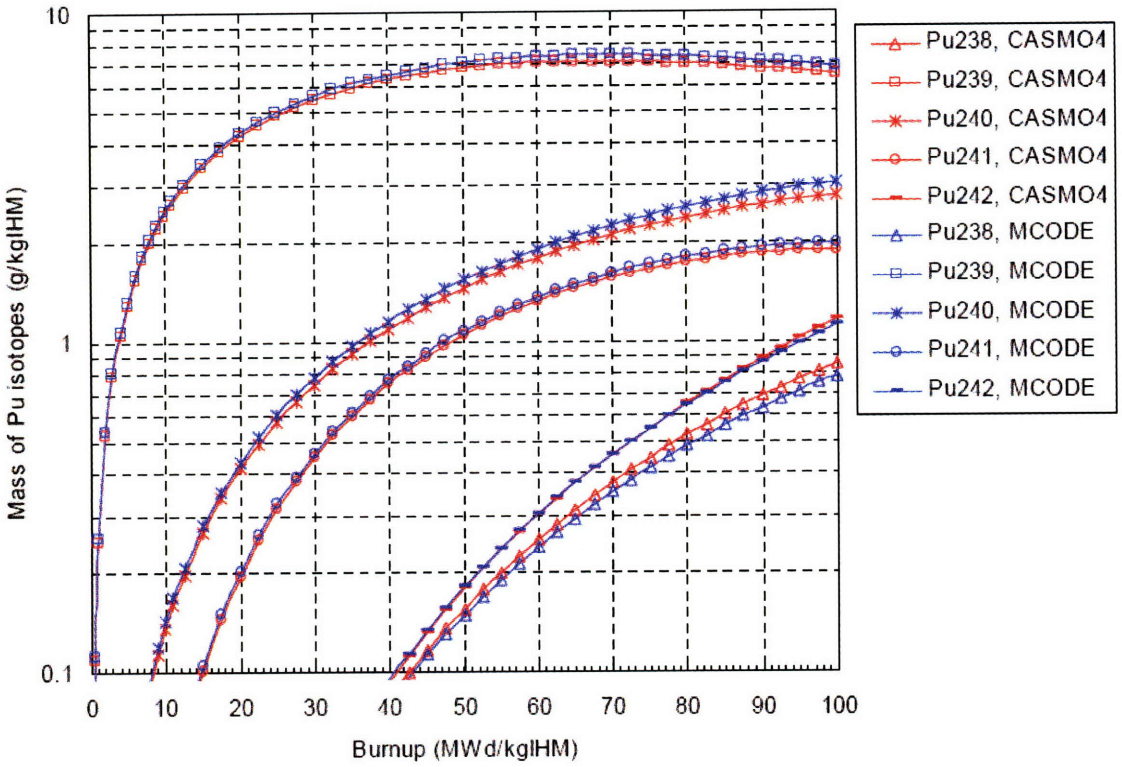

Figure 4-1 Plutonium vector as a function of burnup calculated by CASMO-4 and MCODE (from Xu, 2003)

4.1.4. Economic Updates

Now that the reactor construction and mass flow HLSDs can account for ULWRs, the capital and fuel costs must also include the ULWR contributions. There are two different capital costs for ULWRs depending on how they were created, either through new ULWR construction or by uprating LWRs. The capital costs of these two pathways were based on the capital costs of options 2 and 3 calculated by Westinghouse in Table 1-4.

4.1.4.1. ULWR Construction Capital Cost

The overnight construction cost (the cost of a hypothetical instantaneous construction) for a 1000 MWe LWR in as applied in the last work using CAFCA was 1700 $/kWe [Busquim e Silva, 2008] while in Table 1-4, it is 1313 $/kWe (option 1) [Kazimi et al, 2004]. Thus, to calculate the overnight construction cost for ULWRs, the capital cost of option 3 (1103 $/kWe) was simply multiplied by the ratio between the costs from CAFCA and Table 1-4 (1700/1313). This yields a value of 1428 $/kWe (approximately 1430 $/kWe) for new ULWR construction. This cost does not need to be scaled down even though the uprate in CAFCA is 500 MWe as opposed to the 600 MWe for the reference PWRs since it is in units of $/kWe. Table 4-3 compares the values used in the Westinghouse study [Kazimi et al, 2006] and in CAFCA [Busquim e Silva, 2008].

4.1.4.2. ULWR Uprate Capital Cost

To calculate the overnight uprate cost, option 2b from Table 1-4 was used as the base cost of the structural components. The top number in Table 4-2 (which is this base cost) does not include the cost of replacement power and the unused fuel so it can be designated as the 'component uprate cost'. The component uprate cost includes the costs for larger steam generators, new recirculation pumps, a new pressurizer, and additional balance of plant to

accommodate the additional power. Once this component uprate cost for Westinghouse PWRs is converted into a component uprate cost used for LWRs in CAFCA, additional costs and savings are factored in to produce the total capital cost for uprates. For the aforementioned calculation (detailed in Table 4-2), the following assumptions were made:

1.) The component uprate total cost ($828,600,000) is scaled down proportionately as the power uprate changes from 600 MWe for Westinghouse PWRs to the 500 MWe for LWRs in CAFCA.

2.) The component uprate total cost is then multiplied by the LWR cost ratio, described in Section 4.1.4.1, to obtain correct costs for use in CAFCA.

3.) The uprate construction is timed to coincide with a scheduled steam generator replacement so the cost of the steam generators ($150,000,000) can be deducted from the uprate construction total cost [Beccherle, 2007].

4.) By using a transitional refueling scheme when converting from solid to annular fuel, all of the remaining solid fuel is used before the uprate construction thus there is no extra cost for the unused fuel [Beccherle, 2007].

5.) The replacement power cost is only calculated for 9 out of the 12 months that the reactor is offline. 3 months of replacement power have already been considered for the scheduled steam generator replacement and do not contribute to the cost of the uprate [Beccherle, 2007].

6.) The cost of electricity for the replacement power was assumed to be $0.035/kWhe, approximately the average cost of electricity calculated by CAFCA in the once-through cycle for the next 30 years (see Figure 4-8).

The replacement power cost was calculated as follows:

$$C_{rp} = C_{Elec} \cdot (\tau_{offline} - 2160) \cdot CF \cdot P \tag{4.14}$$

where C_{Elec} is the cost of electricity ($0.035/kWhe) assumed by [Xu et al, 2004], $\tau_{offline}$ is the offline period (1 year or 8640 hours), CF is the capacity factor (0.9) assumed in CAFCA [Busquim e Silva, 2008], P is the electric power rating (10^6 kWe), and C_{rp} is the total cost of the replacement power, calculated to be $204.12 M. As previously mentioned, the offline period was subtracted by 2160 hours (3 months).

The ULWR uprate total capital cost in Table 4-2 is divided by the 500 MWe of added power to obtain the ULWR uprate capital cost of 1896 $/kWe (approximated as 1900 $/kWe) in Table 4-3. This is comparable to the 1817 $/kWe as proposed by Westinghouse [Kazimi et al, 2006] even though the replacement power was calculated at a price of $0.035/kWhe compared to Westinghouse's $0.019/kWhe. The increase in cost of replacement power was almost entirely offset by using an optimized solid to annular fuel transition scheme (Beccherle, 2007) and timing the uprate with a scheduled steam generator replacement which, together, yielded savings from the cost of steam generators, unused fuel, and the 3 month replacement power credit.

Table 4-2 Calculation of uprate construction cost for CAFCA

$828,600,000	Component Uprate Cost (Westinghouse)
x 500/600	Westinghouse to CAFCA added power ratio
$690,500,000	
x 1700/1313	Westinghouse to CAFCA cost ratio
$894,021,325.21	Component Uprate Cost (CAFCA)
- 150,000,000	Cost of steam generators
$744,021,325.21	
+ $0	Unused fuel cost
$744,021,325	
+ $204,120,000	Nine months of replacement power (at $0.035/kWhe)
$948,131,325	**ULWR uprate total capital cost**

Table 4-3 Westinghouse and CAFCA capital costs in [$/kWe]

	Westinghouse	CAFCA [Busquim]
LWR Construction Cost	1313	1700
ULWR Construction Cost	1103	1430
ULWR Uprate Cost	1817*	1900**

* On additional 600 MWe only
** On additional 500 MWe only

4.1.4.3. **Up to Date Costs**

Although the costs used in CAFCA are more recent than those used in the Westinghouse study, they still require more recent updates to more accurately reflect costs in the year 2008. As of February 2008, the overnight construction cost for a Gen. III LWR is around $3,000/kWe while the overnight decommissioning costs are closer to $500/kWe for all reactors (around 40% higher than in the previous CAFCA reference values). This increase is mainly due to the increased cost of concrete and steel. The construction costs of the reactors from Table 4-3 along with the construction costs of advanced reactors were multiplied by the new LWR cost ratio (3000/1700) and are shown in Table 4-5. The decommissioning costs were simply changed from $350 to $500/kWe.

The uprate cost, however, was calculated a little differently: only the component uprate cost was multiplied by the ratio instead of the entire uprate cost which also includes replacement power and steam generator costs. The replacement power cost was added and the steam generator costs (also multiplied by the 3000/1700 cost ratio) were deducted from this updated uprate component cost to yield a total uprate capital cost of $1.5171B as shown in Table 4-4. Dividing this value by the power added (500 MWe) yielded approximately 3035 $/kWe as shown in Table 4-5.

Table 4-4 Calculation of updated uprate construction cost for CAFCA

$828,600,000	Component Uprate Cost (Westinghouse)
x 500/600	Westinghouse to CAFCA added power ratio
$690,500,000	
x 1700/1313	Westinghouse to CAFCA cost ratio
$894,021,325.21	Component Uprate Cost (CAFCA)
x 3000/1700	Cost update
$1,577,684,692	
- $264,705,882	Cost of steam generators ($150 M x 3000/1700)
$1,312,978,810	
+ $0	Unused fuel cost
$1,312,978,810	
+ $204,120,000	Nine months of replacement power (at $0.035/kWhe)
$1,517,098,810	**ULWR uprate total capital cost**

Table 4-5 Cost updates for CAFCA (from Kazimi, 2008)

cost updates		
Overnight Construction Costs [$/KWe]		
	old	updated
LWR	1700	3000
ULWR (new)	1430	2520
ABR	2500	4400
FBR	2500	4400
Overnight Uprate Cost [$/KWe]		
ULWR (uprated)	1900	3035*
Overnight Decommissioning Costs [$/KWe]		
	old	new
LWR	350	500
ULWR	350	500
ABR	350	500
FBR	350	500

* On the additional 500 MWe only

4.1.4.4. Economic Updates in CAFCA

In updating the Capital Cost HLSD, three new cost calculation features were implemented for: 1) new ULWRs, 2) uprated ULWRs, and 3) existing LWRs that are still paying annuities. To calculate the capital cost, the *overnight construction cost* $C_{overnight}^{constr}$ (from the new costs in Table 4-5) was multiplied by the electric power generated by reactors under 20 years old since $C_{overnight}^{constr}$ is paid during the amortization period of the plant (20 years) through annual payments (annuities) of Y_{constr}, given an effective discount rate r and tax rate on equity, τ

$$Y_{constr} = C_{overnight}^{constr} \cdot \left(\frac{e^{r \cdot T_{constr}} - 1}{r \cdot T_{constr}} \right) \cdot \frac{1}{(1-\tau)} \cdot \left(\frac{e^{r \cdot L_e} \cdot (e^r - 1)}{e^{r \cdot L_e} - 1} - \frac{\tau}{L_e} \right) \qquad (4.15)$$

where L_e is the *amortization period*, T_{constr} is the *plant construction time.* To account for the capital costs of constructing and uprating ULWRs (features 1 and 2), the annuity for each case was calculated from the values in Table 4-6 and multiplied by the electricity produced from the additional electric power added to the fleet.

The third implementation was necessary due to the capital cost updates in Table 4-5; the new LWR overnight construction costs should only be applied to new reactors (presumably Gen. III) constructed after 2007. However, CAFCA SD did not make the distinction between existing and newly constructed LWRs so all existing LWRs under 20 years old would have been paying the updated construction cost annuity. To fix this discrepancy, a separate fleet of LWRs was created for the existing Generation II reactors under 20 years old. These LWRs would pay a lower construction cost annuity based on the old LWR overnight construction cost in 4-5.

Table 4-6 Capital cost values for new reactor types

Reactor Type	Overnight Construction Cost [$/kWe]	Construction Time [years]	Tax Rate	Discount Rate	Amortization Period [years]
LWR (Gen II)	1700	4	38%	7.55%	20
LWR (Gen III)	3000	4	38%	7.55%	20
ULWR (new)	2520	4	38%	7.55%	20
ULWR (uprate)	3035	1	38%	7.55%	20

A major correction made to the original CAFCA SD version was the calculation of the cost of fuel enrichment. Originally, the cost of fuel enrichment was the product between the total enriched fuel mass per year [kg/y] and the cost of enrichment [$/kg]. This has been correctly changed to the product between the *separative work unit* (SWU) per year [kg/y] and the cost of enrichment where SWU requirements are evaluated as

$$SWU_{LWR}(t) = P_{UO_2}(t)\cdot V(x_P^{LWR}) + T_{UO_2}(t)\cdot V(x_T^{LWR}) - F_U(t)\cdot V(x_F^{LWR}) \qquad (4.16)$$

where $P_{UO_2}(t)$ is the *mass of enriched uranium for UO_2 per year*, x_P^{LWR} is the *enrichment of the product for UO_2*, $T_{UO_2}(t)$ is the *mass of the UO_2 tails*, x_T^{LWR} is the *enrichment of the tails*, $F_U(t)$ is the *mass rate of natural uranium feed enrichment for traditional fuel per year*, x_F^{LWR} is the *enrichment of the feed for UO_2*, and $V(x)$ is defined as:

$$V(x) = (2\cdot x - 1)\cdot \ln\left(\frac{x}{1-x}\right) \qquad (4.17)$$

The *Uranium mass feeding the conversion process per year, $M_{CON}(t)$*, and the *Uranium mass feeding the milling process per year, $M_{MIL}(t)$* are evaluated as

$$M_{CON}(t) = \frac{F_U(t)}{(1-L_C)} \qquad (4.18)$$

$$M_{MIL}(t) = \frac{M_{CON}(t)}{(1-L_M)} \qquad (4.19)$$

where L_M is the Uranium milling process losses, and L_C is the Uranium conversion process losses. In addition, the *mining mass rate,* $M_{MIN}(t)$, is considered as equal to $M_{MIL}(t)$.

The *cumulative demand for natural Uranium* is represented by one stock, $S_D^U(t)$. The inflow for this stock is the sum of the *mining mass rate for traditional, young CONFU,* and *old CONFU* fuels, $M_{MIN}(t) + M_{MIN}^{Young}(t) + M_{MIN}^{Old}(t)$. $S_{Do}^U(t)$ is the initial demand at time t = 0 [Busquim e Silva, 2008]:

$$\frac{dS_D^U(t)}{dt} = M_{MIN}(t) + M_{MIN}^{Young}(t) + M_{MIN}^{Old}(t), S_{Do}^U(t) \tag{4.20}$$

4.2. High Burnup Reactors in Once Through Cycle

The introduction of ULWRs to the open fuel cycle in the U.S. was simulated in various scenarios to demonstrate CAFCA SD's new capabilities and to analyze their impact on the fuel cycle economics and uranium resources. Three cases of ULWR introduction at a given date were compared to the standard case with only LWRs using solid fuel: Case A) construction of new ULWRs only, Case B) simultaneous new construction and uprate of 50% of available LWRs (P_{UA} = 50%), and Case C) simultaneous new construction and uprate of 100% of available LWRs (P_{UA} = 100%). All 3 cases have the parameters listed in Table 4-7:

Table 4-7 Main simulation parameters

Simulation period	100 years
Nuclear annual growth rate	2.4%
ULWR introduction date	2017
LWR lifetime	60 years
ULWR lifetime	60 years
Capacity Factor (all reactors)	0.90
Initial LWR fleet	current U.S. fleet*
U.S. spent fuel "legacy"	50,000 MT

*reactor age distribution in Appendix D

All of the aforementioned fuel and cost assumptions in Tables 4-1, 4-2, and 4-3 were applied. Table 4-8 lists the fuel costs in the model and the associated masses of each fuel cycle process:

Table 4-8 Fuel cycle costs and average corresponding masses per reactor per year

	Costs	Mass per LWR	Mass per ULWR
Ore Purchase	120 $/kg	180 MT/yr	320 MT/yr
Conversion Process	12 $/kg	177 MT/yr	317 MT/yr
Enrichment Process	140 $/kg SWU	132 MT SWU/yr	276 MT SWU/yr
UO2 Fuel Fabrication	250 $/kg	19.1 MT/yr	17.2 MT/yr
Spent Fuel Interim Storage	200 $/kg	15.2 MT/yr	14 MT/yr

4.2.1. Construction Results

CAFCA SD constructs or uprates reactors based solely on the power demand, as shown in Figure 4-2, which was set to grow at a rate of 2.4% annually:

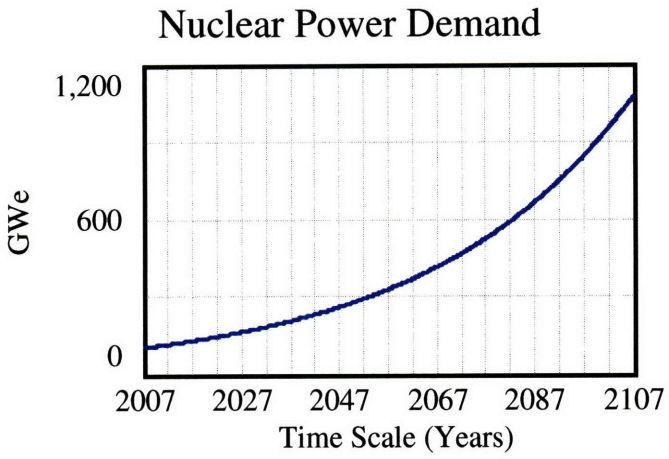

Figure 4-2 Nuclear power demand growth curve

Therefore the total fleet of LWRs and ULWRs should also grow exponentially, as seen in Figure 4-3:

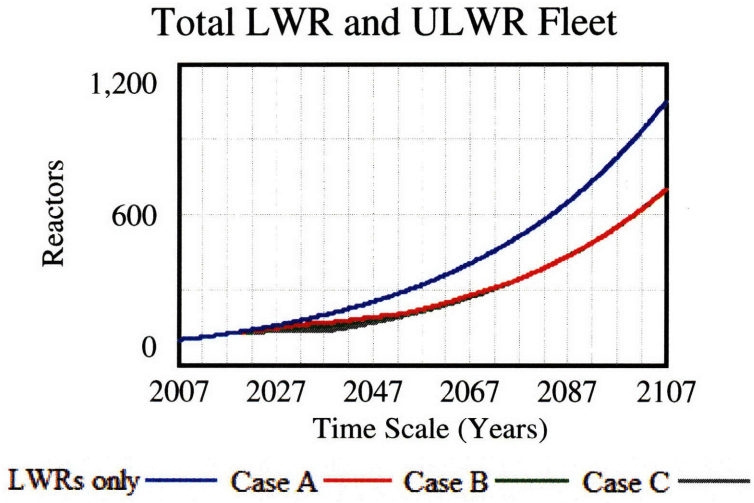

Figure 4-3 Combined LWR and ULWR growth for the various cases

where the LWRs and ULWRs graphed individually are shown in Figures 4-4 and 4-5:

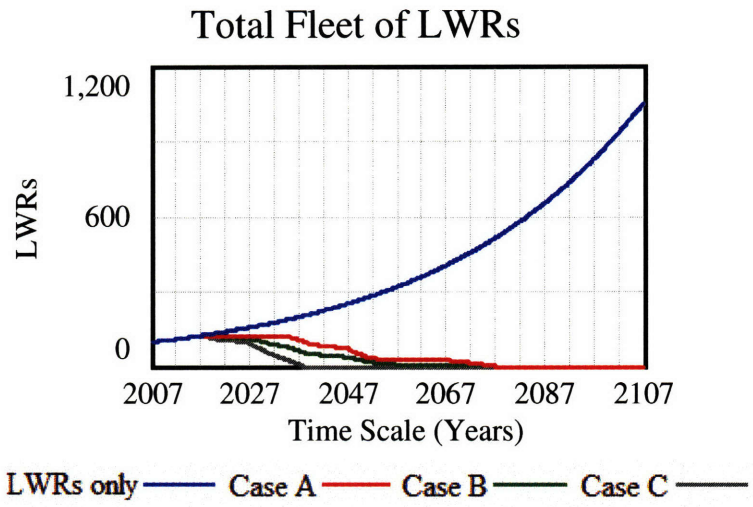

Figure 4-4 Total LWR fleet for the various cases

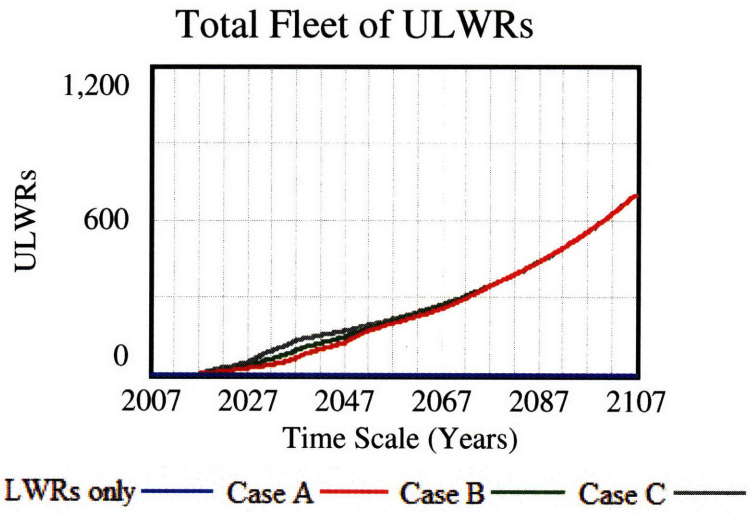

Figure 4-5 Total ULWR fleet for the various cases

Figure 4-4 shows that eventually for cases A, B, and C, the entire fleet will consist of ULWRs. For the cases utilizing ULWRs, the total number of reactors is lower than that of the LWRs only case since fewer ULWRs are required to satisfy the same power demand as LWRs. Both the LWR and ULWR (Cases A, B, and C) growth rates match that of the nuclear power

demand in Figure 4-2. This was due to the correct modeling of the ULWR adjustment as shown in Figure 4-6 and defined in Equation 4.2.

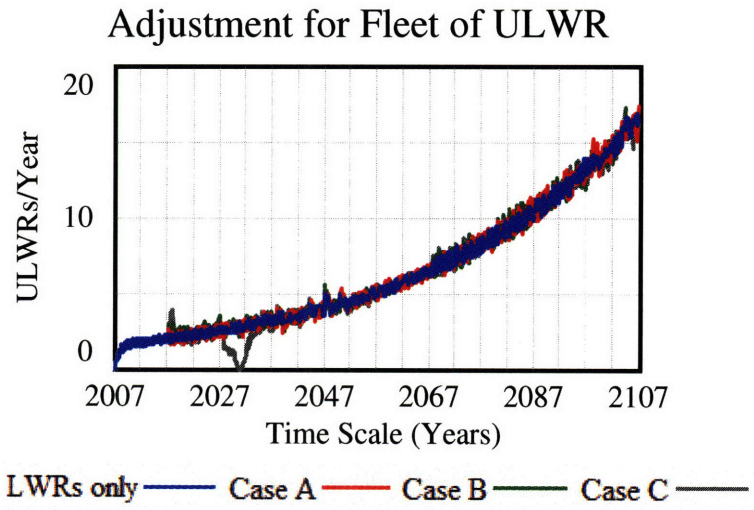

Figure 4-6 Power demand versus reactor supply adjustment for ULWRs

The large fluctuations in the adjustment occur only for Case C when 100% of the available LWRs are uprated. This is because from 2027 to 2037, uprates occur at a rate that is higher than required to maintain the power demand as shown in Figure 4-7:

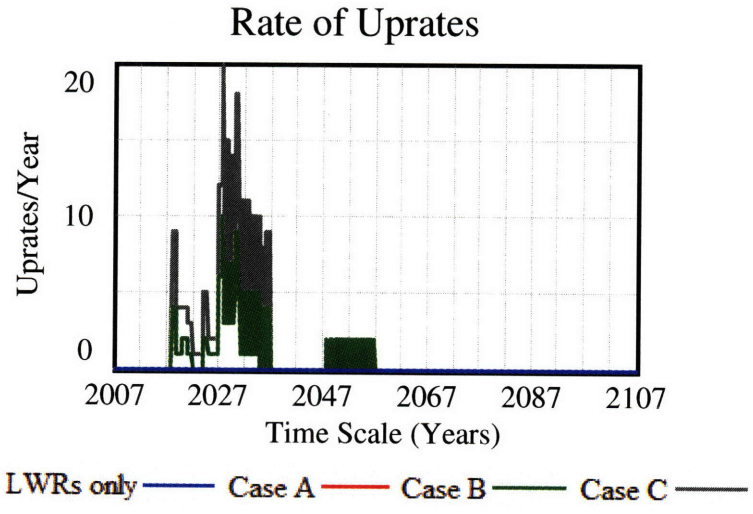

Figure 4-7 Instantaneous rate at which uprates are occurring

It has been shown that the fluctuations in adjustment do not occur if the $P_{UA} < 90\%$ so most of the LWRs can still be uprated without supplying more electricity than the demand. The second peak for Case B occurring from 2047 to 2057 indicates the uprating of 40 year-old LWRs that were not uprated when they were 20 years old.

4.2.2. **Economic Results**

Figures 4-8 through 4-10 show the total cost of electricity and its various components for all the cases:

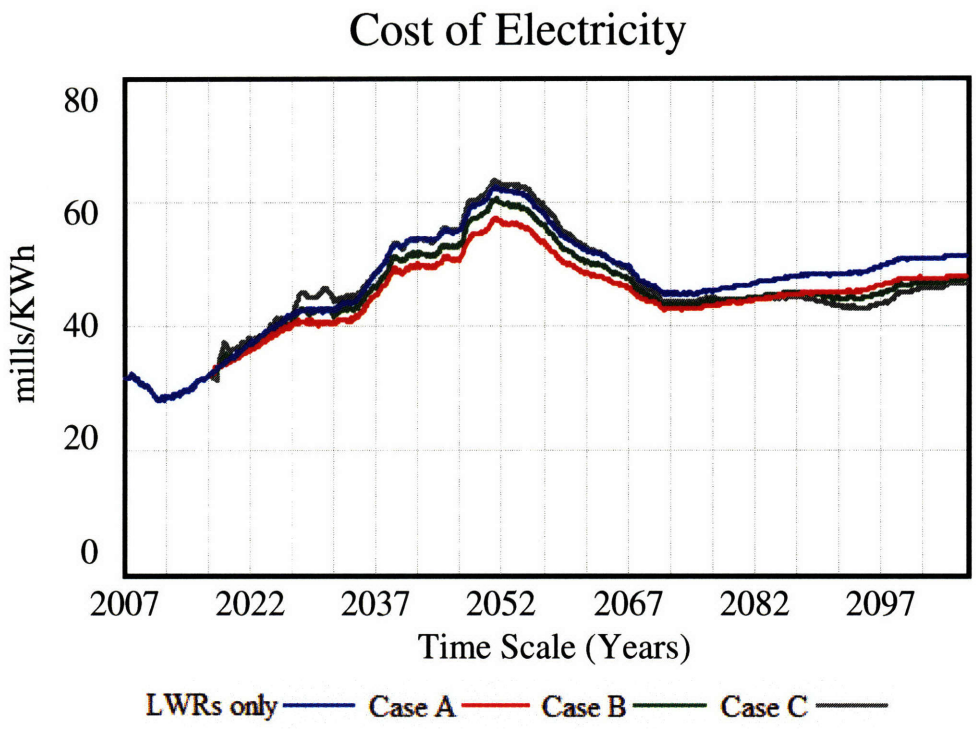

Figure 4-8 Cost of electricity from nuclear power for various cases

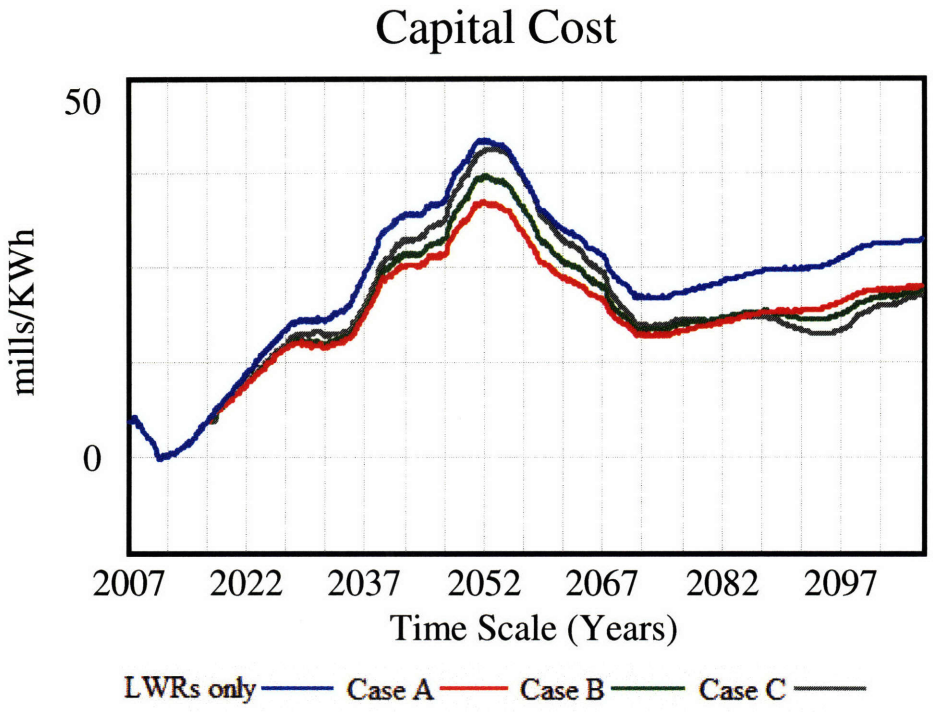

Figure 4-9 Capital costs of reactors for various cases

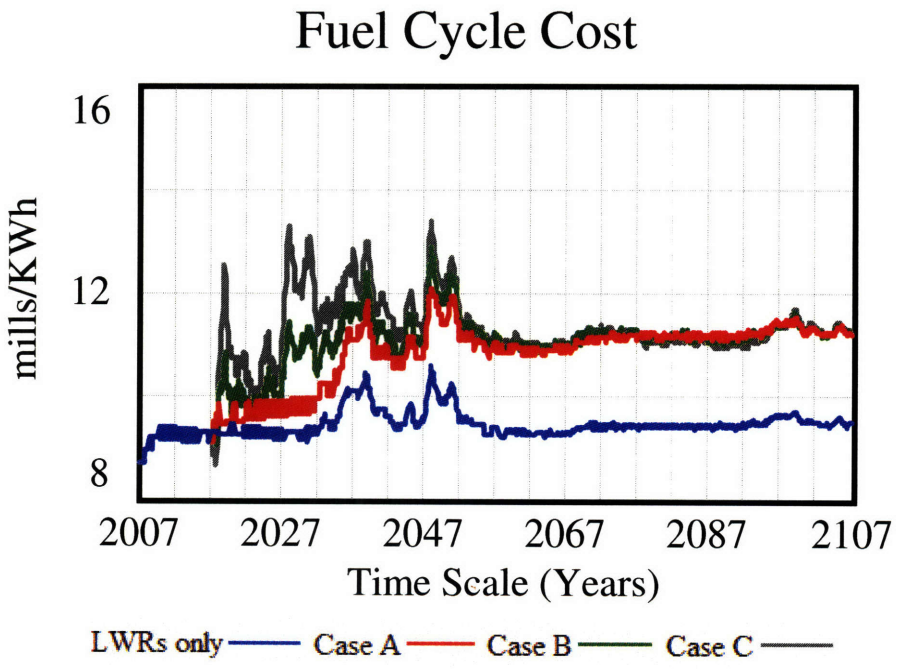

Figure 4-10 Fuel cycle costs for various cases

The total cost of electricity is the sum of the capital cost, fuel cycle cost, and operations and maintenance cost (a constant 9 mills/kWh). All cases have very similar curves for the capital cost. This can be explained as follows: the first dip in cost is due to the decrease in the number of Gen. II LWRs that pay construction cost annuities as they age past 20 years. Then the capital cost increases as new Gen. III LWRs are constructed. The capital cost starts to level off at around the year 2030 as equilibrium is reached, but then shoots up again at around 2037 as the decommissioning rate of Gen. II LWRs hits its first peak (as seen in Figure 4-11). When the decommissioning rate hits its second peak at around the year 2048, the capital cost climbs again due to a surge in new construction to replace the lost electrical output. The capital costs then gradually decrease as reactors finish paying the construction annuities.

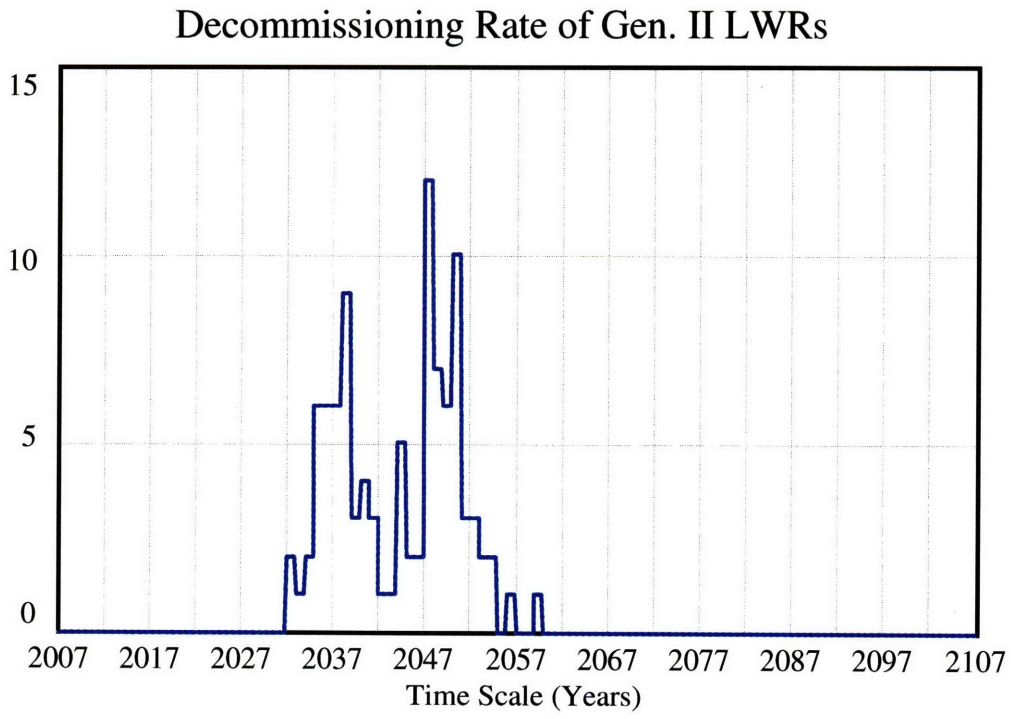

Figure 4-11 Decommissioning rate of initial fleet of LWRs

The divergence in fuel cost among the different cases occurs at 2017 and can be attributed to the beginning of feeding ULWRs with annular fuel. Although the mass loading is less, the increase in product enrichment from 4.51 wt% to 8.7 wt% more than doubles the SWU requirement per unit mass of fuel as calculated from Equation 4.16. As seen in Figure 4-12, the total SWU requirements for cases using annular fuel are a fixed ratio higher than that of the LWRs only case. The fuel cost spikes when a large group of LWRs is uprated since all uprated and new ULWRs require a fresh core of annular fuel, which is more than 3 times the amount of fuel required annually by equilibrium cores. Eventually, the fuel cost starts to converge at around 2050 for all cases and a constant difference is established between LWR and ULWR fuel costs.

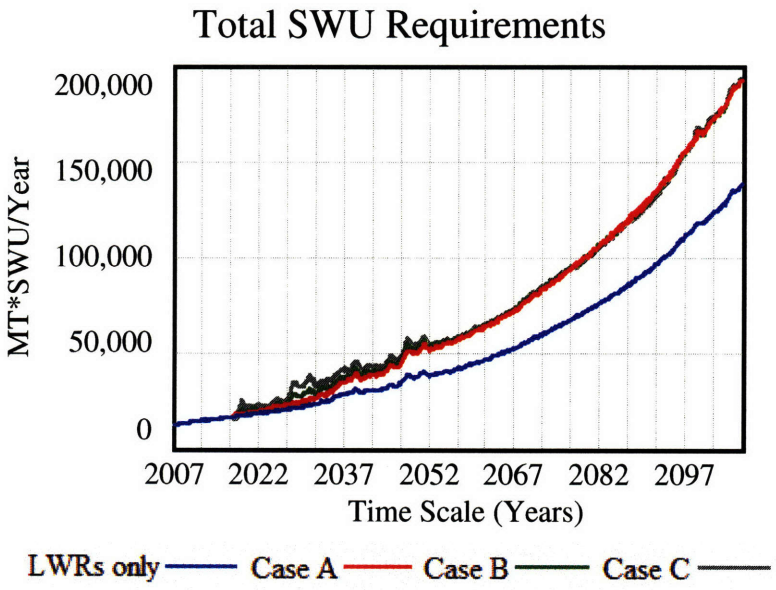

Figure 4-12 Total SWU requirements in the enrichment process for various cases

From Figure 4-8 it is shown that overall Case A, where only new construction of ULWRs takes place, results in the cheapest cost of electricity (an average reduction of 2-3 mills/kWh from the LWRs only case). This was expected since ULWRs had the lowest overnight construction cost. Cases B and C showed that any uprates of existing LWRs would increase the

overall cost of electricity due to its high overnight construction cost but this was able to be offset as long as new ULWR construction also took place.

4.2.3. Impact on Resources

The cases using ULWRs have fewer reactors and less fuel loading per reactor at any given year, so the total spent fuel, shown in Figure 4-13, is substantially less. However the natural uranium mining rate, shown in Figure 4-14, is still higher due to the fuel's higher enrichment. Although Table 4-1 indicates that ULWR spent fuel has a higher Pu and MA composition, the total amount of TRUs is less for the cases involving ULWR, as shown in Figure 4-15, due to fewer reactors and smaller fuel loading per reactor. The mass flows per reactor for each stage of the fuel cycle are shown in Table 4-8.

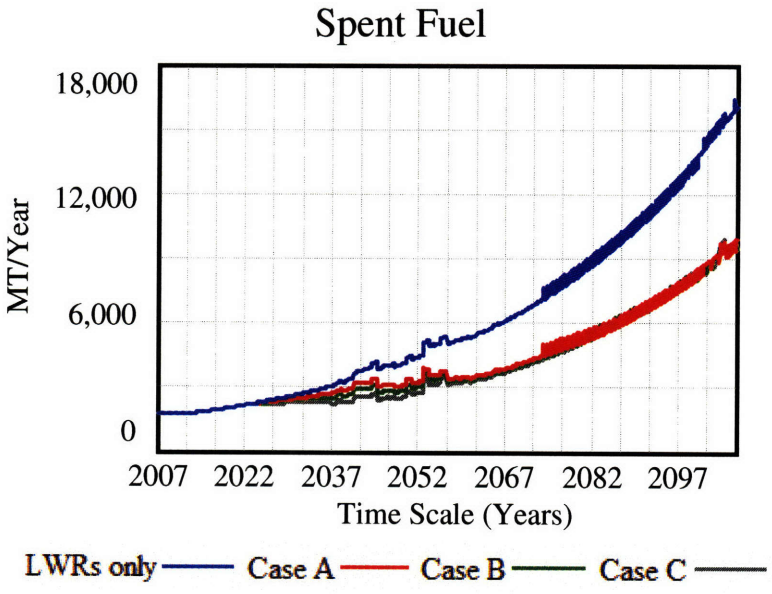

Figure 4-13 Cumulative spent fuel from various cases

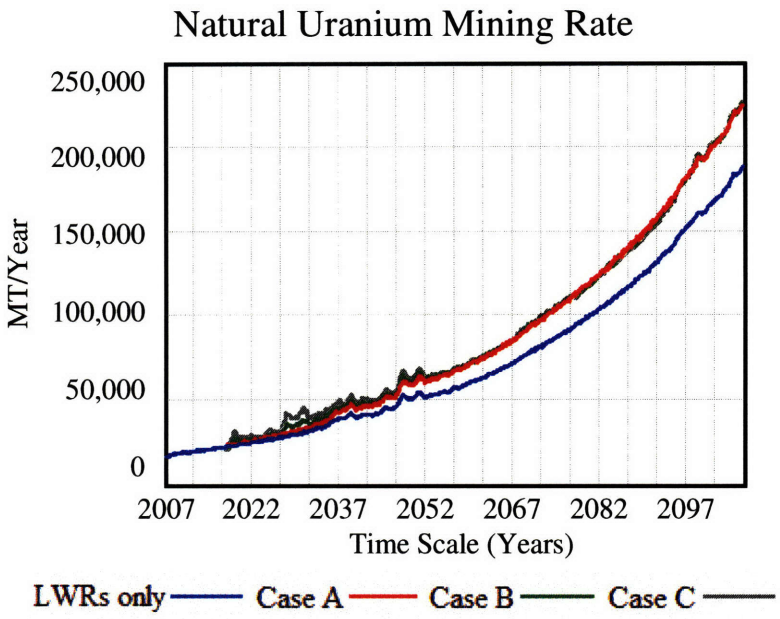

Figure 4-14 Natural uranium mining rate for various cases

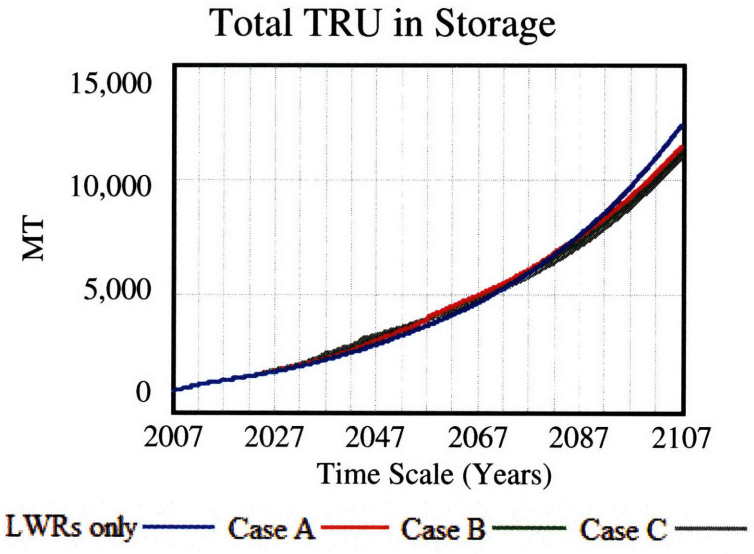

Figure 4-15 Cumulative TRU in storage for various cases

4.3. Summary

The fuel cycle systems code CAFCA SD was modified to include the implementation of high burnup annular fuel for light water reactors. This entailed creating a new fleet of reactors (ULWRs) that generate 50% more power and use higher enrichment fuel than LWRs. ULWRs are created through two ways: new construction and uprating LWRs. The LWR Construction, Mass Flow, Capital Cost, and Fuel Cost HLSDs were all updated to include this new type of reactor. The economic results show that creating ULWRs through new construction only yielded the greatest reduction in cost of electricity (2-3 mills/kWh less than the LWRs only cost). Any simultaneous uprates would increase capital costs and yield a lesser reduction in electricity cost, but the electricity cost would still be comparable to that of a cycle using only LWRs.

5. Conclusions and Recommended Future Work

5.1. Conclusions

A range of topics relating to high performance annular fuel was covered in this study to supplement the Annular Fuel Project or to address unresolved issues. The results of the study concluded that using IXAF is a very feasible approach to uprate current PWRs or to employ in future reactors for high power density in terms of neutronics, thermal hydraulics, and economics.

5.1.1. Shutdown Margin

Using the CMS code suite (CASMO-4/TABLES-3/SIMULATE-3), the whole-core shutdown margin was calculated to be sufficient for the entire fuel cycle if 25% B-10 enriched boron carbide are used for the control rods in place of traditional Ag-In-Cd.

Using MCNP-4, various Ag-In-Cd control rod shapes were modeled to determine if an increase in control rod surface area or moderator volume would increase the rod worth. This actually was shown to have the opposite effect of reducing the worth since ultimately the control rod worth is proportional to the control material volume.

5.1.2. Inner Channel Flow Thermal Hydraulic Issues

Using the thermal hydraulic code VIPRE-01, a whole core model of the uprated PWR using annular fuel was modified to simulate crud and corrosion growth in the inner channel of the hot rod. Very conservative conditions were assumed to account for the errors in the computational representation of fluid flow and heat transfer. The model calculated that a MDNBR of 1.3 was able to be maintained under transient conditions with a combined crud and corrosion thickness of 50μm, which is more than the typical thicknesses found in PWRs during

refueling periods. The model also calculated that the same margin was able to be maintained with a hypothetical entrance blockage of 35 to 40% under normal operating conditions.

5.1.3. Fuel Cycle Impact

Modifications were made to CAFCA SD to allow it to properly calculate the impact of uprated light water reactors using high performance annular fuel. An additional feature of separating the LWR fleet into Gen. II and Gen. III reactors was implemented to accurately represent old and new construction cost annuities.

Simple cases were run to demonstrate the code's new capabilities that produced consistent results with predictions:

1.) Fewer ULWRs are constructed to meet the same power demand as LWRs due to their higher power rating.

2.) Annular fuel is an average 2 mills/kWh more expensive than traditional solid fuel due to its higher SWU requirements for higher fuel enrichment.

3.) Creating ULWRs only through new construction (no uprates) resulted in the greatest reduction in cost of electricity.

4.) Increasing the percentage of ULWRs from uprates increases the cost of electricity due to its higher overnight construction cost and fuel costs.

5.) 20% more uranium ore is required to provide the U-235 for the higher enriched annular fuel for the same amount of electricity generated.

6.) The amount of spent fuel decreases by 50% at the end of the century due to the lower mass loading per reactor and the lower number of overall reactors to meet the same power demand.

7.) The ULWR fleet produces slightly less TRUs than the LWR fleet due to its smaller mass loading and fewer reactors.

5.2. Future Work

Other methods to increase the shutdown margin which deserve further investigation are extended control rodlets which originate from a rod cluster assembly that extend to adjacent assemblies. This would increase the number of control rods and increase the total worth without requiring a change the control material. Future designs for annular fuel assemblies with high power densities should leave more volume for control rods or at least keep in mind the shutdown margin during the preliminary stages of the design.

For the inner channel thermal-hydraulics, it is recommended to examine more correlations for the entrance form loss coefficient due to a blockage. Although it is highly unlikely that a correlation exists that depicts the exact situation of a partial blockage, calculating the form loss coefficient from multiple correlations defines the uncertainty due to the model adopted. Also, future annular fuel designs with long cycles should consider increasing the inner channel diameter to leave enough margins for possibly thicker crud and corrosion buildup.

For CAFCA, it is recommended to that power uprate of PWRs be made a variable value in CAFCA from 0 to 50%, since not all plants may be interested in the 50% uprate. This would entail automatically modifying the spent fuel composition, fuel enrichment, and economics, which may require extensive reprogramming of the current code structure. Correlations may be employed to determine spent fuel vectors rather than coupling with a depletion code.

Another recommendation is to allow variation of the age at which LWRs are available for uprate. Currently it can be varied while changing a few parameters but would be more user-friendly if only one variable had to be changed.

Appendices

Appendix A: Heat Flow Calculation

An approximate model was developed to explain the uneven heat flow due to annular geometry that was calculated by VIPRE-01. In the model the following approximations were assumed:

- Equal inner and outer cladding thickness
- Equal thickness crud layer on both claddings (no ZrO_2)
- Equal temperature difference across the crud layer for both claddings

For heat conduction in the crud (inner or outer):

$$q' = \frac{\Delta T}{R} \tag{A.1}$$

where q' is the linear heat flux, ΔT is the temperature difference across the crud layer, and R is the thermal resistance in the crud where:

$$R_i = \frac{\ln\left(\frac{b}{a}\right)}{2\pi H K_{crud}} \quad \text{for the inner cladding} \tag{A.2}$$

$$R_o = \frac{\ln\left(\frac{d}{c}\right)}{2\pi H K_{crud}} \quad \text{for the outer cladding} \tag{A.3}$$

where H is the active height of the rod; K_{crud} is the thermal conductivity of the crud; a, b, c, and d are the crud layer boundaries in terms of pellet radii shown below:

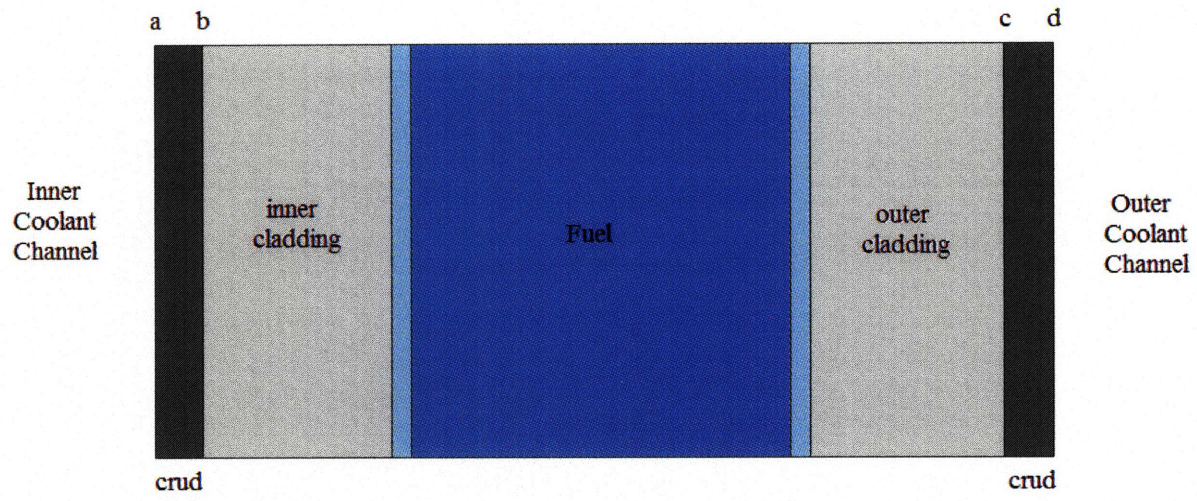

If we assume the dimensions of the annular pin in Table 1-2 and a crud thickness of 20 μm, then we obtain the following values for the radii in Equations A.2 and A.3:

	a	*b*	*c*	*d*
radii [cm]	0.8613	0.8633	1.5367	1.5387

Assuming H = 1m, we get:

$$R_i = \frac{\ln\left(\frac{0.8633}{0.8613}\right)}{2\pi K_{crud}} = \frac{3.69x10^{-4}}{K_{crud}}$$

$$R_o = \frac{\ln\left(\frac{1.5387}{1.5367}\right)}{2\pi K_{crud}} = \frac{2.07x10^{-4}}{K_{crud}}$$

Thus, for any value of K_{crud}, the inner thermal resistance will almost be twice as large. Now if we add the thermal resistances of the fuel, gap, and cladding before the crud layer to determine the thermal resistance inside and outside of the point in the fuel where the temperature gradient is zero, then we obtain:

$$R_{in} = R_1 + \frac{3.69x10^{-4}}{K_{crud}} \tag{A.4}$$

$$R_{out} = R_2 + \frac{2.07x10^{-4}}{K_{crud}} \tag{A.5}$$

where R_{in} is the total thermal resistance for heat conducting to the inner channel, R_{out} is the total thermal resistance for heat conducting to the outer channel; similarly, R_1 and R_2 are the thermal resistances from the fuel, gap, and cladding for heat conducting to the inner and outer channels, respectively. If R_1 and R_2 are on the same order of magnitude as R_i and R_o, then one can easily see that as K_{crud} decreases, the crud thermal conductivity term will dominate and increase the ratio between R_{in}/R_{out} thus causing the heat flux to be directed toward the outer channel if ΔT is the same. To reiterate, this was a very simplistic model to explain the uneven heat flow towards the inner and outer channels in annular fuel.

Appendix B: Code Descriptions

The following descriptions of the codes used for this research are meant to be brief and to serve as general introductions. More details on the codes can be found in each code's reference manual as listed in the bibliography section.

Studsvik's Core Management System (CMS)

The Studsvik core management system consists of CASMO-4, TABLES-3, and SIMULATE-3. Combined together, these three licensing-level codes are capable of simulating steady-state LWR core operations accurately and are widely used by utilities and regulatory bodies. In general, the codes are run in series, i.e., CASMO-4 runs various depletion cases for each fuel assembly type, TABLES-3 then reads CASMO-4's output which contains mainly two-group cross sections and tabulates them into a binary-format library, and finally, SIMULATE-3 draws upon data from the generated library to run whole core calculations [Edenius, 1995].

CASMO-4 is a multi-group two-dimensional transport theory code entirely written in Fortran 77. As a deterministic lattice physics code, it is used for burnup calculations of individual LWR assemblies or pin cells. The code can represent geometries consisting of cylindrical fuel rods of varying compositions in a square/hexagonal lattice. However, it is unable to accurately model annular fuel so the user must make an artificial modification to the input which is described in section 2.1.1.2. The CASMO-4 assembly output files include data on the individual assembly or pin cell such as the eigenvalue, power distribution, reaction rates, flux discontinuity factors, and few-group parameters for any region of the assembly. It also outputs a card image file that is readable by TABLES-3 to generate binary cross section libraries. Three-dimensional core conditions vary considerably from location to location, so in order to do a 3-D

PWR core analysis, a series of CASMO-4 assembly depletion calculations is needed under different core conditions [Edenius, 1995].

Given a lot of CASMO-4 runs for a fuel segment under various core conditions, a data correlation is needed to establish a dependence of CASMO-4 results on various core parameters. TABLES-3 is for such service, which links CASMO to SIMULATE via reading CASMO card image files and producing a master binary library for SIMULATE use. The types of data processed by TABLES-3 include: two-group cross sections, discontinuity factors, fission product data, detector data, pin power reconstruction data, kinetics data, and isotopics data [Edenius, 1995].

SIMULATE-3 is an advanced three-dimensional, two-group nodal code for LWR steady-state core analysis. It performs a coupled neutronics/thermal hydraulics iteration to calculate the detailed core power distribution. The reactor core is represented by dividing into a small number of sizable regions called nodes. Homogenized parameters for each of these nodes are constructed from the lattice physics code, i.e., CASMO-4. The code is capable of calculating whole-core parameters such as overall reactivity, power distribution, depletion, and for the purpose of this study, total control rod worth and indirectly, the shutdown margin. Detailed comparisons with critical assembly measurements have demonstrated that PWR pin-by-pin power distributions have root mean square (rms) differences of about 1.0% relative to measured data. Peak pin powers were predicted with rms differences of less than 0.5% relative to measured data [Edenius, 1995].

MCNP-4C

MCNP is a general purpose, generalized-geometry, continuous energy, coupled neutron/ photon/electron Monte Carlo N-Particle transport code developed at the Los Alamos National Laboratory (LANL) [Breismeister, 2000].

The stochastic model is preeminently realistic (a theoretical experiment) where the spatial and energy treatment are in principle exact. The geometry modeling is fairly generalized, which treats an arbitrary three-dimensional configuration of user-defined materials in geometric regions bounded by first- and second-degree surfaces and/or fourth-degree elliptical tori. Surfaces are defined by supplying coefficients to the analytic equations. In this way, very complex geometrical configurations can be initiated, such as a human brain. No approximations are needed in the three-dimensional problem setup. The continuous-energy Monte Carlo method is then adopted for this three-dimensional problem, where each neutron trajectory is followed according to laws of neutron interaction with matter as in reality. Random numbers are used to determine the probability of an interaction. Note that MCNP itself is a generalized particle transport code whereas our interest is focused on the neutron criticality calculations (reactor analysis), i.e., kcode problems. The Monte Carlo random walk works by running equal numbers of neutron histories in batches, or cycles, representing each generation of neutrons. Source neutrons are distributed throughout all fissionable materials. Each neutron is emitted isotropically with its energy sampled from a fission spectrum. These neutrons then wonder around until they escape or are absorbed. In particular, when a fission is induced, the subsequent fission neutrons are not followed further. Rather, the location is stored for producing the next generation or cycle of neutrons. At the end of each cycle, the eigenvalue is evaluated as the ratio of the number of fission neutrons and the number of source neutrons in that cycle. Track length estimators are applied in order to obtain the reaction rates in the fuel [Breismeister, 2000].

Unlike deterministic codes (such as CASMO-4), MCNP is universally applicable to any neutron transport calculation, e.g., not limited to LWRs. Using MCNP, one can model the desired system as detailed as he/she wants. However, one should be aware that Monte Carlo methods only provide global answers and are not efficient for problems where a local answer is desired everywhere in phase space. Besides the number of neutron histories, the actual MCNP running time also depends on the desired result information. Another issue is that the typical Monte Carlo convergence is inversely proportional to the square root of the number of neutron histories. It is therefore much more computationally demanding compared to deterministic methods, e.g., hours of MCNP calculations are needed in order to achieve acceptable statistical errors whereas CASMO-4 takes only minutes to solve the same problem. This method was even once thought of as a last resort for attacking complex problems. But, it is believed that, as the trend of computer power increase continues, Monte Carlo based codes will become more widely used in the future [Breismeister, 2000].

VIPRE-01

VIPRE-01 is a systems thermal-hydraulics code designed for nuclear power utility thermal-hydraulic analysis applications. It was designed to help evaluate nuclear reactor core safety limits including MDNBR, critical power ratio, fuel and clad temperatures, and coolant state in normal operation and assumed accident conditions [EPRI, 1985].

VIPRE-01 predicts the three-dimensional velocity, pressure, and thermal energy fields and fuel rod temperatures for single- and two-phase flow in PWR and BWR cores. It solves the finite-difference equations for mass, energy, and momentum conservation for an interconnected array of channels assuming incompressible, thermally expandable homogeneous flow. The equations are solved with no time step or channel size restrictions for stability. Although the formulation is homogeneous, nonmechanistic models are included for subcooled boiling and vapor/liquid slip in two-phase flow [EPRI, 1985].

Like most other core thermal-hydraulic codes, the VIPRE-01 modeling structure is based on subchannel analysis. The core or section of symmetry is defined as an array of parallel flow channels with lateral connections between adjacent channels. A channel may represent a true subchannel within a rod array, a closed tube or a larger flow area representing several subchannels or rod bundles. The shape and size of the channels and their interconnections are essentially arbitrary. The user has a great deal of flexibility for modeling reactor cores or any other fluid flow geometry [EPRI, 1985].

MCODE 2.2

MCODE Version 2.2 is a linkage program, which combines the continuous-energy Monte Carlo code, MCNP-4C, and the one-group depletion code, ORIGEN-2.2, to perform burnup calculations for nuclear fission reactor systems. MCNP is used as the advanced physics modeling tool providing the neutron flux solution and detailed reaction rates in the pre-defined spatial burnup zones. ORIGEN, in turn, carries out multi-nuclide depletion calculations in each region and updates the corresponding material composition in the MCNP model. The MCNP/ORIGEN coupling follows the predictor-corrector approach. During a burnup timestep, end-of-timestep material compositions are first predicted based on the flux solution at the beginning-of-timestep. Using the predicted end-of-timestep material compositions, an MCNP run is performed to compute the neutron flux and detailed reaction rates, which are then used in a corrector burnup step. The final end-of-timestep material compositions are obtained as the average value of the results from the predictor and corrector steps [Xu et al., 2006].

Appendix C: Sample Inputs

CASMO-4

```
* FUEL SEGMENT: XU81024G10 USING BORON CRD at 25% B10
*
* CASE MATRICES:
*    - BASE CASE WITH INSTANTANEOUS BRANCHES
*    - LOW TFU HISTORY WITH BRANCHES TO NOMINAL
*    - LOW TMO HISTORY WITH BRANCHES TO NOMINAL
*    - LOW BOR HISTORY WITH BRANCHES TO NOMINAL
*    - HIGH TFU HISTORY WITH BRANCHES TO NOMINAL
*    - HIGH TMO HISTORY WITH BRANCHES TO NOMINAL
*    - HIGH BOR HISTORY WITH BRANCHES TO NOMINAL
*

TTL * IXAF ASSEMBLY DESIGN, PQN-02, 13X13 LATTICE

***** STATE POINT PARAMETERS *****
TFU=800 TMO=583.1 BOR=600 VOI=0.0
SIM 'XU81024G10' 8.1 10 24 24  * ITYPE, ENR, WBA, IBAP, IBAO

***** OPERATING PARAMETERS *****
PRE 155.1296  * CORE PRESSURE, bars
PDE 156.75 'KWL'  * POWER DENSITY, kW/liter

***** MISCELLANEOUS OPTIONS *****
THE 0  * NO THERMAL EXPANSION

***** MATERIAL COMPOSITIONS *****
* FUE 1  8.1 w/o ENR              (+20% U-238)
*     2  8.1 w/o ENR, 10wt% Gd2O3 (+30% U-238)
FUE 1 /1.90270E+21 92234=1.52868E+19 92238=2.55596E+22 8000=4.64149E+22
FUE 2 /1.65272E+21 64154=7.15550E+19 64155=4.91214E+20 64156=6.82822E+20
       64157=5.22717E+20 64158=8.29586E+20 64152=6.90454E+18 64160=7.30328E+20
       92234=1.32785E+19 92238=2.40518E+22  8000=4.53221E+22
SPA 10.81934 0.1800E-4,,8.154/718=84.59 347=15.41
B4C 1.76 0.0 / 5000=106.9126 6000=21.74 * B10 Concentration 25/18.3 higher

***** GEOMETRY SPECIFICATION *****
PWR 13 1.651 21.5
PIN 1    0.4315 0.4890 0.4950 0.7050 0.7110 0.7685/
      'COO'  'CAN'  'AIR'   '1'   'AIR'  'CAN'
PIN 2    0.4315 0.4890 0.4950 0.7050 0.7110 0.7685/
      'COO'  'CAN'  'AIR'   '2'   'AIR'  'CAN'
PIN 5 0.7110 0.7685/'COO' 'BOX'  * GUIDE TUBE
PIN 9 0.7110 0.7685/'COO' 'BOX'
PIN 9 0.5751 0.5789 0.6259  0.7110 0.7685/'B4C' 'AIR' 'CRS' 'COO' 'BOX'
      //1 'RCC' 'ROD'
LPI 5
    1 2
    1 1 1
    1 1 1 2
    2 1 9 1 1
    1 1 2 1 1 2
    1 1 1 1 1 1 1

***** BASE CASE WITH INSTANTANEOUS BRANCHES *****
DEP -100 105 110 115 120 125 130 135 140 145 150
STA
COE ,,0 0.5 1 2 3 4 5 6 7 8 9 10 15 20 25 30 40 50 60 70 80 90 100 110 120 130
```

```
      140 150
TMO 293.2 333.2 449.8 505.4 546.8 565.8 583.1 600.0 616.5
+ TFU 293.2 449.8 549.8 565.8 800 1100
TMO 293.2 333.2 449.8 505.4 546.8 565.8 583.1 600.0 616.5
+ BOR 0 1200 1800 2400
TMO 293.2 333.2 449.8 505.4 546.8 565.8 583.1 600.0 616.5 ROD 'RCC'
SDC 100 100 100 100 100 1691.5 6574.5 8766.0 26298.0 43830.0/'DT'

***** LOW TFU HISTORY WITH BRANCHES TO NOMINAL *****
TTL * LOW TFU HISTORY
TFU=565.8 TMO=583.1 BOR=600 VOI=0.0
DEP -100 105 110 115 120 125 130 135 140 145 150
STA
COE ,,0 0.5 1 2 3 4 5 6 7 8 9 10 15 20 25 30 40 50 60 70 80 90 100 110 120 130
      140 150
TFU 800

***** LOW TMO HISTORY WITH BRANCHES TO NOMINAL *****
TTL * LOW TMO HISTORY
TFU=800 TMO=565.8 BOR=600 VOI=0.0
DEP -100 105 110 115 120 125 130 135 140 145 150
STA
COE ,,0 0.5 1 2 3 4 5 6 7 8 9 10 15 20 25 30 40 50 60 70 80 90 100 110 120 130
      140 150
TMO 583.1

***** LOW BOR HISTORY WITH BRANCHES TO NOMINAL *****
TTL * LOW BOR HISTORY
TFU=800 TMO=583.1 BOR=0.0 VOI=0.0
DEP -100 105 110 115 120 125 130 135 140 145 150
STA
COE ,,0 0.5 1 2 3 4 5 6 7 8 9 10 15 20 25 30 40 50 60 70 80 90 100 110 120 130
      140 150
BOR 600

***** HIGH TFU HISTORY WITH BRANCHES TO NOMINAL *****
TTL * HIGH TFU HISTORY
TFU=1100 TMO=583.1 BOR=600 VOI=0.0
DEP -100 105 110 115 120 125 130 135 140 145 150
STA
COE ,,0 0.5 1 2 3 4 5 6 7 8 9 10 15 20 25 30 40 50 60 70 80 90 100 110 120 130
      140 150
TFU 800

***** HIGH TMO HISTORY WITH BRANCHES TO NOMINAL *****
TTL * HIGH TMO HISTORY
TFU=800 TMO=600.0 BOR=600 VOI=0.0
DEP -100 105 110 115 120 125 130 135 140 145 150
STA
COE ,,0 0.5 1 2 3 4 5 6 7 8 9 10 15 20 25 30 40 50 60 70 80 90 100 110 120 130
      140 150
TMO 583.1

***** HIGH BOR HISTORY WITH BRANCHES TO NOMINAL *****
TTL * HIGH BOR HISTORY
TFU=800 TMO=583.1 BOR=1200.0 VOI=0.0
DEP -100 105 110 115 120 125 130 135 140 145 150
STA
COE ,,0 0.5 1 2 3 4 5 6 7 8 9 10 15 20 25 30 40 50 60 70 80 90 100 110 120 130
      140 150
BOR 600

END
```

TABLES-3

```
'COM' 78901234567890123456789012345678901234567890123456789012345678901234567890
'COM'    1         2         3         4         5         6         7         8

'TIT' 'FUE SEG: XU700 (+20% U-238)'/
'PWR' 0 155.1296/
'LIB' 'ADD'/
'OPT' 4 1/
'CAS' '../C4/c4.XU700.b.cax'/
'EXP' 40 1  0 0.5 1 2 3 4 5 6 7 8 9 10 11 12.5 15 17.5 20 25 30 35 40 45 50
            55 60 65 70 75 80 85 90 95 100 105 110 115 120 130 140 150/
'RES' 28 1  0 0.5 1 2 3 4 5 6 7 8 9 10 15 20 25 30 40 50 60 70 80 90 100 110
            120 130 140 150/
'TFU'  6 5  293.2 449.8 549.8 565.8 800 1100/
'TMO'  9 7  293.2 333.2 449.8 505.4 546.8 565.8 583.1 600.0 616.5/
'BOR'  5 2  0 600 1200 1800 2400/
'HTFU' 3 2  565.8 800 1100/
'HTMO' 3 2  565.8 583.1 600/
'HBOR' 3 2  0 600 1200/
'CRD'  2 1  '   ' 'RCC'/
'SDC' 11 1  0 0.1 0.2 0.3 0.4 0.5 2.1915 8.766 17.532 43.83 87.66/
'BAS.MAC' 3 'EXP' 'TFU' 'TMO'/
'DEL.MAC' 3 'EXP' 'BOR' 'TMO'/
'DEL.MAC' 3 'EXP' 'CRD' 'TMO'/
'DEL.MAC' 2 'EXP' 'HTFU'/
'DEL.MAC' 2 'EXP' 'HTMO'/
'DEL.MAC' 2 'EXP' 'HBOR'/
'DEL.MAC' 2 'EXP' 'SDC'/
'EPS.MAC' 10*0.000/
'BAS.FPD' 3 'EXP' 'TFU' 'TMO'/
'DEL.FPD' 3 'EXP' 'BOR' 'TMO'/
'DEL.FPD' 3 'EXP' 'CRD' 'TMO'/
'DEL.FPD' 2 'EXP' 'HTFU'/
'DEL.FPD' 2 'EXP' 'HTMO'/
'DEL.FPD' 2 'EXP' 'HBOR'/
'DEL.FPD' 2 'EXP' 'SDC'/
'EPS.FPD' 10*0.000/
'BAS.DFS' 3 'EXP' 'TFU' 'TMO'/
'DEL.DFS' 3 'EXP' 'BOR' 'TMO'/
'DEL.DFS' 3 'EXP' 'CRD' 'TMO'/
'DEL.DFS' 2 'EXP' 'HTFU'/
'DEL.DFS' 2 'EXP' 'HTMO'/
'DEL.DFS' 2 'EXP' 'HBOR'/
'DEL.DFS' 2 'EXP' 'SDC'/
'EPS.DFS' 10*0.000/
'ADF' 1 1 0 0 1 1 0 0/
'PIN.PIN'/
'EPS.PIN' 10*0.000/
'STA'/

'TIT' 'FUE SEG: XU750 (+20% U-238)'/
'LIB' 'ADD'/
'CAS' '../C4/c4.XU750.b.cax'/
'STA'/

'TIT' 'FUE SEG: XU800 (+20% U-238)'/
'LIB' 'ADD'/
'CAS' '../C4/c4.XU800.b.cax'/
'STA'/

'TIT' 'FUE SEG: XU810'/
'LIB' 'ADD'/
```

```
'CAS' '../C4/c4.XU810.b.cax'/
'STA'/

'TIT' 'FUE SEG: XU81024G80'/
'LIB' 'ADD'/
'CAS' '../C4/c4.XU81024G80.b.cax'/
'STA'/

'TIT' 'FUE SEG: XU81024G10'/
'LIB' 'ADD'/
'CAS' '../C4/c4.XU81024G10.b.cax'/
'STA'/

'TIT' 'FUE SEG: XU81028G80'/
'LIB' 'ADD'/
'CAS' '../C4/c4.XU81028G80.b.cax'/
'STA'/

'TIT' 'FUE SEG: XU81028G12'/
'LIB' 'ADD'/
'CAS' '../C4/c4.XU81028G12.b.cax'/
'STA'/

'TIT' 'FUE SEG: XU81032G80'/
'LIB' 'ADD'/
'CAS' '../C4/c4.XU81032G80.b.cax'/
'STA'/

'TIT' 'FUE SEG: XU850 (+20% U-238)'/
'LIB' 'ADD'/
'CAS' '../C4/c4.XU850.b.cax'/
'STA'/

'TIT' 'FUE SEG: XU900 (+20% U-238)'/
'LIB' 'ADD'/
'CAS' '../C4/c4.XU900.b.cax'/
'STA'/

'TIT' 'FUE SEG: XU90016G60'/
'LIB' 'ADD'/
'CAS' '../C4/c4.XU90016G60.b.cax'/
'STA'/

'TIT' 'FUE SEG: XU90020G80'/
'LIB' 'ADD'/
'CAS' '../C4/c4.XU90020G80.b.cax'/
'STA'/

'TIT' 'FUE SEG: XU90024G60'/
'LIB' 'ADD'/
'CAS' '../C4/c4.XU90024G60.b.cax'/
'STA'/

'TIT' 'FUE SEG: XU90024G80'/
'LIB' 'ADD'/
'CAS' '../C4/c4.XU90024G80.b.cax'/
'STA'/

'TIT' 'FUE SEG: XU90024G12'/
'LIB' 'ADD'/
'CAS' '../C4/c4.XU90024G12.b.cax'/
'STA'/

'TIT' 'FUE SEG: XU90028G80'/
'LIB' 'ADD'/
```

```
'CAS' '../C4/c4.XU90028G80.b.cax'/
'STA'/

'TIT' 'FUE SEG: XU90028G14'/
'LIB' 'ADD'/
'CAS' '../C4/c4.XU90028G14.b.cax'/
'STA'/

'TIT' 'FUE SEG: XU90032G80'/
'LIB' 'ADD'/
'CAS' '../C4/c4.XU90032G80.b.cax'/
'STA'/

'TIT' 'FUE SEG: XU90040G60'/
'LIB' 'ADD'/
'CAS' '../C4/c4.XU90040G60.b.cax'/
'STA'/

'TIT' 'FUE SEG: XU950 (+20% U-238)'/
'LIB' 'ADD'/
'CAS' '../C4/c4.XU950.b.cax'/
'STA'/

'TIT' 'FUE SEG: XU100 (+20% U-238)'/
'LIB' 'ADD'/
'CAS' '../C4/c4.XU100.b.cax'/
'STA'/

'TIT' 'FUE SEG: XU300'/
'LIB' 'ADD'/
'CAS' '../C4/c4.XU300.b.cax'/
'STA'/

'TIT' 'FUE SEG: XU400'/
'LIB' 'ADD'/
'CAS' '../C4/c4.XU400.b.cax'/
'STA'/

'TIT' 'FUE SEG: XU500'/
'LIB' 'ADD'/
'CAS' '../C4/c4.XU500.b.cax'/
'STA'/

'TIT' 'FUE SEG: XU585'/
'LIB' 'ADD'/
'CAS' '../C4/c4.XU585.b.cax'/
'STA'/

'TIT' 'FUE SEG: XU85016G60'/
'LIB' 'ADD'/
'CAS' '../C4/c4.XU85016G60.b.cax'/
'STA'/

'TIT' 'FUE SEG: XU85024G10'/
'LIB' 'ADD'/
'CAS' '../C4/c4.XU85024G10.b.cax'/
'STA'/

'TIT' 'FUE SEG: XU870'/
'LIB' 'ADD'/
'CAS' '../C4/c4.XU870.b.cax'/
'STA'/

'TIT' 'FUE SEG: XU87020G60'/
'LIB' 'ADD'/
```

```
'CAS' '../C4/c4.XU87020G60.b.cax'/
'STA'/

'TIT' 'FUE SEG: XU87040G80'/
'LIB' 'ADD'/
'CAS' '../C4/c4.XU87040G80.b.cax'/
'STA'/

'END'/

'COM' 78901234567890123456789012345678901234567890123456789012345678901234567890
'COM'    1         2         3         4         5         6         7         8

'TIT' 'XU-PWR RADIAL REFLECTOR'/
'REF' 'RADIAL' 0 155.1296/
'LIB' 'ADD'/
'CAS' '../C4/c4.XURADREF.cax'/
'BOR'  4 2  0 600 1200 2400/
'HBOR' 4 2  0 600 1200 2400/
'TMO'  4 4  293 353 425 563.1/
'HTMO' 4 4  293 353 425 563.1/
'BAS.MAC' 2 'TMO' 'BOR',,'HTMO' 'HBOR'/
'BAS.DFS' 2 'TMO' 'BOR',,'HTMO' 'HBOR'/
'STA'/

'TIT' 'XU-PWR BOTTOM REFLECTOR'/
'REF' 'AXIAL' 0 155.1296/
'LIB' 'ADD'/
'CAS' '../C4/c4.XUBOTREF.cax'/
'STA'/
'END'/

'COM' 78901234567890123456789012345678901234567890123456789012345678901234567890
'COM'    1         2         3         4         5         6         7         8

'TIT' 'XU-PWR TOP REFLECTOR'/
'REF' 'AXIAL' 0 155.1296/
'LIB' 'ADD'/
'CAS' '../C4/c4.XUTOPREF.cax'/
'TMO'  5 4  293 353 425 563.1 603.1/
'HTMO' 5 4  293 353 425 563.1 603.1/
'BOR'  4 2  0 600 1200 2400/
'HBOR' 4 2  0 600 1200 2400/
'BAS.MAC' 2 'TMO' 'BOR',,'HTMO' 'HBOR'/
'BAS.DFS' 2 'TMO' 'BOR',,'HTMO' 'HBOR'/
'STA'/
'END'/
```

SIMULATE-3

```
'COM' 789012345678901234567890123456789012345678901234567890123456789012345678901234567890
'COM'    1         2         3         4         5         6         7         8
'COM'
'COM' 150%-POWER PWR CORE FUELED WITH IXAF FUEL, PQN-02
'COM' 72 RELOAD FUEL ASSEMBLIES WITH 5.85 w/o AXIAL BLANKETS
'COM'           24 LOW-ENRICHED FUEL AT 8.1 w/o CENTER ENRICHMENT
'COM'           48 HIGH-ENRICHED FUEL AT 9.0 w/o CENTER ENRICHMENT
'COM'
'COM' CYCLE 10: EQUILIBRIUM CYCLE CORE

'DIM.PWR' 15/
'DIM.CAL' 24 2 2/  * 24 AXIAL NODES, QUARTER CORE, 2X2 NODES PER ASSY
'DIM.DEP' 'EXP' 'SAM' 'HTMO' 'HBOR' 'HTFU' 'PIN' 'EBP'/  * DEPLETION ARGUMENTS

'TIT.CAS' 'CYCLE 10 (EQC)'/

'FUE.NEW' 'TYPE01' 'M101'  4 11/  * XU81024G10
'FUE.NEW' 'TYPE01' 'M105'  8 12/  * XU81028G80
'FUE.NEW' 'TYPE01' 'M113'  4 12/  * XU81028G80
'FUE.NEW' 'TYPE01' 'M117'  8 13/  * XU81032G80
'FUE.NEW' 'TYPE01' 'M201'  8 33/  * XU90028G80
'FUE.NEW' 'TYPE01' 'M209'  8 33/  * XU90028G80
'FUE.NEW' 'TYPE01' 'M217'  8 32/  * XU90024G60
'FUE.NEW' 'TYPE01' 'M225'  8 34/  * XU90040G60
'FUE.NEW' 'TYPE01' 'M233'  4 31/  * XU90016G60
'FUE.NEW' 'TYPE01' 'M237'  4 33/  * XU90028G80
'FUE.NEW' 'TYPE01' 'M241'  8 33/  * XU90028G80

'COM'  -R-  -P-  -N-  -M-  -L-  -K-  -J-  -H-  -G-  -F-  -E-  -D-  -C-  -B-  -A-
'FUE.SER' 4/
01 1                      K218 L231 L201 K209 L204 L229 K219
02 1            K234 L242 M218 M210 M202 L102 M203 M211 M219 L243 K240
03 1       K238 M234 M226 L218 L209 L105 M238 L108 L212 L219 M227 M235 K235
04 1       L245 M229 L238 L118 K232 M242 K212 M243 K230 L119 L240 M231 L247
05 1  K221 M221 L221 L121 L233 M118 K202 M114 K203 M119 L236 L123 L223 M223 K223
06 1  L228 M213 L214 K227 M121 K245 M106 L113 M107 K243 M123 K226 L216 M215 L225
07 1  L206 M205 L110 M245 K205 M109 K242 M102 K247 M111 K207 M247 L112 M207 L208
08 1  K215 L103 M239 K214 M115 L116 M103 K101 M104 L115 M116 K213 M240 L104 K216
09 1  L207 M208 L111 M248 K208 M112 K248 M101 K241 M110 K206 M246 L109 M206 L205
10 1  L226 M216 L215 K225 M124 K244 M108 L114 M105 K246 M122 K228 L213 M214 L227
11 1  K224 M224 L224 L124 L235 M120 K204 M113 K201 M117 L234 L122 L222 M222 K222
12 1       L248 M232 L239 L120 K229 M244 K211 M241 K231 L117 L237 M230 L246
13 1       K236 M236 M228 L220 L211 L107 M237 L106 L210 L217 M225 M233 K237
14 1            K239 L244 M220 M212 M204 L101 M201 M209 M217 L241 K233
15 1                      K220 L230 L203 K210 L202 L232 K217
 0 0

'RES' './RES/s3.XU18.11.c9.res' 20000/

'CRD.GRP' 1
4*0             00 00 00 00 00 00 00            4*0
2*0       00  9 00  3 00  2 00  3 00  9 00      2*0
  0    00 00 00  6 00  8 00  8 00  7 00 00 00     0
  0     9 00  1 00 00 00  5 00 00 00  1 00  9     0
    00 00  7 00  4 00 00 00 00 00  4 00  6 00 00
    00  3 00 00 00  2 00  4 00  2 00 00 00  3 00
    00 00  8 00 00 00 00 00 00 00 00 00  8 00 00
    00  2 00  5 00  4 00  1 00  4 00  5 00  2 00
    00 00  8 00 00 00 00 00 00 00 00 00  8 00 00
    00  3 00 00 00  2 00  4 00  2 00 00 00  3 00
    00 00  6 00  4 00 00 00 00 00  4 00  7 00 00
```

```
  0     9 00  1 00 00 00  5 00 00 00  1 00  9     0
  0    00 00 00  7 00  8 00  8 00  6 00 00 00     0
2*0       00  9 00  3 00  2 00  3 00  9 00      2*0
4*0             00 00 00 00 00 00 00            4*0/
'CRD.ZON' 1 1 'ARO' 0 0.0 0 365.76/  * NO CONTROL ROD
'CRD.ZON' 2 1 'AIC' 0 0.0 0 7.57 10 365.76/  * AIC CONTROL ROD
'CRD.DAT' 226 1.585/
'CRD.TYP' 1
4*0              1  1  1  1  1  1  1            4*0
2*0        1 02  1 02  1 02  1 02  1 02  1      2*0
  0     1  1  1 02  1 02  1 02  1 02  1  1  1     0
  0    02  1 02  1  1  1 02  1  1  1 02  1 02     0
     1  1 02  1 02  1  1  1  1 02  1 02  1  1
     1 02  1  1  1 02  1 02  1 02  1  1  1 02  1
     1  1 02  1  1  1  1  1  1  1  1  1 02  1  1
     1 02  1 02  1 02  1 02  1 02  1 02  1 02  1
     1  1 02  1  1  1  1  1  1  1  1  1 02  1  1
     1 02  1  1  1 02  1 02  1 02  1  1  1 02  1
     1  1 02  1 02  1  1  1  1  1 02  1 02  1  1
  0    02  1 02  1  1  1 02  1  1  1 02  1 02     0
  0     1  1  1 02  1 02  1 02  1 02  1  1  1     0
2*0        1 02  1 02  1 02  1 02  1 02  1      2*0
4*0              1  1  1  1  1  1  1            4*0/
'CRD.SEQ'  1  000 000 000 000 115 226 226 226 226 226/  * CD
'CRD.SEQ'  2  000 000 000 115 226 226 226 226 226 226/  * CC
'CRD.SEQ'  3  000 000 115 226 226 226 226 226 226 226/  * CB
'CRD.SEQ'  4  000 115 226 226 226 226 226 226 226 226/  * CA
'CRD.SEQ'  5  226 226 226 226 226 226 226 226 226 226/  * SE
'CRD.SEQ'  6  226 226 226 226 226 226 226 226 226 226/  * SD
'CRD.SEQ'  7  226 226 226 226 226 226 226 226 226 226/  * SC
'CRD.SEQ'  8  226 226 226 226 226 226 226 226 226 226/  * SB
'CRD.SEQ'  9  226 226 226 226 226 226 226 226 226 226/  * SA
'CRD.SEQ' 10  226 226 226 226 226 226 226 226 226 226/  * NO BANK REGION
'CRD.PAS' 10 6/

'COM' OUTPUT EDIT OPTIONS
'BAT.EDT' 'ON'/
'FUE.BAT'  1
          21 01 12 02 26 06 11 26
          01 26 02 26 06 12 06 16
          12 02 26 03 27 16 06 17
          02 26 03 14 13 15 05 25
          26 06 27 13 16 07 16  0
          06 12 16 15 07 04 26  0
          11 06 06 05 16 24  0  0
          26 16 17 25  0  0  0  0/
'COM'       -FRESH-        -ONCE-         -TWICE-
'BAT.LAB' 01 '0L2410'   11 '1L2410'   21 '2L2410'
          02 '0L2880'   12 '1L2880'
          03 '0L3280'   13 '1L3280'
          04 '0H1660'   14 '1H1660'   24 '2H1660'
          05 '0H2460'   15 '1H2460'   25 '2H2460'
          06 '0H2880'   16 '1H2880'   26 '2H2880'
          07 '0H4060'   17 '1H4060'   27 '2H4060'/
'PRI.STA' '2EXP' '2RPF'/

'COR.OPE' 150 150 2250/  * 150% POWER OPERATION
'ITE.BOR' 1500/
'ITE.SRC' 'SET' 'EOLEXP',,0.0001,,,'KEF' 1.000 0.000005 'MINBOR'/

'DEP.CYC' 'CYCLE10' 0.0 10/
'DEP.STA' 'AVE' 0.0 0.15 0.25 0.5 -0.5 32/
'WRE' './RES/s3.XU18.11.eqc.res' -32/

'STA'/
```

```
'XPN.RES' './RES/s3.XU18.11.eqc.res' 0 0.15 0.5 1 3 5 7 9 11 13 15 17 19 21 23 25
25.991/

'TIT.CAS' 'HZP, NO XENON, PK SM'/
'COR.OPE' 0./
'DEP.FPD' 8/  * NO XE PK SM
'ITE.BOR' 1500/
'BAT.EDT' 'OFF'/
'XPN.STA'/
'END'/
```

MCNP-4C

```
 1/8th Full Assembly model of PWR annular fuel
c   13x13 Lattice with 4.95w/o UO2 Fuel and 150% Power Density
c  Cross Shaped Control rods in
c
c
c   cell specification
c
c    mt  density             geometry
  4  4  7.06685e-02 -1        u=2 imp:n=1            $ internal coolant 583.1K
  6  3  4.34384e-02  1 -2      u=2 imp:n=1            $ internal clad 593K
  8  2  3.76497e-05  2 -3      u=2 imp:n=1            $ internal gap
 10  1  6.96225e-02  3 -4      u=2 imp:n=1 vol=2343.37  $ fuel pellet 600K
 12  2  3.76497e-05  4 -5      u=2 imp:n=1            $ external gap
 13  3  4.34384e-02  5 -6      u=2 imp:n=1            $ external clad 593K
 14  4  7.06685e-02  6         u=2 imp:n=1            $ extenal coolant 583.1K
 24  4  7.06685e-02 -1         u=6 imp:n=1            $ internal coolant 583.1K
 26  3  4.34384e-02  1 -2      u=6 imp:n=1            $ internal clad 593K
 28  2  3.76497e-05  2 -3      u=6 imp:n=1            $ internal gap
 32  2  3.76497e-05  4 -5      u=6 imp:n=1            $ external gap
 33  3  4.34384e-02  5 -6      u=6 imp:n=1            $ external clad 593K
 34  4  7.06685e-02  6         u=6 imp:n=1            $ extenal coolant 583.1K
 41  4  6.98055e-02 -8         u=5 imp:n=1            $ coolant in guide tube 587.3K
 42  3  4.34384e-02  8 -9      u=5 imp:n=1            $ guide tube 587.3K
 43  4  6.98055e-02  9         u=5 imp:n=1            $ coolant out of guide tube 587.3K
 44  5  -10.16      -101 102 -103 104  u=4 imp:n=1          $ AIC CRD center
 45  2  3.76497e-05  10 -11     u=4 imp:n=1           $ gap btwn CRD and CRS
 46  16 -7.9         11 -12     u=4 imp:n=1           $ Stainless steel (347) CRS
 47  4  7.06685e-02  12 -8      u=4 imp:n=1           $ external coolant 583.1K
 48  3  4.34384e-02  8 -9       u=4 imp:n=1           $ guide tube 583.1K
 49  4  7.06685e-02  9         u=4 imp:n=1           $ coolant out of guide tube 583.1K
 50  5  -10.16      -10 -101 102 103  u=4 imp:n=1          $ AIC CRD north
 51  5  -10.16      -10 101 -103 104  u=4 imp:n=1          $ AIC CRD east
 52  5  -10.16      -10 -104 102 -101  u=4 imp:n=1         $ AIC CRD south
 53  5  -10.16      -10 -102 -103 104  u=4 imp:n=1         $ AIC CRD west
 54  2  3.76497e-05  -10 103 101  u=4 imp:n=1          $ water sector northeast
 55  2  3.76497e-05  -10 101 -104 u=4 imp:n=1          $ water sector southeast
 56  2  3.76497e-05  -10 -102 -104 u=4 imp:n=1         $ water sector southwest
 57  2  3.76497e-05  -10 -102 103 u=4 imp:n=1          $ water sector northwest
101  0          -21 22 -23 24 imp:n=1 u=1 lat=1 fill=-6:6 -6:6 0:0
       2 2 2 2 2 2 2 2 2 2 2 2 2
       2 2 2 2 2 2 2 2 2 2 2 2 2
       2 2 2 2 4 2 2 2 4 2 2 2 2
       2 2 2 2 2 2 2 2 2 2 2 2 2
       2 2 4 2 2 2 2 2 2 4 2 2 2
       2 2 2 2 2 2 2 2 2 2 2 2 2
       2 2 2 2 2 2 5 2 2 2 2 2 2
       2 2 2 2 2 2 2 2 2 2 2 2 2
       2 2 4 2 2 2 2 2 2 4 2 2 2
       2 2 2 2 2 2 2 2 2 2 2 2 2
       2 2 2 2 4 2 2 2 4 2 2 2 2
       2 2 2 2 2 2 2 2 2 2 2 2 2
       2 2 2 2 2 2 2 2 2 2 2 2 2
110  0          -25  26  -27  28     u=12      fill=1  imp:n=1 $ core
111  4 7.06685e-02  25:-26:  27: -28     u=12           imp:n=1 $ interassembly coolant
```

```
 120  4 7.06685e-02 -51  52  -53   54     u=16 lat=1 fill=12 imp:n=1
 130  0           61  62 -501  402 -408        fill=16 imp:n=1 $ FA
 1000 0           -61:-62: 501:-402: 408              imp:n=0 $ outside
c   end of cell specification

c
c   surface specification
c
c   trn card  constants for equations
  1  cz  0.4315         $ Inner surface of inner clad
  2  cz  0.4890         $ Outer surface of inner clad
  3  cz  0.49500         $ Inner fuel surface (cylinder #1)
  4  cz  0.70500         $ Outer fuel surface (cylinder #10)
  5  cz  0.7110         $ Inner surface of outer clad
  6  cz  0.7685         $ Outer surface of outer clad
  8  cz  0.7110         $ Inner surface of guide tube
  9  cz  0.7685         $ Outer surface of guide tube
  10 cz  0.5751         $ Outer surface of control rod
  11 cz  0.5789         $ Inner surface of CRS
  12 cz  0.6259         $ Outer surface of CRS
  101 px  0.2800         $ cross northeast vertical line
  102 px -0.2800         $ cross northwest vertical line
  103 py  0.2800         $ cross northeast horizontal line
  104 py -0.2800         $ cross southeast horizontal line
  21  px  0.8255         $ pin pitch
  22  px -0.8255         $ pin pitch
  23  py  0.8255         $ pin pitch
  24  py -0.8255         $ pin pitch
  25  px  10.73150        $ FA width
  26  px -10.73150        $ FA width
  27  py  10.73150        $ FA width
  28  py -10.73150        $ FA width
  51  px  10.75000        $ FA pitch
  52  px -10.75000        $ FA pitch
  53  py  10.75000        $ FA pitch
  54  py -10.75000        $ FA pitch
 *61  p  1 -1  0  0     $ symmetry  1
 *62  py 0.0           $ symmetry
 *402 pz  0.000          $ core-bottom
 *408 pz  400.00         $ core-top
 *501 px  10.750001       $ boundary
c   end of surface specification

c
c   data specification
c
c
phys:n   20   0.0
c
c
c    3. tmp free-gas thermal temperature card
c   t1n t2n...n=index of time,t1n=temp for cell 1 at time n
#       tmp1
   4   5.0246e-08       $583.1K
   6   5.1099e-08       $593K
   8   2.5300e-08       $293K
  10   5.1702e-08       $600K
```

```
  12  2.5300e-08
  13  5.1099e-08      $593K
  14  5.0246e-08      $583.1K
  24  5.0246e-08      $583.1K
  26  5.1099e-08      $593K
  28  2.5300e-08
  32  2.5300e-08
  33  5.1099e-08      $593K
  34  5.0246e-08      $583.1K
  41  5.0246e-08      $583.1K
  42  5.0246e-08      $583.1K
  43  5.0246e-08      $583.1K
  44  5.1702e-08      $600K
  45  2.5300e-08
  46  5.1099e-08      $593K
  47  5.0246e-08      $583.1K
  48  5.0246e-08      $583.1K
  49  5.0246e-08      $583.1K
  50  5.1702e-08      $600K
  51  5.1702e-08      $600K
  52  5.1702e-08      $600K
  53  5.1702e-08      $600K
  54  2.5300e-08
  55  2.5300e-08
  56  2.5300e-08
  57  2.5300e-08
 101  5.0246e-08      $583.1K
 110  5.0246e-08      $583.1K
 111  5.0246e-08      $583.1K
 120  5.0246e-08      $583.1K
 130  5.0246e-08      $583.1K
1000  2.5300e-08
c
c   material specification
c
awtab  34079 78.240500 38089 88.143700 38090 89.135400
      44106 104.998000 46107 105.987000
      47111 109.953000 48115 113.919000
      50126 124.826000 51124 122.842000 51125 123.832000
      52127 125.815000 52129 127.800000 53131 129.781998
      54133 131.764008 56140 138.709000 57140 138.707993
      58141 139.697998 58143 141.684998 58144 142.677000
      59142 140.691000 59143 141.682999 61151 149.625000
      62153 151.608002 63156 154.585007
      63157 155.577000 65160 157.562000
c
c   4.95 wt% U-235  (10.31g/cc, 6.96225e-02)
m1      8016.60c  4.6415e-2
      92234.78c  9.30160e-6
      92235.53c  1.16270e-3
      92238.53c  2.20355e-2
c   AIR (gap)
m2    8016.60c  3.76497E-05
c
c   Zircaloy-4  (6.550g/cc)
m3      8016.60c 3.08257e-4
      24000.50c 7.58604e-5
```

```
      26000.55c 1.48326e-4
      40000.60c 4.24242e-2
      50000.35c 4.81797e-4
c
c    H2O (15.5MPa at 583.1K)  (0.705g/cc)
m4     8016.60c 2.35652e-2
       1001.60c 4.71033e-2
mt4    lwtr.04t
c
c    AIC control material (10.16 g/cc)
m5     47000.55c -80
       48000.50c -5
       49000.60c -15
c
c      Stainless Steel-347 (7.9 g/cc)
m16    14000.50c -0.51
       24000.50c -17.4
       25055.50c -1.99
       26000.50c -68.4
       28000.50c -11.7
c
c
ksrc   1.0   0.2    0.0
     1.0   0.2    5.0
     1.0   0.2   10.0
     1.0   0.2   15.0
c
c
mode   n
kcode  3000   1.0  5   150
prdmp   150 150 150
print
```

VIPRE-01

```
*                                                                    *
*  1/8 core, 13x13 annular pins, using PWR power distribution        *
*  30um corrosion + crud various k_crud                               *
**********************************************************************
1,0,0                                                *vipre.1
1/8 core, 13x13 PQN02 annular pins,PWR power distribution          *vipre.2
geom,49,49,20,0,0,0  *normal geometry input                        *geom.1
144.0,0.0,0.5                                        *geom.2
1,0.0675,0.9503,0.7127,1,2,0.045,0.542,
2,0.1350,1.9007,1.9007,2,3,0.045,0.542,4,0.045,0.650,
3,0.0675,0.9503,0.9503,1,5,0.045,0.542,
4,0.1350,1.9007,1.9007,2,5,0.045,0.650,7,0.045,0.650,
5,0.131727,1.911534,1.911534,2,6,0.045,0.542,8,0.045,0.650, *affected channel
6,0.065863,0.955767,0.955767,1,9,0.045,0.542, *affected channel
7,0.1350,1.9007,1.9007,2,8,0.045,0.650,11,0.045,0.650,
8,0.131727,1.911534,1.433651,2,9,0.045,0.650,12,0.045,0.650, *affected channel
9,0.131727,1.911534,1.433651,2,10,0.045,0.542,13,0.045,0.650, *affected channel
10,0.0675,0.9503,0.9503,1,14,0.045,0.542,
11,0.1350,1.9007,1.9007,2,12,0.045,0.650,16,0.045,0.650,
12,0.1350,1.9007,1.4255,2,13,0.045,0.650,16,0.045,0.650,
13,0.1350,1.9007,1.4255,2,14,0.045,0.650,16,0.045,0.650,
14,0.1350,1.9007,1.9007,2,15,0.045,0.542,17,0.045,0.650,
15,0.0675,0.9503,0.9503,1,17,0.045,0.542,
16,0.4051,5.7020,5.7020,2,17,0.045,1.842,18,0.135,0.657,
17,0.3376,4.7517,4.7517,1,18,0.135,0.657,
18,0.9440,12.35430268,12.3543,1,19,0.300,2.282,
19,5.294,74.126,69.849,2,20,0.300,4.232,21,0.270,4.938,
20,5.766,80.303,76.026,2,21,0.300,4.938,22,0.300,6.348,
21,11.514,160.368,151.815,1,23,0.600,7.054,
22,11.533,160.606,152.053,2,23,0.600,6.348,25,0.300,12.697,
23,23.066,321.212,304.106,2,24,0.600,7.054,25,0.600,12.697,
24,11.533,160.606,152.053,1,25,0.600,11.286,
25,161.459,2248.483,2128.741,1,26,2.698,19.499,
26,322.92,4496.97,4257.48,
27,0.0454,0.5339,0.5339,
28,0.0454,0.5339,0.5339,
29,0.0454,0.5339,0.5339,
30,0.0907,1.0678,1.0678,
31,0.0454,0.5339,0.5339,
32,0.0454,0.5339,0.5339,
33,0.0907,1.0678,1.0678,
34,0.088886,1.056872,1.056872, *affected channel
35,0.0454,0.5339,0.5339,
36,0.0454,0.5339,0.5339,
37,0.0907,1.0678,1.0678,
38,0.0907,1.0678,1.0678,
39,0.0454,0.5339,0.5339,
40,0.4536,5.3388,5.3388,
41,0.5444,6.4066,6.4066,
```

```
42,3.629,42.711,42.711,
43,3.629,42.711,42.711,
44,7.258,85.422,85.422,
45,7.258,85.422,85.422,
46,14.517,170.843,170.843,
47,7.258,85.422,85.422,
48,101.62,1195.90,1195.90,
49,203.23,2391.80,2391.80                    *geom.4
prop,0,0,2,1  *internal EPRI functions                    *prop.1
rods,1,46,1,2,6,0,0,0,0,0,0  *six material types,two types of geo.  *rods.1
0.0,0.0,0,0                                  *rods.2
-1                                          *rods.3
1.55  *chopped cosine, with peak to average=1.55          *rods.5
******rods geometry input                              *rods.9
1,1,1.657,1,1,0.25,2,0.25,
-1,1,1.657,1,27,0.5,
2,1,1.582,1,1,0.125,2,0.25,3,0.125,
-2,1,1.582,1,28,0.5,
3,1,1.544,1,2,0.25,4,0.25,
-3,1,1.544,1,29,0.5,
4,1,1.557,1,2,0.25,3,0.25,4,0.25,5,0.25,
-4,1,1.557,1,30,1,
5,1,1.576,1,3,0.125,5,0.25,6,0.125,
-5,1,1.576,1,31,0.5,
6,1,1.544,1,4,0.25,7,0.25,
-6,1,1.544,1,32,0.5,
7,1,1.587,1,4,0.25,5,0.25,7,0.25,8,0.25,
-7,1,1.587,1,33,1,
8,2,1.685,1,5,0.25,6,0.25,8,0.25,9,0.25,
-8,2,1.685,1,34,1,
9,1,1.655,1,6,0.125,9,0.25,10,0.125,
-9,1,1.655,1,35,0.5,
10,1,1.557,1,7,0.25,11,0.25,
-10,1,1.557,1,36,0.5,
11,1,1.66,1,7,0.25,8,0.25,11,0.25,12,0.25,
-11,1,1.66,1,37,1,
12,1,1.668,1,9,0.25,10,0.25,13,0.25,14,0.25,
-12,1,1.668,1,38,1,
13,1,1.554,1,10,0.125,14,0.25,15,0.125,
-13,1,1.554,1,39,0.5,
14,1,1.586,1,11,0.5,12,0.5,13,0.25,16,2.5,18,1.25,
-14,1,1.586,1,40,5,
15,1,1.554,1,13,0.25,14,0.5,15,0.375,16,0.5,17,2.5,?
18,1.875
-15,1,1.554,1,41,6,
16,1,1.587,1,18,3.25,19,36.75,
-16,1,1.587,1,42,40,
17,1,1.587,1,20,40,
-17,1,1.587,1,43,40,
18,1,1.587,1,18,0.125,21,79.875,
-18,1,1.587,1,44,80,
19,1,1.382,1,22,80,
```

```
-19,1,1.382,1,45,80,
20,1,1.261,1,23,160,
-20,1,1.261,1,46,160,
21,1,1.226,1,24,80,
-21,1,1.226,1,47,80,
22,1,0.941,1,25,1120,
-22,1,0.941,1,48,1120,
23,1,0.942,1,26,2240,
-23,1,0.942,1,49,2240,                          *rods.9
0                                               *rods.9
1,tube,0.605,0.339882,5                         *rods.68
2,1,0.0224921,0.0,?  *inner cladding              *rods.69
2,2,0.0024488,0.0,?  *inner gap                   *rods.69
8,3,0.0826772,1.0,?  *fuel ring                   *rods.69
2,4,0.0024409,0.0    *outer gap                   *rods.69
2,1,0.0225000,0.0    *outer cladding              *rods.69
2,tube,0.60846,0.336413,9  *Crud rod              *rods.68
2,5,0.001181,0.0,?   *inner crud                  *rods.69
2,6,0.001735,0.0,?      *inner corrosion             *rods.69
2,1,0.021311,0.0,?  *inner cladding               *rods.69
2,2,0.0024488,0.0    *inner gap                   *rods.69
8,3,0.0826772,1.0,?  *fuel ring                   *rods.69
2,4,0.0024409,0.0,?  *outer gap                   *rods.69
2,1,0.021319,0.0,?  *outer cladding               *rods.69
2,6,0.00173,0.0        *outer corrosion             *rods.69
2,5,0.001181,0.0     *outer crud                  *rods.69
1,18,409.0,clad                                 *rods.70
0.0,0.0671,7.3304509,?
25,0.0671,7.3304509
50,0.0671,7.33045093,?
65,0.0671,7.33045093
80.33,0.0671,7.33045093,?
260.33,0.07212,8.11585329
692.33,0.07904,9.80167423,?
1502.33,0.08955,13.2923001
1507.73,0.11988,13.3211893,?
1543.73,0.14089,13.5166505
1579.73,0.14686,13.717249,?
1615.73,0.1717,13.9231981
1651.73,0.1949,14.1347101,?
1687.73,0.18388,14.3519980
1723.73,0.1478,14.5752746,?
1759.73,0.112,14.804753
1786.73,0.085,14.9810589,?
2240.33,0.085,18.5665964
2,1,0.025,igap                                  *rods.70
1,1.240834,0.2156263   *Cp=5195J/kg-K *gap=6000          *rods.71
3,23,650.617,FUO2                               *rods.70
86,0.05677357,4.73275874,?
176,0.06078589,4.29917259
266,0.06366347,3.93877428,?
356,0.06581210,3.63454049
```

```
446,0.06747631,3.37435643,?
536,0.06880819,3.1493668
626,0.06990545,2.95294976,?
716,0.07083283,2.78005572
806,0.07163441,2.62676801,?
896,0.07234099,2.49000319
986,0.07297458,2.36730189,?
1076,0.07355124,2.25667975
1166,0.07408294,2.1565193,?
1256,0.07457886,2.06549023
1346,0.07504628,1.98248979,?
1436,0.07549123,1.90659753
1526,0.0759191,1.83704065,?
1616,0.07633503,1.77316713
1706,0.0767443,1.7144247,?
1796,0.07715268,1.66034425
1886,0.07756663,1.61052668,?
1976,0.07799351,1.5646323
2500,0.079364,1.33988                                    *rods.71
4,1,0.025,ogap                                          *rods.70
1,1.240834,0.2149314   *Cp=5195J/kg-K *gap=6000          *rods.71
5,1,368.3,crud       *crud K varies                      *rods.70
1,0.1,1.156352                                          *rods.71
6,1,368.3,rust                                          *rods.70
1,0.1,1.156352       *ZrO2 props  5.9g/cm^3 2W/mk 418J/kgK      *rods.71
oper,1,1,0,1,0,1,0,0,0                                  *oper.1
-1.0,1.3,0.0,0.005,                                     *oper.2
0                                                       *oper.3
*27,39,52,53,54,55,56,57,58,59
2248.12,562.46,7316.516,195.5139,0.0                          *oper.5
0            *no forcing functions                      *oper.12
corr,2,2,0                                              *corr.1
epri,epri,epri,none                                     *corr.2
0.2                                                     *corr.3
ditb,thsp,thsp,w-3l,cond,g5.7    *correlation for boiling curve   *corr.6
w-3s,w-3l            *dnb analysis by w-3l              *corr.9
0.0          *w-3s input data                           *corr.10
0.042,0.066,0.986  *w-3l input data                           *corr.11
drag,1,1,4                                              *drag,1
0.32,-0.25,0.0,64.0,-1.0,0.0                                  *drag.2
0.605,0.65                                              *drag.7
7.333,-0.2,0.0,7.333,-0.2,0.0
grid,0,3                                                *grid.1
0.6,0.4,1.0,                                            *grid.2
26,9                                                    *grid.4
1,2,3,4,5,6,7,8,9,10,11,12,13,14,15,16                        *grid.5
17,18,19,20,21,22,23,24,25,26                                 *grid.5
0.0,2,12.007874,1,32.007874,1,52.007874,1,?
72.007874,1,92.007874,1,112.007874,1,132.007874,1
144.0,3                  *grid loc.              *grid.6
23,2
27,28,29,30,31,32,33,34,35,36,37,38,39,40,41,42,
```

```
43,44,45,46,47,48,49,
0.0,2,144.0,3
0
cont                                        *cont.1
0.0,0,150,50,3,1,  *iterative solution                *cont.2
0.0,0.0,0.001,0.0,0.0,0.9,1.5,1.0                     *cont.3
5,0,0,0,0,0,1,1,0,0,0,1,0,0                         *cont.6
1000.,0.0,0.0,0.0,0.0,0.0,0.0                       *cont.7
endd
*
*end of data input
0
```

MCODE 2.2

```
 Pin Model of PWR annular fuel MCODE
c   150% Power Density 8.7 enrichment
c
c  by Bo Feng 3/31/08
c
c   cell specification
c
c    mt  density                    geometry
  4  4  7.06685e-02  -1 -7 8          imp:n=1          $ internal coolant 583.1K
  3  3  4.34384e-02   1 -2 -7 8        imp:n=1          $ internal clad 593K
  2  2  3.76497e-05   2 -3 -7 8        imp:n=1          $ internal gap
  1  1  6.912873-02   3 -4 -7 8        imp:n=1          $ fuel pellet 600K
 12  2  3.76497e-05   4 -5 -7 8        imp:n=1          $ external gap
 13  3  4.34384e-02   5 -6 -7 8        imp:n=1          $ external clad 593K
 14  4  7.06685e-02   6 -7 8 -9 10 -11 12  imp:n=1 vol=8.704    $ extenal coolant 583.1K
  5  0            7 -8 9 -10 11 -12   imp:n=0          $ void
c

c   surface specification
c
c   trn card  constants for equations
 1  cz  0.4315        $ Inner surface of inner clad
 2  cz  0.4890        $ Outer surface of inner clad
 3  cz  0.49500       $ Inner fuel surface
 4  cz  0.70500       $ Outer fuel surface
 5  cz  0.7110        $ Inner surface of outer clad
 6  cz  0.7685        $ Outer surface of outer clad
 *7  pz  5.0          $ pin top
 *8  pz -5.0          $ pin bottom
 *9  px  0.8255       $ front boundary (pitch 1.651)
 *10 px -0.8255       $ back boundary
 *11 py  0.8255       $ right boundary
 *12 py -0.8255       $ left boundary
c   end of surface specification

c  Material specification
c
c    8.7 wt% U-235  (10.31g/cc, 600K)
m1       8016.34c 4.608582e-2
       92234.34c 1.621356e-5
       92235.34c 2.026695e-3
       92238.34c 2.100000e-2
c
c    AIR (gap)
m2       8016.60c 3.76497E-05
c
c    Zircaloy-4  (6.550g/cc)
m3       8016.34c 3.08257e-4
      24000.50c 7.58604e-5
```

```
      26000.55c 1.48326e-4
      40000.60c 4.24242e-2
      50000.35c 4.81797e-4
c
c    H2O (15.5MPa at 583.1K)  (0.705g/cc)
m4     8016.34c 2.35652e-2
      1001.34c 4.71033e-2
c
c
kcode   1000   1.0  5   55
prdmp   50 50 50
print
c

c    MCODE Input
1   7.9168 pwrue.lib 600
mce  /home/CODES/mcnp/mcnp
mcxs /home/CODES/mcode/mcnpxs.sum
mcs  2 xus
orge /home/CODES/origen22/origen22
orgl /home/CODES/origen22/libs decay.lib gxuo2brm.lib
tal  1 (1)
pow  2595.0
nor  2 0
cor  1
dep  E   10
       20
       30
       40
       60
       70
       83.4
sta  0
end
```

Appendix D: U.S. Fleet of Reactors

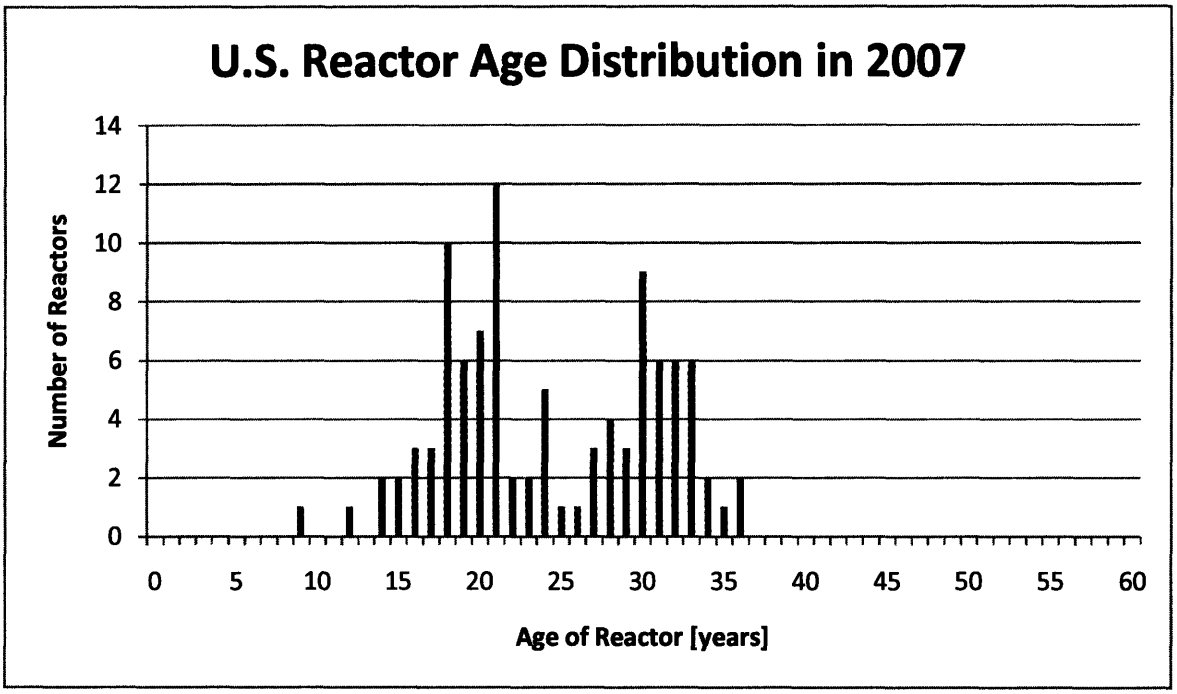

Reactor Age (years)	Number of Reactors
1	0
2	0
3	0
4	0
5	0
6	0
7	0
8	0
9	1
10	0
11	0
12	1
13	0
14	2
15	2
16	3
17	3
18	10
19	6
20	7

Reactor Age (years)	Number of Reactors
21	12
22	2
23	2
24	5
25	1
26	1
27	3
28	4
29	3
30	9
31	6
32	6
33	6
34	2
35	1
36	2
37	0
38	0
39	0
40	0

Reactor Age (years)	Number of Reactors
41	0
42	0
43	0
44	0
45	0
46	0
47	0
48	0
49	0
50	0
51	0
52	0
53	0
54	0
55	0
56	0
57	0
58	0
59	0
60	0

References

[1] Beccherle, J., "Feasibility and Economics of Existing PWR Transition to a Higher Power Core Using Annular Fuel," Master's Thesis, Center for Advanced Nuclear Energy Systems, MIT (Aug 2007).

[2] Bonnet, N., "Sensitivity of Economic Performance of the Nuclear Fuel Cycle to Simulation Modeling Assumptions," Master's Thesis, Center for Advanced Nuclear Energy Systems, MIT (May 2007).

[3] Breismeister, J.F., "MCNP-A General Monte Carlo N-Particle Transport Code," Version 4C Manual. Los Alamos National Laboratory (2000).

[4] Busquim e Silva, R., "Simulation of the Nuclear Fuel Cycle With Recycling: Options and Outcomes," Master's Thesis, Center for Advanced Nuclear Energy Systems, MIT (Feb 2008).

[5] Deshon, J. and K. Edsinger, EPRI. Private Communication (Nov 2007).

[6] DiGiovine, A.S., J.D. Rhodes, III, "SIMULATE-3 User's Manual," Studsvik/SOA-95/15, Studsvik of America, Inc. (1995).

[7] Eaglepicher, http://www.eaglepicher.com/EaglePicherInternet/Technologies/Boron/ (2008).

[8] Edenius, M., K. Eckberg, B.H. Forssen, and D. Knott, "CASMO-4, A Fuel Assembly Burnup Program, User's Manual," Studsvik/SOA-95/1, Studsvik of America, Inc. (1995).

[9] Feng, D., M.S. Kazimi, and P. Hejzlar, "Innovative Fuel Designs for High Power Density Pressurized Water Reactor" MIT-NFC-TR-075 Center for Advanced Energy Systems, MIT (Sept 2005).

[10] Guérin, L. "CAFCA: Code for Advanced Fuel Cycles Assessment," PowerPoint presentation. MIT meta study meeting and M.S. Thesis in progress (Feb 2008).

[11] Idelchik, I.E., "Handbook of Hydraulic Resistance," Second Edition, Revised and Augmented. Hemisphere Publishing Corporation. ISBN 3-540-15962-2. p. 133 Diagram 3-13 (1986).

[12] KAERI, http://atom.kaeri.re.kr (2000).

[13] Kazimi, M.S. et al, "High Performance Fuel Design for Next Generation PWRs," 1st Annual Report, MIT-NFC-PR-048, Center for Advanced Nuclear Energy Systems, MIT (Aug 2002).

[14] Kazimi, M.S., P. Hejzlar, et al., "High Performance Fuel Design For Next Generation PWRs: Final Report," MIT-NFC-PR-082, Center for Advanced Nuclear Energy Systems, MIT (Jan 2006).

[15] Lahoda, E. et al., "High-Power-Density Annular Fuel for Pressurized Water Reactors: Manufacturing Costs and Economic Benefits," Nuclear Technology, Vol. 160, No. 1, pp. 112-134 (Oct 2007).

[16] "Nuclear Fuel Safety Criteria Technical Review," Nuclear Energy Agency, OECD (2001).

[17] Seabrook Station Updated Final Safety Analysis Report, Chapter 4.

[18] VerPlanck, D.M., "TABLES-3 User's Manual," Studsvik/SOA-95/16, Studsvik of America, Inc. (1995).

[19] "VIPRE-01: Thermal Hydraulic Code for Reactor," Volume II Users Manual. EPRI-NP-2511-CCM-A. Electric Power Research Institute (1985).

[20] Xu, Z. "Design Strategies for Optimizing High Burnup Fuel in Pressurized Water Reactors," PhD Thesis, Center for Advanced Nuclear Energy Systems, MIT (Jan 2003).

[21] Xu, Z., Y. Otsuka, P. Hejzlar, M.J. Driscoll, and M.S. Kazimi, "Neutronic Design of PWR Cores with High Performance Annular Fuel," MIT-NFC-TR-063, Center for Advanced Nuclear Energy Systems, MIT (May 2004).

[22] Xu, Z., P. Hejzlar, and M. Kazimi, "MCODE, Version 2.2-an MCNP-ORIGEN Depletion Program," Center for Advanced Nuclear Energy Systems, MIT (Feb 2006).